AN ^{57}FE MÖSSBAUER STUDY OF PRIMARY LITHIUM/IRON SULFIDE BATTERIES

by

Phillip E. Kovacs

B.Sc., Simon Fraser University, 1983

THESIS SUBMITTED IN PARTIAL FULFILLMENT OF

THE REQUIREMENTS FOR THE DEGREE OF

MASTER OF SCIENCE

in the Department

of

Chemistry

SIMON FRASER UNIVERSITY

September, 1988

APPROVAL

Name: Phillip E. Kovacs

Degree: Master of Science

Title of thesis: An ^{57}Fe Mössbauer Study of
Primary Lithium/Iron Sulfide Batteries

Examining Committee:

Chairman: P. W. Percival, Professor

Senior Supervisor: C. H. W. Jones, Professor

E. J. Wells, Associate Professor

B. L. Funt, Professor

Internal Examiner: J. M. D'Auria, Professor

Date Approved: 20 September 1988

PARTIAL COPYRIGHT LICENSE

I hereby grant to Simon Fraser University the right to lend my thesis, project or extended essay (the title of which is shown below) to users of the Simon Fraser University Library, and to make partial or single copies only for such users or in response to a request from the library of any other university, or other educational institution, on its own behalf or for one of its users. I further agree that permission for multiple copying of this work for scholarly purposes may be granted by me or the Dean of Graduate Studies. It is understood that copying or publication of this work for financial gain shall not be allowed without my written permission.

Title of Thesis/Project/Extended Essay

An ^{57}Fe Mössbauer Study of Primary Lithium / Iron Sulfide Batteries

Author:

(signature)

PHILLIP KOVACS

(name)

Sept 21/1988

(date)

ABSTRACT

Mössbauer spectroscopy has been used to monitor the processes occurring during discharge in Li/FeS_2 and Li/FeS cells. The ^{57}Fe Mössbauer spectra was recorded for partially and fully discharged FeS_2 cathodes at 295, 77.4, and 4.2°K. The low temperature Mössbauer and external magnetic field measurements revealed the presence of superparamagnetic and superferromagnetic Fe° particles, as well as collective magnetic excitations and surface effects. The mean diameter of the iron particles present in a fully discharged cathode was determined to be 27 ± 1Å while the effective field due to interaction with neighbouring particles was found to be 5 ± 1kG.

Studies on partially discharged FeS_2 cathodes suggested that the intermediates formed were dependent on the rate of discharge and type of electrolyte. Elemental iron is formed early in the discharge cycle, with possible evidence for $Li_3Fe_2S_4$ and other Li_xFeS_2 compounds. There is no evidence for the formation of Li_2FeS_2 in FeS_2 cathodes discharged at RT or 55°C.

Analogous studies on FeS cathodes indicated that the Fe° particles formed are larger for cathodes with the same electrolyte and discharged at the same rate. No intermediates were observed and a one step discharge mechanism appears to be operative.

ACKNOWLEDGMENTS

The author would like to express his gratitude to his research supervisor, Dr. C.H.W.Jones for his advice and guidance throughout this work. Sincere thanks are also extended to Dr. R.D.Sharma for many helpful suggestions and discussions. Dr. R.Batchelor is thanked for his assistance in some of the calculations.

Dr. R.McMillan is thanked for providing the cells and discharged cathodes used in this study. R.Fong (MoLi Energy) is thanked for doing the X-ray powder diffraction work.

I would like to thank the S.F.U. Surface Physics group for use of their electromagnet and J.Rudd for his assistance. Dr. S.Mørup is also thanked for providing the source code for MCAL.

The inhabitants of the XRF lab will not be forgotten for creating an unique ambience for research.

SYMBOLS AND ABBREVIATIONS

Symbols

$b(T,B)$	normalized magnetic hyperfine field, $b = H_{obs}/H_{bulk}$
B	external magnetic field
$\langle\cos\theta\rangle_T$	thermal average of $\cos\theta$
$B_i(T,B)$	effective contribution from neighbouring interacting particles to the total internal magnetic hyperfine field
δ	isomer shift
Δ	quadrupole splitting
ΔE_m	energy difference between $\|I,m_I\rangle$ states of a nuclear spin state
E_Q	electric quadrupole interaction energy
f	recoil-free fraction
ΔI	difference between nuclear spin quantum numbers of two nuclear spin states
Δm_I	difference between nuclear magnetic spin quantum numbers of two nuclear spin states
γ_o	gyromagnetic ratio
I	nuclear spin quantum number
k	Boltzmann's constant
K	magnetic anisotropy constant
K_1, K_2	rate constants
m_I	nuclear magnetic spin quantum number
M_S	saturation magnetization
$\mu(T)$	magnetic dipole moment, $\mu = M_S V$
η	asymmetry parameter, $\eta = (V_{xx} - V_{yy})/V_{zz}$
Q	nuclear quadrupole moment
T	temperature
T_α	temperature at which FeS is converted into the paramagnetic α-phase
T_B	blocking temperature
T_β	temperature at which FeS is converted into the β-phase
T_m	temperature at which the relaxation time for magnetic fluctuations approaches the Mössbauer timescale

T_p	magnetic ordering temperature
τ	superparamagnetic relaxation time for reversal of the magnetization about a preferred direction
τ_o	particle frequency factor (10^{-10}-10^{-12}s)
τ_L	nuclear Larmor precession time
τ_m	Mössbauer measurement time
u_x, u_y, u_z	direction cosines
V	volume
V_{zz}	one of the diagonal elements of the 3 × 3 second rank tensor describing the electric field gradient surrounding the nucleus

Abbreviations

ANL	Argonne National Laboratory
B_{appl}	externally applied magnetic field
b.c.c.	body centered cubic
EFG	electric field gradient
ESCA	electron spectroscopy for chemical analysis
f.c.c.	face centered cubic
H_{bulk}	magnetic hyperfine field of large magnetically ordered crystals, $H_{hf}(V=\infty,T)$
H_D, H_{dem}	demagnetizing field created by the uncompensated poles of the surface atoms on a microcrystal
H_{dip}	magnetic field due to dipole-dipole interactions between neighbouring particles
hfd	hyperfine field distribution
hfs	hyperfine splitting
H_{hf}, H_{int}	internal magnetic field
H_{obs}	observed magnetic hyperfine field
IMA	ion micro-probe analysis
IS	isomer shift
OCV	open circuit voltage
PC	propylene carbonate
QS	quadropole splitting
RT	room temperature
SEM	scanning electron microscopy

SF	superferromagnetic
SP	superparamagnetic
THF	tetrahydrofuran
UHV	ultra high vacuum
w.r.t.	with respect to

TABLE OF CONTENTS

LIST OF TABLES

LIST OF FIGURES

I. INTRODUCTION

Over the last twenty years, technological progress has increased the demand for light-weight, compact electrical power sources which are portable. Existing batteries barely meet these requirements and this has led to a considerable interest in battery research.

The high electrochemical reactivity, low electron affinity and low weight per unit of electricity delivered, makes lithium an attractive prospect for use as an anode. There are now several Li cells, which have been commercialized in various parts of the world, with a lifetime as high as 10 years.

In battery research, an understanding of the physical and chemical properties of the anode, cathode, electrolyte and solvent and of the various processes occurring within the battery are essential for the future improvement and design of batteries. The ideal arrangement would be to study intact cells without perturbing them. The techniques which are available for the study of complete, intact cells, however, are very limited in the types of information which they can provide. The common approach has been to disassemble the cells at various stages in their life, and apply modern analytical chemical and structural tools to gain further insight into the physical and chemical processes occurring during discharge.

One area of research which has received a great deal of attention is high temperature, rechargeable Li/Iron sulfide systems in which the electrolyte is a molten salt. A second area is ambient temperature primary and secondary Li batteries based on organic electrolyte solutions.

Although ambient temperature, non-aqueous, primary Li/Iron sulfide cells have been extensively studied in the last decade, the discharge mechanism is still not fully understood. The purpose of the present work was to further investigate the processes occurring during discharge in Li/FeS_2, and Li/FeS cells which have been developed by MoLi Energy Inc. The amorphous character of the cathodes in these batteries makes x-ray diffraction impractical as an analytical technique for the determination of phase composition of the cathode for example. The use of ^{57}Fe Mössbauer spectroscopy as an analytical technique can provide further insight into the reactions occurring at the cathode in the primary Li/iron sulfide batteries during discharge. Mössbauer spectroscopy allows the study of the iron chalcogenide cathodes in discharged battery cells *in situ*, and when disassembled.

II. THE LI/FES AND LI/FES_2 BATTERY SYSTEMS

II.1 Primary Batteries

The electropositive character of Li makes it an ideal material for battery anodes, and essentially all non-aqueous systems on the market today incorporate Li as the anode. Reactions of transition metal compounds with alkali metals may occur by one of three mechanisms:

1. **Displacement** - involves complete disruption of the crystal lattice and formation of a new solid phase.
2. **Insertion** - some structural rearrangement, however some elements of the structure of the starting host are preserved.
3. **Intercalation** - alkali metal cations occupy interstitial sites in the host lattice with minimal structural changes occuring.

In a primary battery, the reaction occurring at the cathode is usually of the displacement type and the reaction is then irreversible with intermediate phases formed which are structurally different from the starting and final material. Some advantages of employing displacement reactions are:

1. A wide range of potential cathode materials can be used.
2. A constant voltage is obtained.

3. Thermodynamically stable products are formed, allowing accurate predictions of energy densities and voltages.
4. Enhanced ionic motion possible.
5. A wide variety of compatible electrolytes is usually available.
6. The electrolyte is not consumed in the cell reaction.

Some corresponding disadvantages are:

1. There is a possibility of energy losses due to lack of microscopic reversibility.
2. New phases formed during discharge may result in polarization losses, and/or slow kinetics.
3. There is a possibility that the intermediate phases can form passive films which may decrease the utilization of the cathode.
4. Such batteries often require high temperatures.

II.2 Fabrication of the Li/FeS_2 and Li/FeS Batteries

II.2a The Cathode

Two crystalline forms are known for FeS_2, marcasite, which has a rhombic structure and pyrite, which has a NaCl structure. Of the two, pyrite is the more stable in moist air with the resulting reaction products being $FeSO_4$ and H_2SO_4. The bonding within the crystal is covalent with the iron in FeS_2 being ferrous while the sulfur is present as an S_2^{-2} group. Both the

sulfur and the iron accept 2e- on discharge, so that the overall reaction involves 4e- per mole of FeS_2.

$$FeS_2 + 4e^- \longrightarrow Fe^\circ + 2S^{-2} \qquad (1)$$

At room temperature, FeS exhibits antiferromagnetic behaviour and possesses a hexagonal superstructure closely related to the Ni-As prototype. As the temperature is raised to $T_\alpha \approx 420°K$, there is a transition to an antiferromagnetic α-phase with a corresponding decrease in the Fe atom layer separation of $\approx 1\%$ [1]. At a temperature of $T_\beta \approx 625°K$, the α-phase becomes a paramagnetic β-phase. At temperatures above T_β, the structure is of the Ni-As type and the conductivity increases by several orders of magnitude. The iron in FeS is also ferrous and the sulfur is present as S^{-2}. The overall reaction on discharge involves 2e- per mole of FeS.

$$FeS + 2e^- \longrightarrow Fe^\circ + S^{-2} \qquad (2)$$

Cathode preparation involves first preparing a slurry of finely ground FeS or FeS_2 minerals in cyclohexane. This mixture is then spread to a certain thickness on an aluminum foil, air dried, and then pressed into discs.

II.2b The Electrolyte

Non-aqueous electroytes for Li/solid cathode systems should be:

1. Stable in the presence of metallic lithium and the cathode material over a suitable range of temperatures.
2. Have a high specific conductance to minimize iR losses in the cell.

Solvents are usually aprotic, and are selected according to their dielectric constant, viscosity and electron donor properties or ability to solvate the lithium cation. An ideal solvent which would combine all three of these properties is so far not available, so most non-aqueous electrolytes contain 2 or more solvents to achieve the desired properties.

In general, a good solute should have a low crystal lattice energy, favouring ionization and should posess a relatively large anion. In non-aqueous electrolytes containing a lithium salt as a solute, the Li ion will be solvated, whereas the anion usually will not. As a result, ion transport will be mostly anionic, since the solvated Li ion will be larger than the anion.

The cathodes in the cells used in the early part of this work were pressure-wetted with a 1M $LiAsF_6$/Propylene carbonate (PC) electrolyte, to 40 lbs/in^2. This salt is a desirable electrolyte material because of its unique chemical and physical

stability, high solubility and high conductivity in a number of organic solvents [2]. Other cells that were used in later studies, were prepared with PC electrolytes which contained $LiClO_4$, another common electrolyte.

The stability of Li metal in propylene carbonate solutions can be attributed to the formation of a non-porous, ionically-conducting, insulating film which is impermeable to solvent molecules, while permitting the transport of Li ions through it. The formation and nature of this passive film has been the subject of much experiment and controversy in the past [3-7]. The generally accepted conclusion is that the major component of the passive film is Li_2CO_3 formed in the reaction:

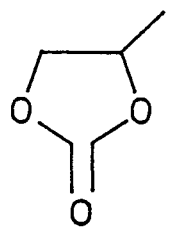

$$+ \quad 2Li \longrightarrow CH_3-CH=CH_2 + Li_2CO_3 \qquad (3)$$

II.2c The Separator

The selection of a suitable separator is also important. The material should be chemically stable in the non-aqueous electrolyte, and should exhibit properties compatible with acceptable cell performance. The low specific conductance of the electrolyte demands that the separator be highly porous and have a low tortuosity factor to minimize conductivity losses. Electrolytic transport and diffusion of the Li ion are also

important since cathodic polarization will depend on the rate at which the ion reaches the cathode. The separator used in the experimental cells consisted of a microporous polypropylene film that was pressure-wetted to open the micropores, and the casing was also constructed from polypropylene.

II.3 Previous Studies on the Discharge Mechanism of Li/FeS and Li/FeS_2 Batteries

II.3a High Temperature Li/Iron Sulfide Batteries

The bulk of research carried out on Li/iron sulfide batteries in the past, has been conducted by Argonne National Laboratories, and their sub-contractors: Eagle-Picher Industries Inc, Rockwell International and Gould Inc.

The batteries developed by these companies have an operating temperature in the range of 400-500°C, and use LiCl-KCl eutectic molten salts as an electrolyte. The nature of these highly corrosive molten salts required the development of exotic structural materials and separators. Lithium-aluminum or Li-Si alloys have been used due to the corrosive and short-circuit problems that were encountered when molten Li was used as a negative electrode.

The electrochemistry of the Li-Al/FeS system has been thoroughly studied, and is now reasonably well understood, although much is still to be learned about the FeS_2 system.

Research on the electrochemistry of high temperature Li/iron sulfide cells was first performed by Vissers *et al* [8], (ANL), in 1974. Metallographic examinations of FeS_2 cathodes that had been cycled several times, revealed that FeS was one of the many intermediate phases formed. Later work was done by Sharma [9], under General Motors Corporation, in 1976. The equilibrium phases formed between Li_2S and FeS were determined using the methods of differential thermal analysis and x-ray diffraction analysis. Martin and Tomczuk, (ANL), using results from x-ray diffraction, cyclic voltammetry and coulometric titration studies on Li/iron sulfide cells, devised a Li-Fe-S phase diagram [10-12]. Further studies on the phase relationships and thermodynamic properties of FeS [13] and FeS_2 electrodes [14], by Tomczuk *et al*, confirmed the predictions from Martin's phase diagram (Fig. 2.1).

Two mechanisms have been proposed for the discharge of the FeS electrode:

Reaction	emf, V vs LiAl
Mechanism 1 (X-phase intermediate)	
1) $2FeS + 2Li^+ + 2e^- \rightarrow Li_2FeS_2 + Fe^\circ$	1.367
2) $Li_2FeS_2 + 2Li^+ + 2e^- \rightarrow 2Li_2S + Fe^\circ$ (X-phase)	1.454
Mechanism 2 (J-phase intermediate)	
3) $26FeS + Li^+ + Cl^- + 6K^+ + 6e^- \rightarrow LiK_6Fe_{24}S_{26}Cl + 2Fe^\circ$	1.955
4) $LiK_6Fe_{24}S_{26}Cl + 51Li^+ + 46e^- \rightarrow 26Li_2S + 24Fe + 6K^+ + Cl^-$ (J-phase)	1.4

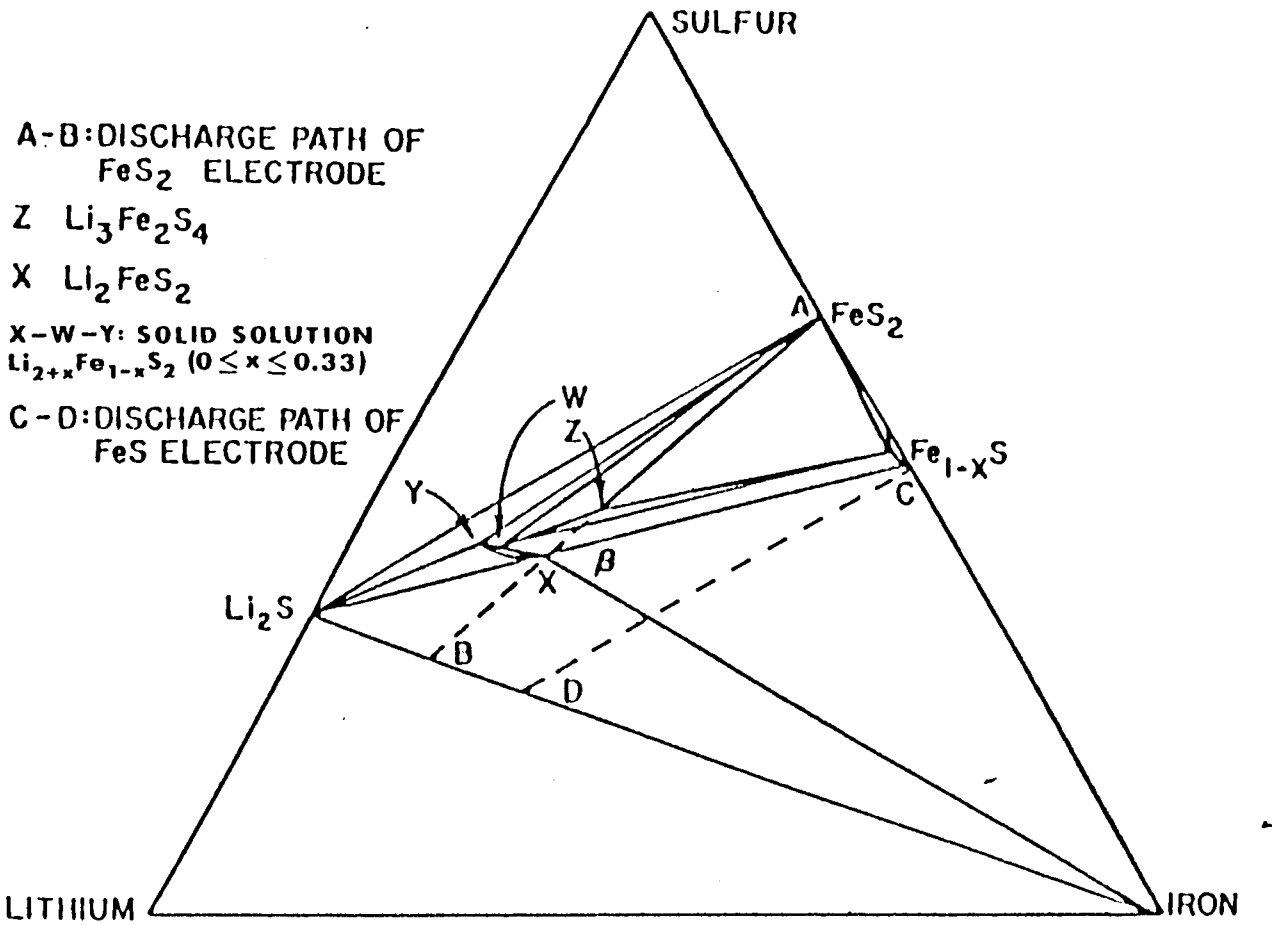

Fig. 2.1: Li-Fe-S phase diagram at 450°C.

The overall reaction is the simple 2e- process:

$$FeS + 2Li \longrightarrow Fe^{\circ} + Li_2S \qquad (4)$$

The actual discharge processes are complicated and are probably a mixture of the two mechanisms. Under certain operating conditions, however, the simple 2-reaction mechanism can occur [13]. Higher operating temperatures and LiCl concentrations favor mechanism 1, while lower temperatures and LiCl concentrations favor mechanism 2. Discharge through the X-phase intermediate is preferred because of the poor reversibility of the J-phase reactions.

Metallographic examination of FeS electrodes have shown that the surface follows a different discharge path than the interior [10], with the surface undergoing the reactions of mechanism 2, while the interior follows the path of reactions for mechanism 2.

An FeS_2 electrode in a LiCl-KCl eutectic molten salt follows a different discharge path [12]:

$$FeS_2 \longrightarrow \underset{\text{(Z-phase)}}{Li_3Fe_2S_4} \qquad (5)$$

$$Li_3Fe_2S_4 \longrightarrow \underset{\text{(W-phase)}}{\approx Li_{11}Fe_4S_{10}} + Fe_{1-x}S \qquad (6)$$

$$\approx Li_{11}Fe_4S_{10} + Fe_{1-x}S \longrightarrow Li_2FeS_2 \qquad (7)$$

$$Li_2FeS_2 \longrightarrow Fe^{\circ} + Li_2S \qquad (8)$$

The J-phase, a major intermediate phase in FeS electrodes, is

only a minor intermediate phase in FeS_2 electrodes. The phases, $Li_4Fe_3S_6$ and $LiFeS_2$ that were earlier reported by Sharma [9], were not observed by Tomczuk in his work [14]. The formation of FeS_2 does not occur at the reverse potential, and the reason behind this is not fully understood.

The phases formed in the FeS_2 electrode during charging are more complex than those formed during discharge, and minor phases are formed with each of the major phases as shown in Table (2.1) [14].

II.3b Ambient Temperature Non-Aqueous Li/Iron Sulfide Batteries

Although there are some Li/FeS_2 ambient temperature cells commercially available, the present understanding of the discharge mechanism is limited. Most of the past research on these cells was carried out during the late 70's to early 80's.

Whittingham (1978) mentions in his comprehensive work on intercalated transition metal dichalcogenides [15], that the first recharge and subsequent discharge of a discharged Li/FeS_2 cell, do not follow the same path taken by the initial discharge (Fig. 2.2).

Work by Brec and Dugast [16,17] on Li_xFeS_2 as a possible cathodic material, was carried out in 1980-81. Thermally prepared Li_2FeS_2 [9] was used as a starting material, and oxidized chemically, or electrochemically to remove quantitative

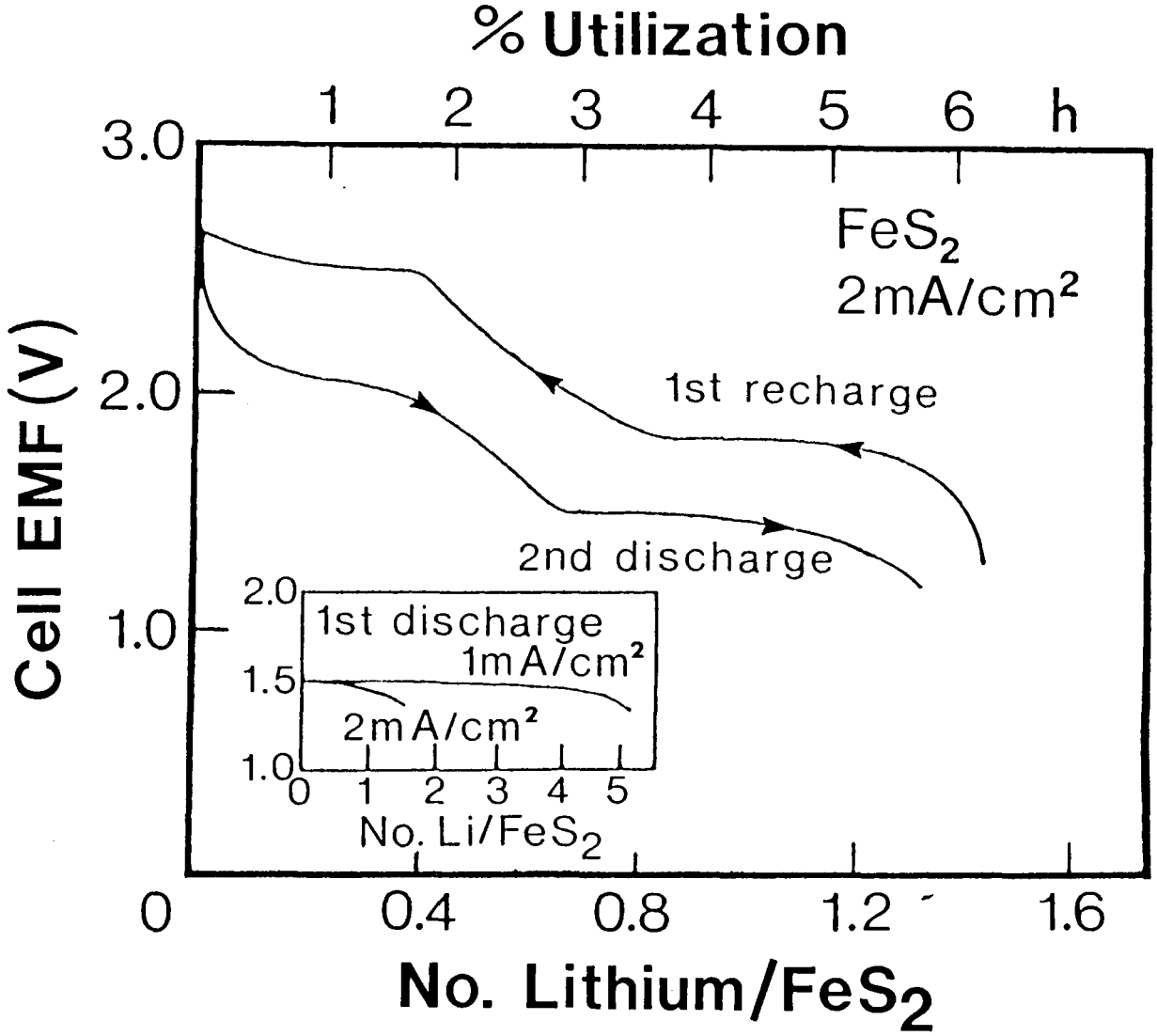

Fig. 2.2: Discharge and recharge curve for a RT Li/FeS_2 cell. The capacity of the FeS_2 electrodes falls drastically on cycling to less than 20% of first cycle capacity after six cycles. The second discharge curve is shaped differently from the initial discharge curve indicating that the same intermediate is not regenerated after reaction with Li (taken from [15]).

Table 2.1

Sulfide Phases During Charging of $LiAl/FeS_2$ Cells Operated at 410°C Using Eutectic Electrolyte

Charge Potential *vs.* (α + β) LiAl	X-ray Findings		Metallographic Findings
	Major Phase	Minor Phase	
1.53	Li_2FeS_2	$LiK_6Fe_{24}S_{26}Cl$	Li_2FeS_2 and trace of $LiK_6Fe_{24}S_{26}Cl$
1.64	$\approx Li_7Fe_2S_6$ and Li_2FeS_2†	$Fe_{1-x}S$	Li_2FeS_2, $Fe_{1-x}S$ and $\approx Li_7Fe_2S_6$
1.72	$Li_3Fe_2S_4$	None detected	$Li_3Fe_2S_4$ only
1.79	$Li_3Fe_2S_4$	None detected	$Li_3Fe_2S_4$ and 5% $Fe_{1-x}S$
1.82	$Li_3Fe_2S_4$	FeS_2 and $Fe_{1-x}S$	Not examined
1.85	FeS_2	$Fe_{1-x}S$	FeS_2 and $Fe_{1-x}S$

†These phases had formed from a phase that was present at cell operating temperature but which decomposed upon cooling to room temperature.

amounts of Li. The Li composition was determined by AAS. From the open circuit voltage data shown in Figure (2.3), five domains were distinguished, with two corresponding to single phases and the rest being bi-phase. The single phases were distinguished by measuring the potential dependence on the value of x over the region of interest.

$$\lambda\text{-phase} \longrightarrow x < 0.02$$
$$\gamma\text{-phase} \longrightarrow 1.09 \leq x < 1.5$$
$$\nu\text{-phase} \longrightarrow 1.5 < x \leq 2$$

In a recent review, Clark [18] points out that given the results of Whittingham the use of data obtained by Brec and Dugast to interpret the FeS_2 mechanism is questionable since the materials studied by them were prepared by chemically or electrochemically **charging** Li_2FeS_2.

The work on high temperature $LiAl/FeS_2$ electrodes by Tomczuk *et al* [14] also contradicts the results of Brec and Dugast. The three Li-Fe-S phases reported by Brec and Dugast could not be detected in any of the FeS_2 electrodes studied. A number of distinct phases were found in the proposed ranges of compositions for the λ and ν-phases. As Tomczuk has pointed out, since no metallographic studies were done it is questionable whether the phases found by Brec and Dugast are indeed single phases.

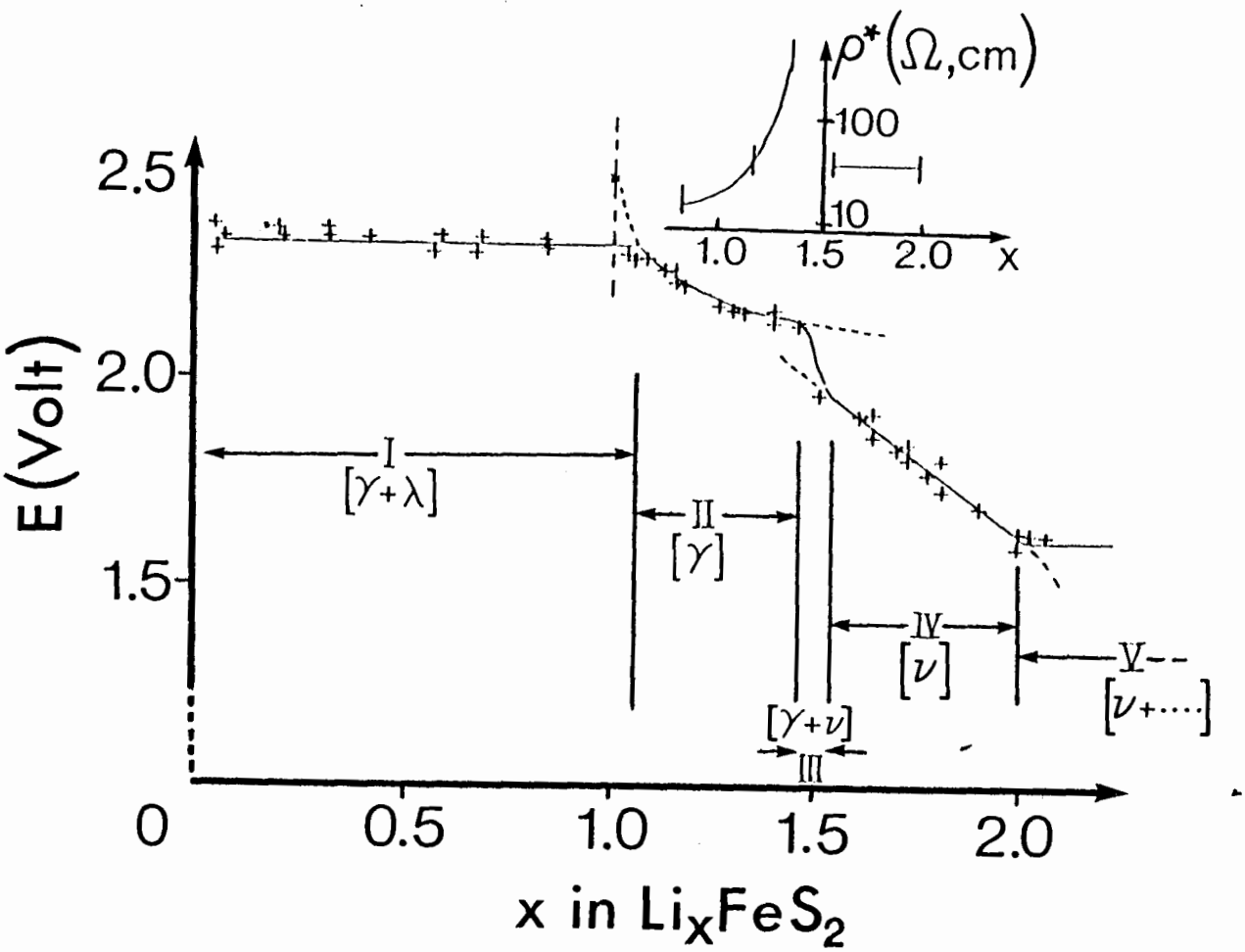

Fig. 2.3: Open circuit voltage curve for the electrochemical oxidation of Li_2FeS_2 (taken from [79]).

In a study carried out in 1982, Iwakura *et al* [19], used the techniques of Electron Spectroscopy for Chemical Analysis (ESCA), Scanning Electron Microscopy (SEM) and Ion Micro-probe Analysis (IMA) in studying the physico-chemical properties and morphology of FeS_2 cathodes. The electrolyte consisted of a 1 M solution of $LiClO_4$ in a 1:1 mixture of propylene carbonate and 1,2-dimethoxyethane. The authors measured OCV's and discharge times for synthesized and natural pyrites that had been pretreated by adsorption of various amounts of O_2 and H_2O. The results indicated that the OCV of Li/FeS_2 cells is determined by the reactions of O_2 and H_2O impurities in the electrolytes with Li, and that at first discharge, the cell voltage decreases as a result of the reactions (Fig. 2.4):

$$4Li + O_2 + 2H_2O \longrightarrow 4LiOH \quad (9)$$

$$4Li + O_2 \longrightarrow 2Li_2O \quad (10)$$

$$2Li + 2H_2O \longrightarrow 2LiOH + H_2 \quad (11)$$

ESCA measurements indicated that the Fe and S species are reduced upon discharge. Using IMA, the Fe and Li ion images showed that the FeS_2 particles are covered with Li during discharge, with the Li content decreasing toward the interior. Their proposed reaction scheme for the discharge of Li/FeS_2 cells in the voltage plateau region of discharge path was:

$$FeS_2 + 2Li \longrightarrow Li_2FeS_2 \quad (12)$$

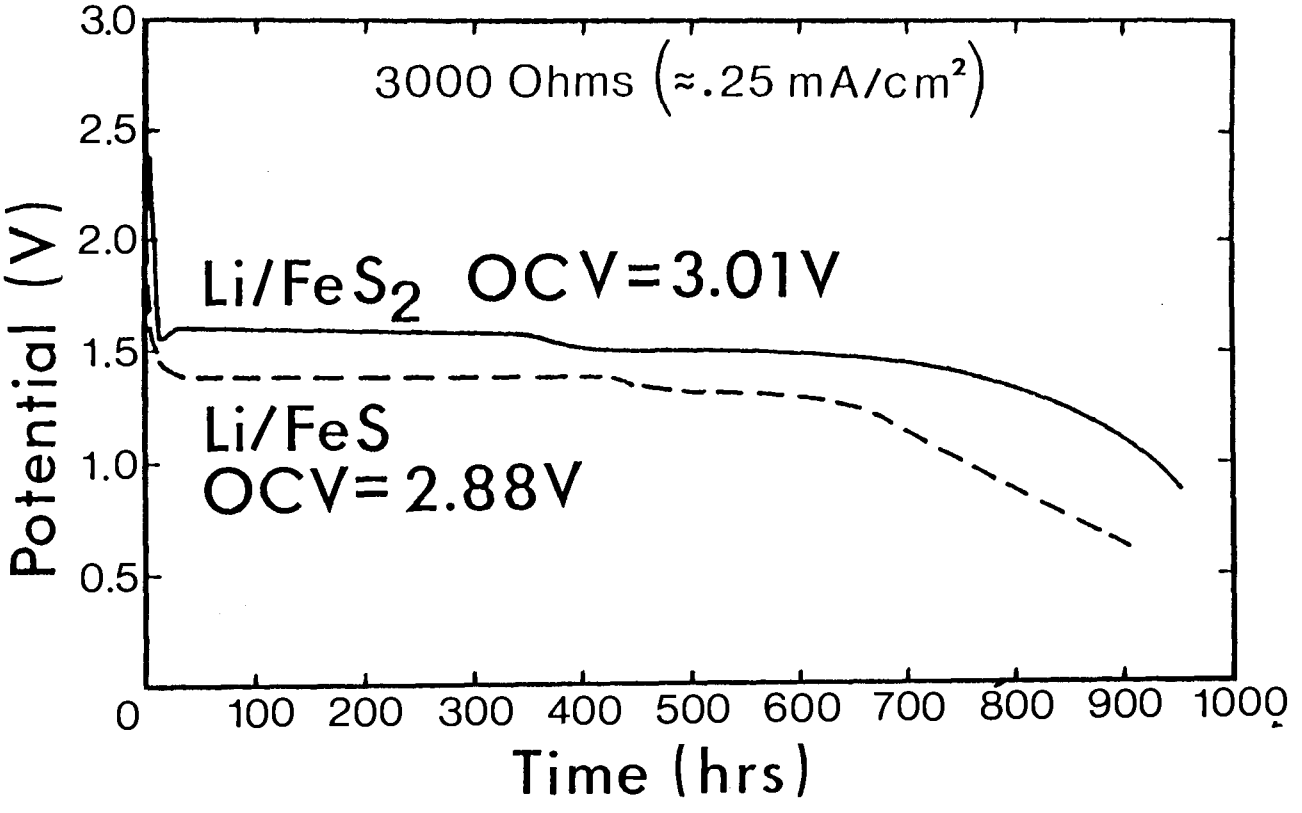

Fig. 2.4: Discharge curves for Li/FeS_2 and Li/FeS cells (taken from [79]).

$$Li_2FeS_2 + 2Li \longrightarrow 2Li_2S + Fe^{\circ} \qquad (13)$$

which is the same intermediate postulated earlier by Ikeda *et al* [20] from IMA and x-ray measurements.

Clark [18] and workers for Union Carbide, have also studied the discharge mechanism for the Li/FeS_2 cell. Using chemical means to determine the Li, Fe and S content in discharged and partially discharged cathodes, they compared their analytically derived compositions with the theoretical compositions based on the discharge mechanism:

$$FeS_2 + 2Li^+ + 2e^- \longrightarrow FeS + Li_2S \qquad (14)$$

$$FeS + 2Li^+ + 2e^- \longrightarrow Fe^{\circ}\ Li_2S \qquad (15)$$

Figure (2.5) displays their results showing the relative amounts of intermediates and products as a function of discharge. Large discrepancies, such as the amount of FeS supposedly formed, the observance of metallic Fe in early discharge, and the presence of unreacted FeS_2 at 80% discharge, suggest that this mechanism is unlikely. Better agreement between theoretical and actual data is achieved assuming a lithiated intermediate during discharge:

$$xe^- + xLi^+ + FeS_2 \xrightarrow{K_1} Li_xFeS_2 \qquad (16)$$

$$(4-x)e^- + (4-x)Li^+ + Li_xFeS_2 \xrightarrow{K_2} 2Li_2S + Fe^{\circ} \qquad (17)$$

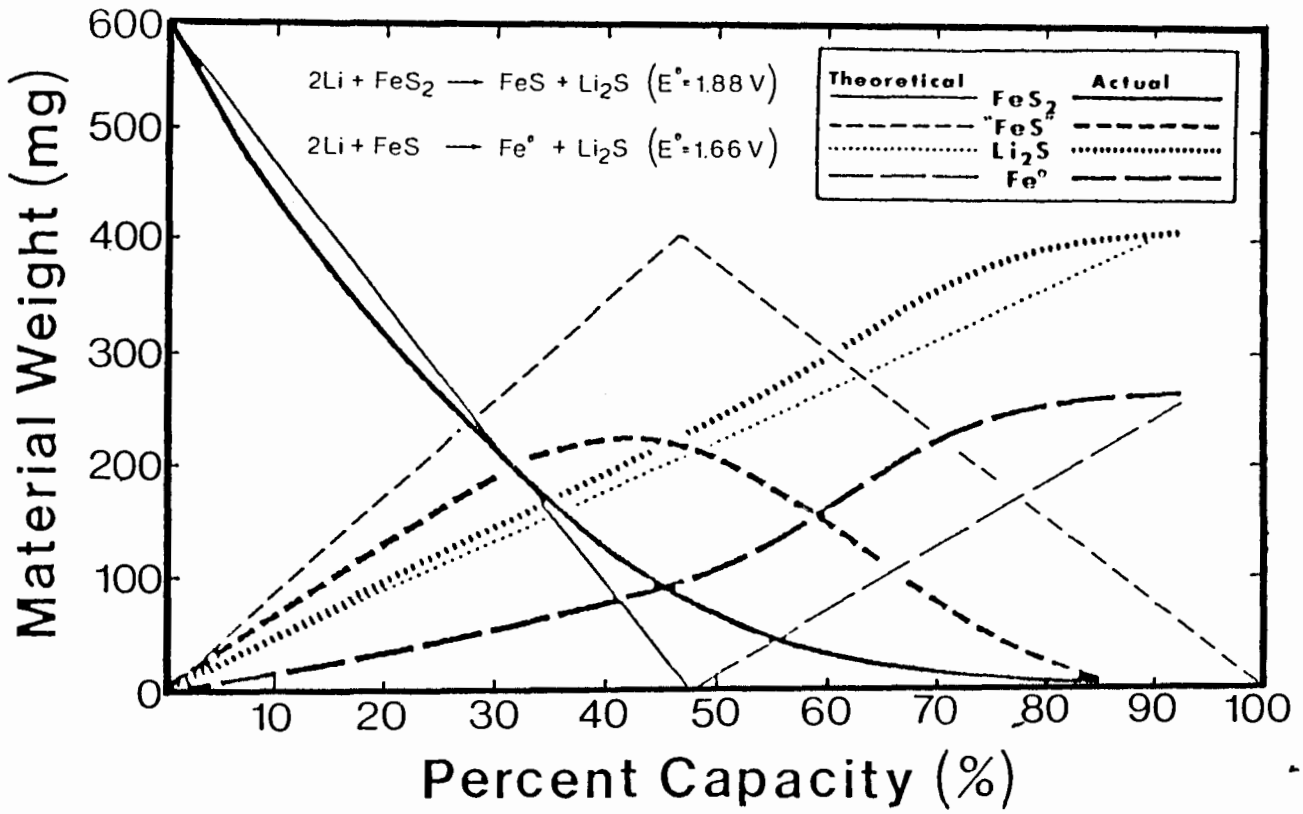

Fig. 2.5: Concentration curves for Li/FeS_2 cell reactants and products. The theoretical concentration curves were calculated using the mechanism based on eqs. (14,15) (taken from [79]).

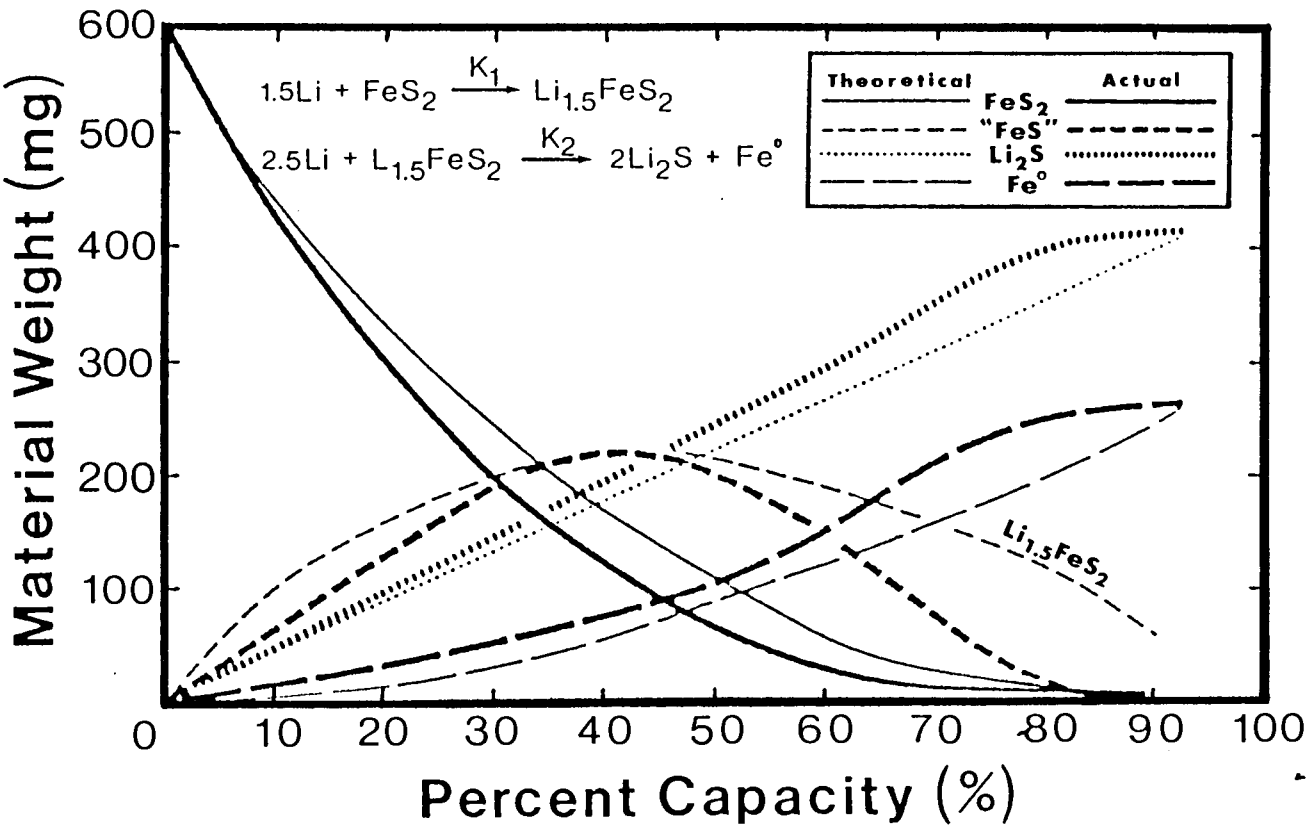

Fig. 2.6: Concentration curves for Li/FeS_2 cell reactants and products. The theoretical concentration curves were calculated using the mechanism based on eqs. (16,17) (taken from [79]).

The best fit to experimental data, shown in Figure (2.6), yields a value of x=1.5. However, this mechanism can not account for the discrepancies in the qualitative amount of Fe° found. Another proposed mechanism suggests the possibility of dual chemical and electrochemical reactions:

$$3FeS_2 + 6Li^+ + 6e^- \longrightarrow 2Li_2FeS_2 + Li_2S_2 + Fe^\circ \quad \text{(electrochemical)} \qquad (18)$$

$$Li_2S_2 + Fe^\circ \longrightarrow Li_2FeS_2 \quad \text{(chemical)} \qquad (19)$$

$$3Li_2FeS_2 + 6Li^+ + 6e^- \longrightarrow 3Fe^\circ + 6Li_2S \quad \text{(electrochemical)} \qquad (20)$$

A weakness of this proposed mechanism is that the calculated standard potential (E°) for the overall discharge of Li_2S_2 to Li_2S is too high to be acceptable. The true nature of the intermediate(s) is not completely understood at this time, but the idea of two competing steps is generally accepted.

Aker and coworkers [21] at Ray-O-Vac Corporation are currently studying the possibilities of an ambient temperature non-aqueous Li/FeS cell. The discharge curve for the Li/FeS system is similar to the Li/FeS_2 system in that it also has two plateau regions (Fig. 2.4). Such a pattern suggests a two-step discharge mechanism, and has led Aker *et al* to propose a lithiated FeS intermediate:

$$Li + FeS \longrightarrow LiFeS \qquad (21)$$

$$Li + LiFeS \longrightarrow Li_2S + Fe^\circ \qquad (22)$$

II.3c ^{57}Fe Mössbauer Studies of Cells

Another technique which appeared to hold out some promise in the study of the cathodes in Li/FeS_2 and Li/FeS cells was ^{57}Fe Mössbauer Spectroscopy.

Clark and coworkers [84] attempted to use ^{57}Fe Mössbauer spectroscopy in their study of the Li/FeS_2 cell system but with rather disappointing results and they did not pursue this avenue of investigation.

The present research was initiated as a joint collaboration between Moli Energy and Simon Fraser University. Preliminary work carried out by J.Aramini in 1983 at SFU suggested that ^{57}Fe Mössbauer spectroscopy could indeed provide useful information and hence the present investigation was launched. It was initially hoped that experiments could be carried out on the FeS_2 and FeS cathodes *in situ* and cells were specifically designed for this purpose. However it was later found that low temperature (4.2°K) experiments could provide much useful information and these experiments required removal of the cathodes from the cell.

III. ^{57}FE MÖSSBAUER OF MAGNETIC MICROCRYSTALS

III.1 Mössbauer Theory

In Mössbauer spectroscopy the interaction between an appropriate nucleus and its electronic environment is probed by carefully modulating the energy of the γ-ray emitted by a suitable source. The effect of this modulation is observed by determining the change in the transmission of the γ-radiation through the experimental sample of interest. A typical Mössbauer spectrum displays the intensity of the transmitted radiation as a function of modulation energy, expressed in Doppler energy units of mms^{-1}.

The ^{57}Fe nucleus is the most widely studied element in Mössbauer spectroscopy because it has several advantages over other Mössbauer active nuclei. The 14.4keV γ-ray emitted from the decay of ^{57}Co to ^{57}Fe (Fig. 3.1) following electron capture, has a very narrow energy distribution, or linewidth. The low energy of the γ-ray results in large percent resonant absorptions. This results in good spectral resolution even at room temperature. The precursor radioactive nuclide (^{57}Co) is inexpensive to make, and has a suitable half life of several months.

A number of parameters characteristic of the sample can be obtained from a spectrum. Among these are:

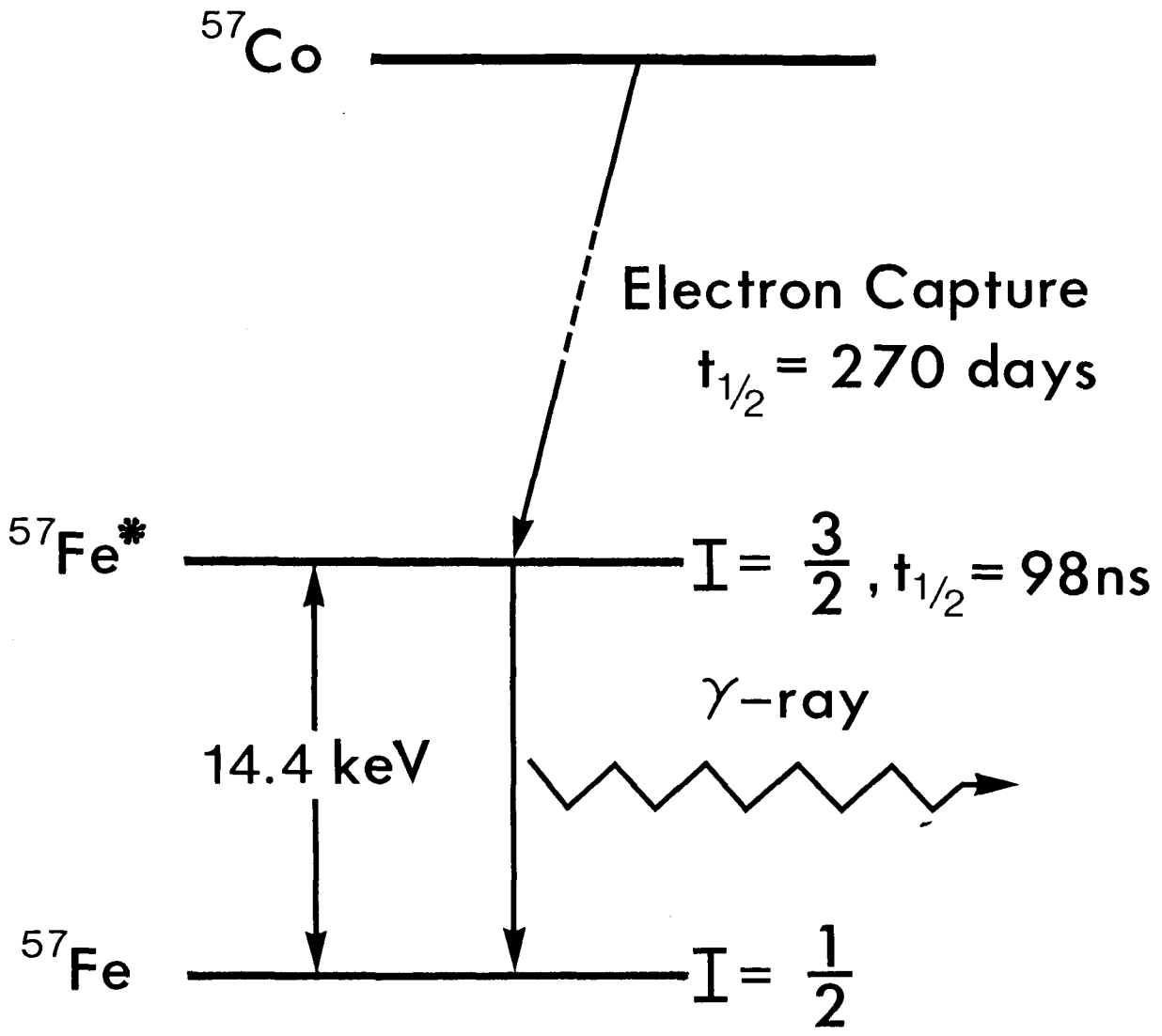

Fig. 3.1: Simplified energy level scheme showing the decay of radioactive ^{57}Co to excited state and then ground state ^{57}Fe.

1. Isomer shift (IS)
2. Quadrupole hyperfine interaction (QS)
3. Magnetic hyperfine interaction (hfs)
4. Area under the resonance curve

The area under a resonance curve can provide information about the recoil-free fraction, f and the relative number of chemically different atoms of the same element which are present. The recoil-free fraction is the probability that a γ-ray will be absorbed without recoil, and the temperature dependence of ln f can be used to extract lattice dynamical information from a series of Mössbauer experiments.

III.1a Isomer Shift

The IS arises from the coulombic interaction between the nucleus and the surrounding electrons, and from changes in the size of the nucleus during a γ-ray absorption. The experimental value for the IS can easily be found from a Mössbauer spectrum as the separation of the resonance line (or the centroid of a multiplet) from zero Doppler velocity. If the same source is used to look at various absorbers of a given Mössbauer nuclide, then the IS will be a linear function of the charge density at the nucleus of the absorber. For ^{57}Fe the IS decreases linearly with increasing s-electron density at the nucleus, so that an increase in the s-electron density will produce a shift of the resonance line to negative velocities. IS values are always

reported with respect to a standard absorber (α-Fe in the case of ^{57}Fe Mössbauer spectroscopy).

Contributions to the electron density from inner, core shell s-electrons remain constant with changes in chemical environment, so that only changes in valence shell orbital populations are important. The p, d, and f electrons, which have zero density at the nucleus, can still indirectly affect the electron density by screening the outer s-electrons. In the case of ^{57}Fe, the magnitude of IS is determined mainly by the occupation of the 3d and 4s states. The absolute value of the IS parameter can yield useful information about the formal oxidation state (ferrous or ferric ion) and the spin state (high or low spin).

III.1b Quadrupole Splitting

The QS parameter arises from the interaction between the nuclear quadrupole moment (Q) and the electric field gradient (EFG). The value of Q is a measure of the deviation from spherical symmetry of the nucleus and can vary for different states of excitation. Since Q is a constant for a Mössbauer nuclide in different compounds, under constant conditions, the quadrupole interaction energy will depend then on the EFG. The EFG is a tensor quantity that characterizes the asymmetric electric field due to an asymmetric charge distribution or ligand arrangement. Nuclei in states having a nuclear spin of

$I=0,\frac{1}{2}$ will have a zero quadrupole moment, so that only nuclei in states with $I>\frac{1}{2}$ can interact with an inhomogeneous electric field. Such an interaction will cause the nuclear state to be split into substates $|I,\pm m_I\rangle$, where $m_I=(I,I-1,.....-I)$ and is called the nuclear magnetic spin quantum number. These substates will have an energy E characterized by the magnitude of $|m_I|$, each being doubly degenerate. This degeneracy, however, can be removed by the influence of a magnetic field.

Figure (3.2a) illustrates how the first excited nuclear level ($I=\frac{3}{2}$) for a ^{57}Fe nuclide is split, while the ground state ($I=\frac{1}{2}$) is not. The QS parameter will be the energy difference between these substates, and is reflected in the difference between the positions of the two resonance peaks as shown in Figure (3.2b). The QS can provide information about the electronic structure, bond properties and molecular symmetry. The temperature dependence of the QS can provide a sensitive measure of both changes in bond angles and distances with temperature, and of the thermally driven population of various electronic sublevels of the Mössbauer active atom.

III.1c Magnetic Hyperfine Interactions

Nuclei with spin $I>0$ will have a magnetic dipole moment μ which can interact with a magnetic field H at the nucleus, be it an internal or an externally applied field. A nuclear Zeeman effect is observed in which each nuclear level is split into

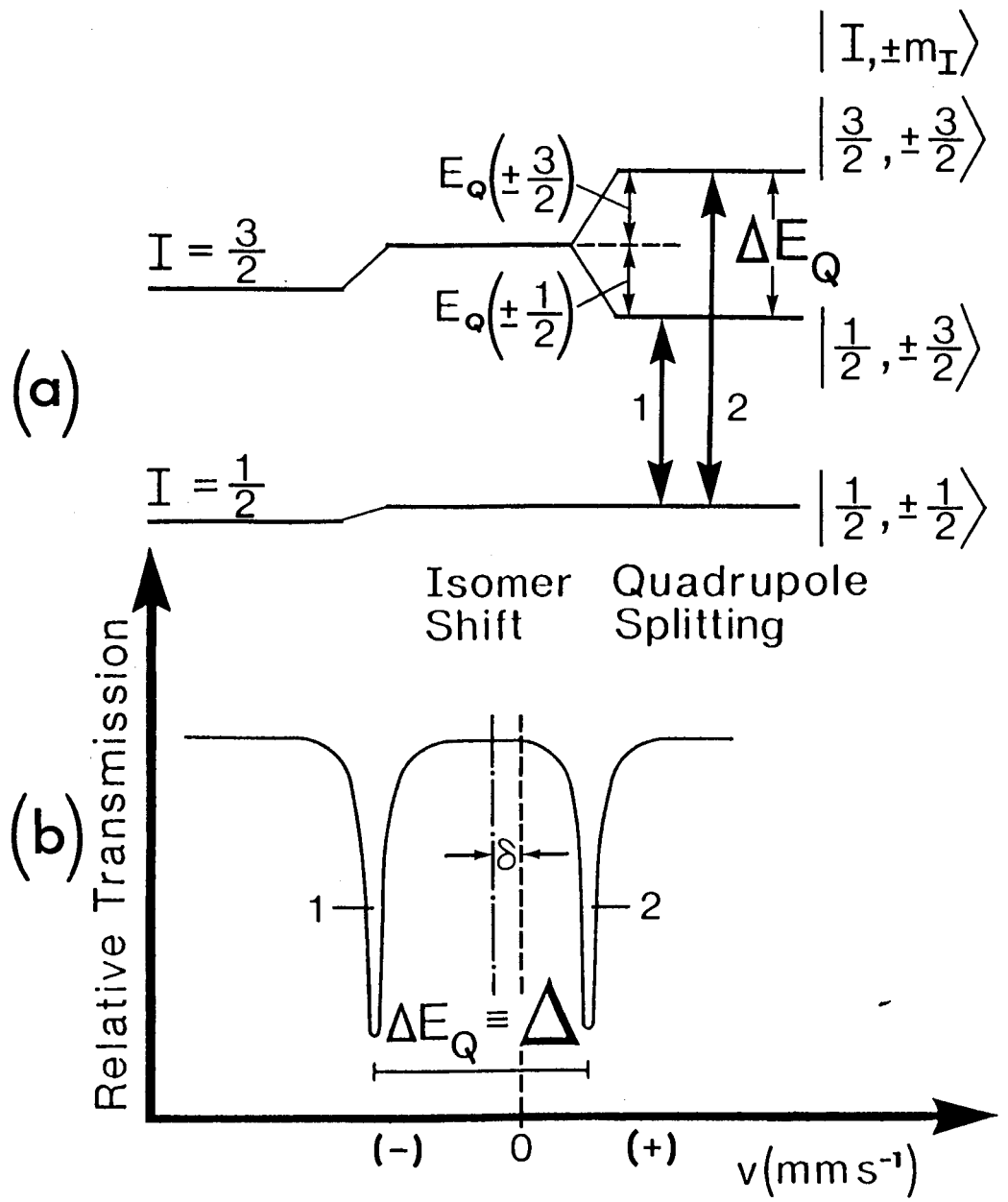

Fig. 3.2a: Quadrupole splitting for a nucleus with $I=\frac{3}{2}$ in the excited state. The electric quadrupole interaction splits the $I=\frac{3}{2}$ level into two sublevels.

Fig. 3.2b: Resultant theoretical Mössbauer absorption spectrum that would be produced by the two possible transitions between the ground state $|\frac{1}{2},\pm\frac{1}{2}\rangle$, and the two excited states ($|\frac{3}{2},\pm\frac{1}{2}\rangle$ and $|\frac{3}{2},\pm\frac{3}{2}\rangle$). The quadrupole splitting parameter Δ and the isomer shift δ are shown in the spectrum.

$2|I|+1$ lines. Only γ-ray transitions which obey the selection rules, $\Delta I=1$, $\Delta m_I=0,\pm1$ are allowed. The six possible transitions between $I=\frac{1}{2}$ and $I=\frac{3}{2}$ for ^{57}Fe are shown in Figure (3.3a). The intensities for each transition will differ since the relative transition probabilities vary according to the states involved. The intensity pattern 3:2:1:1:2:3 is characteristic of iron nuclei which possess an internal magnetic field. In most cases, the nuclear state is simultaneously perturbed by both magnetic dipole and electric quadrupole interactions. This results in unequal spacing between the sublevels of the excited state (Fig. 3.3b).

III.2 Superparamagnetism

Mössbauer spectroscopic studies of composite materials have in many cases revealed the presence of magnetic microcrystals. An understanding of these phenomena as well as their influence on Mössbauer spectra is essential in applications of Mössbauer spectroscopy in materials science. In addition to its sensitivity to relaxation effects, Mössbauer spectrosocopy has several other advantages in studies of microcrystalline samples, and it has therefore become an important technique for the study of magnetic microcrystals.

There exists in small particles of magnetically ordered material, a critical size below which the particle consists of a *single magnetic domain*. This is due to the fact that in a

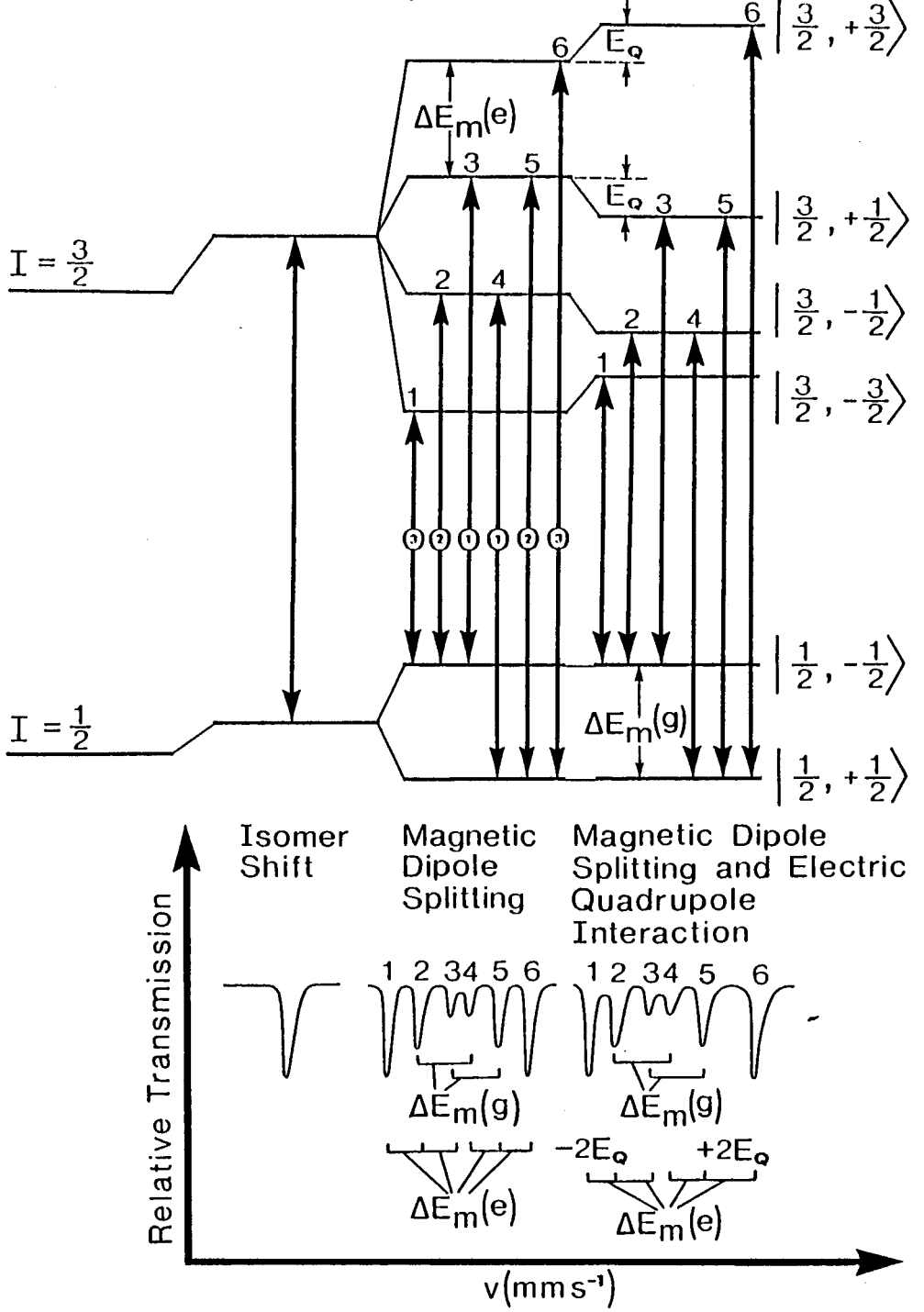

Fig. 3.3a: Magnetic dipole splitting with and without a **small** electric quadrupole perturbation ($V_{zz}>0$). For $V_{zz}<0$, the sublevels $|+\frac{3}{2}\rangle$, and $|-\frac{3}{2}\rangle$ are lowered while the $|+\frac{1}{2}\rangle$ and $|-\frac{1}{2}\rangle$ sublevels are raised.

Fig. 3.3b: The resultant theoretical Mössbauer absorption spectrum for the six possible transitions. The ground state splitting ($\Delta E_m(g)$) and the excited state splitting ($\Delta E_m(e)$) are shown.

particle smaller than the critical size, the increase in magnetic energy due to the formation of domain walls is larger than the energy loss obtained by splitting the particle into smaller magnetic domains.

The *exchange interaction* between neighbouring ions in the single domain particle results in the coupling of spins, which may result in ferromagnetism, ferrimagnetism, or antiferromagnetism depending on the relative orientation of the spins. The entire spin system can be rotated in space without changing the exchange energy providing the rotation is coherent (i.e. the relative orientation between spins is not changed).

Other interactions lead to a dependence of the total magnetic energy on the direction of the exchange-coupled spin system, such that certain directions will correspond to a minimum in the total magnetic energy. These low energy directions called the *easy directions*, are separated by *anisotropy energy barriers*. The magnitude of these energy barriers will be the sum of contributions due to interactions from the crystal lattice, shape, stress, magnetic moment and surface of the particle. Each interaction will have an associated anisotropy constant, with the sum being the *magnetic anisotropy constant*.

In the absence of an applied magnetic field the magnetization direction in large magnetically ordered crystals is along an easy direction. However, since the anisotropy energy

decreases with a decrease in particle size, for sufficiently small particles (<100Å) the thermal energy will be comparable to the anisotropy energy. The magnetization will then fluctuate randomly between the easy directions and such fluctuations are called *superparamagnetism*. There are also small fluctuations about any one of the easy directions and these are called *collective magnetic excitations*. The *blocking temperature* T_B is defined as the temperature below which the particle exhibits magnetic ordering. At T_B the height of the anisotropy energy barriers $E(T_B)$ will be comparable in magnitude to the thermal energy kT_B. This temperature is not uniquely defined but is related to the time scale of the experimental method. For most systems studied the magnetic anisotropy can be considered uniaxial with a total magnetic energy described by the expression:

$$E(\theta) = KV\sin^2\theta \qquad (23)$$

where K is the magnetic anisotropy constant, V is the volume of the particle, and θ is the angle between the magnetization direction and the easy direction. The two energy minima at $\theta=0$ and $\theta=\pi$ are separated by an anisotropy energy barrier equal to KV. The superparamagnetic relaxation frequency (τ^{-1}) is the rate at which the magnetization vector fluctuates between easy directions, and was first derived by Néel [22].

$$\tau = \tau_o \exp^{\{KV/kT\}} \qquad (24)$$

where τ_o is of the order of 10^{-10}-10^{-12}s, k is Boltzmann's constant, and T is the temperature. Later it was shown by Brown [23,24,25] that for a particle with uniaxial anisotropy energy and magnetic energy given by (23), the SP relaxation time for $KV/kT \geq 1$ was given by:

$$\tau \simeq \frac{M_S \pi^{\frac{1}{2}}}{K\gamma_o} \left[\frac{KV}{kT} \right]^{\frac{1}{2}} \exp\left[\frac{KV}{kT} \right] \qquad (25)$$

where M_S is the *saturation magnetization*, and γ_o is the gyromagnetic ratio of the electron.

III.3 Effect of Superparamagnetic Relaxation on Mössbauer Spectra

The time scale for the observation of magnetically split Mössbauer spectra is approximately given by the nuclear Larmor precession time, τ_L, of the nuclear magnetic moment. For ^{57}Fe Mössbauer spectroscopy a six line magnetic hyperfine spectrum will be observed when $\tau >> \tau_L$, and when $\tau << \tau_L$ then a paramagnetic spectrum is observed with one or two lines. In the intermediate range where $\tau \approx \tau_L$, complex spectra with broadened lines can be observed. In Mössbauer studies of magnetic microcrystals the blocking temperature T_B is often defined as

the temperature at which τ equals the nuclear Larmor precession time of the nucleus in its excited state. Wickman [26] calculated the theoretical ^{57}Fe Mössbauer spectra for a uniaxial particle at different relaxation times and found that the magnetic splitting is resolved when $\tau \gtrsim 2.5 \times 10^{-9}$s. This value can be used for an empirical definition of T_B.

Samples will usually contain a distribution of particle sizes and magnetic anisotropy constants. Since τ is sensitive to KV (eq. (24,25)) there will be a distribution in KV values, and hence a distribution in relaxation times resulting in line broadening. In many cases a small fraction of the particles will have relaxation times within the critical region (10^{-8}-10^{-9}s), so the spectra will be the sum of a magnetically split component and a paramagnetic component.

Mørup and Topsøe [27] have shown that collective magnetic excitations can influence Mössbauer spectra far below the T_B. Since the time scale for these fluctuations is shorter than the Mössbauer observation time (τ_L), the magnetic splitting of the Mössbauer spectrum is proportional to the average value of the hyperfine field:

$$H_{hf}(V,T) = H_{hf}(V=\infty,T)\ \langle\cos\theta\rangle_T \qquad (26)$$

where $H_{hf}(V=\infty,T)$ is the hfs of the bulk crystal (absence of collective magnetic excitations). The term $\langle\cos\theta\rangle_T$ is the thermal average of $\cos\theta$, the angle which the magnetization

vector makes with the easy direction. In the low temperature limit,

$$\langle \cos\theta \rangle_T \simeq 1 - kT/2KV \qquad (27)$$

Thus magnetic splitting in small particles will be lower than the magnetic splitting found in bulk crystals by a factor of kT/2KV.

For particles with three-dimensional magnetic anisotropy the magnetic energy is expressed as a function of the direction cosines u_x, u_y and u_z:

$$E = E(u_x, u_y, u_z) \qquad (28)$$

The easy directions can be defined as the z direction, and by choosing the x and y directions so that $(\partial^2 E/\partial u_x \partial u_y) = 0$, then for $KV/kT \geq 1$ [28]:

$$H_{hf}(V,T) \simeq H_{hf}(V=\infty,T)\left[1 - \frac{1}{2}kT\left\{\left[\frac{\partial^2 E}{\partial u_x^2}\right]_o^{-1} + \left[\frac{\partial^2 E}{\partial u_y^2}\right]_o^{-1}\right\}\right] \qquad (29)$$

Since the magnetic energy $E(u_x, u_y, u_z)$ is proportional to the volume V, eq. (29) can also be written as:

$$H_{hf}(V,T) = H_{hf}(V=\infty,T)\,[1 - kT/2\kappa V] \qquad (30)$$

where

$$\kappa = \left\{ \left[\frac{\partial^2 E}{\partial u_x^2} \right]^{-1} + \left[\frac{\partial^2 E}{\partial u_y^2} \right]^{-1} \right\}^{-1} V^{-1} \qquad (31)$$

III.4 Application of an External Magnetic Field

Mössbauer spectra of systems exhibiting superparamagnetism are very sensitive to magnetic fields above the blocking temperature T_B, and can be used to obtain the mean particle-size through studies with applied external magnetic fields. In the presence of an external magnetic field, B, applied along the symmetry axis, eq. (23) must include an energy term for the interaction of the magnetic moment of the particle with the applied magnetic field B,

$$E(\theta) = KV\sin^2\theta - B\mu\cos\theta \qquad (32)$$

where the magnetic moment μ of the particle is equal to the product of the saturation magnetization M_S, and the volume of the particle. If the applied field is large enough ($B \geq 2K/M_S$) then the magnetic energy will only have one minimum (Fig. 3.4). The magnetization can then be considered to be fixed in one of the easy directions, and this is the situation in large, magnetically ordered crystals.

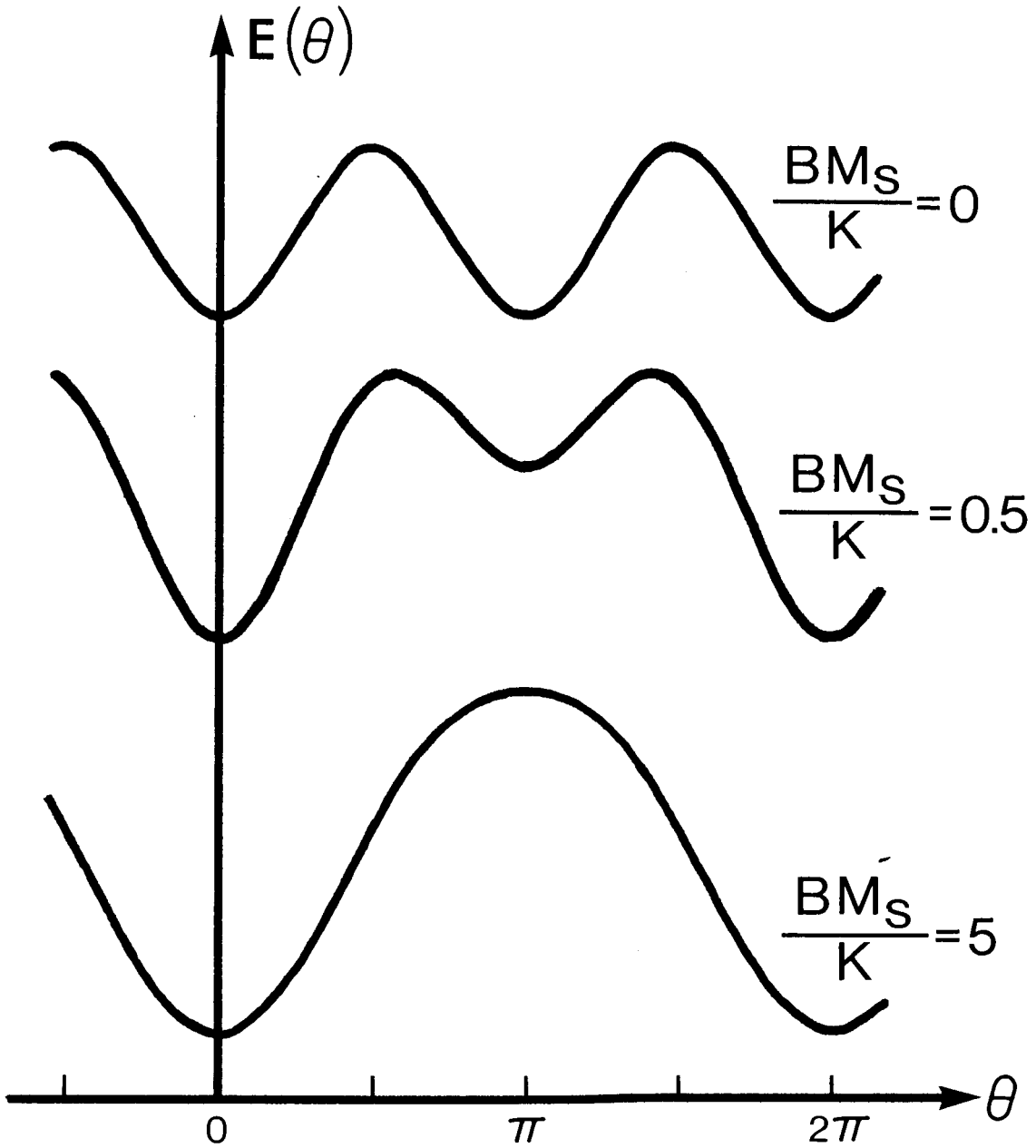

Fig. 3.4: Magnetic energy as given by eq. (32) for various values of $\frac{BM_S}{K}$ (taken from [56]).

The magnetization of a ferromagnetic microcrystal, averaged over a time that is large compared to the time scale of the fluctuations, is given by:

$$\langle M \rangle = M_S \frac{\int_0^{\pi} \exp\left[-\frac{E(\theta)}{kT}\right] \cos\theta \sin\theta \, d\theta}{\int_0^{\pi} \exp\left[-\frac{E(\theta)}{kT}\right] \sin\theta \, d\theta} \qquad (33)$$

When the effect of the anisotropy is negligible compared to the influence of the applied field, eq. (33) reduces to a classic Langevin function.

$$\langle M \rangle = M_S \, L\left[\frac{\mu B}{kT}\right] = M_S \coth\left[\frac{\mu B}{kT}\right] - M_S \frac{kT}{\mu B} \qquad (34)$$

The hyperfine field is proportional to $\langle M \rangle$ so that the observed magnetic splitting can be written:

$$H_{hf}(V,T,B) = B + H_{hf}(V=\infty,T) \, L\left[\frac{\mu B}{kT}\right] \qquad (35)$$

In the limit of low and high fields the Langevin function is

given by the simple expressions.

$$L\left[\frac{\mu B}{kT}\right] = \frac{\mu B}{kT} \qquad \frac{\mu B}{kT} << 1 \tag{36}$$

$$L\left[\frac{\mu B}{kT}\right] = 1 - \frac{kT}{\mu B} \qquad \frac{\mu B}{kT} >> 1 \tag{37}$$

The relative intensities of the Mössbauer lines depend on the direction of the magnetic field at the nucleus relative to the γ-ray direction. If the magnetic field is parallel or perpendicular to the γ-ray direction, the relative areas of the six lines of a ^{57}Fe spectrum are given by 3:0:1:1:0:3 and 3:4:1:1:4:3 respectively.

III.5 The Demagnetizing Field in Small Particles

In a ferromagnetic particle the arrangement of the atomic magnetic dipoles can result in uncompensated magnetic poles at the surface, and these create a *demagnetizing field*, H_D. This field adds to the magnetic hyperfine field at the Mössbauer nucleus, and it therefore contributes to the magnetic splitting of the Mössbauer spectrum. In multidomain, or large particles, the domain boundaries are arranged in such a way so as to minimize the total magnetic energy, and hence the demagnetizing field is negligible.

The contribution of the demagnetizing field to the splitting of the nuclear states, is significant for magnetic microcrystals. For single domain systems, the uncompensated poles at the particle surface will create a demagnetizing

$$H_D = - NM_S \qquad (38)$$

field in the interior of the particle. N is a demagnetizing coefficient which depends on the shape of the particle and the magnetization direction. For spherical particles, the demagnetizing coefficient would be equal to $\frac{4}{3}\pi$. The contribution of shape anisotropy to the anisotropy barrier is a direct result of the demagnetizing field, and is reflected by an increase or decrease in the magnetic splitting of the Mössbauer spectrum.

Knudsen and Mørup [29] have found the effects of the demagnetizing field is most noticeable when the magnetization direction is determined by other contributions to the magnetic anisotropy energy constant. In metallic iron the demagnetizing field increases the magnetic splitting of the Mössbauer spectrum because H_D and the hyperfine field are both antiparalell to the magnetization. As a result, the magnetic field acting at the nuclei in a spherical single-domain particle of α-Fe should be larger than the bulk value by $\simeq$7kG [29,30].

III.6 Surface Effects

Magnetism at surfaces and interfaces of 3d transition metals has received considerable experimental and theoretical interest in the past. The reduced symmetry and the lower coordination number at the surface or interface may induce new magnetic phenonema. Freeman and coworkers [31,32] have calculated spin-dependent energy dispersion, electronic density of states, and spin-densities for a 7-layer Fe (001) film. Their results predict an enhancement of the magnetic moment per Fe atom of ~32% at the **clean** Fe (001) surface as compared to the bulk. However it has been shown by Ohnishi *et al* [32] that contributions to H_{int} from polarized bulk conduction electrons (H_{ce}) are different at the free Fe (001) surface than the those in the bulk, since H_{ce} changes sign from negative in the interior to positive at the topmost surface layer. This results in a predicted **reduction** in the magnitude of $H_{int}(T\sim0)$ by ~32% (relative to the bulk) of the first layer Fe atoms of a clean Fe (001) surface. The total-spin-density map for a 7-layer Fe (001) film with a clean surface is shown in Figure (3.5). The positive spin-density extends far into the vacuum region (the wave function of the surface atoms becoming more atomic like) resulting in a large increase of the Fe moment at the surface. Covering the Fe (001) surface with Ag atoms results in an increased spin-density around the Fe atom, and a lower enhancement of ~11% is predicted for the magnetic moment of the interface Fe atom [33]. As the Ag atom restores the negative

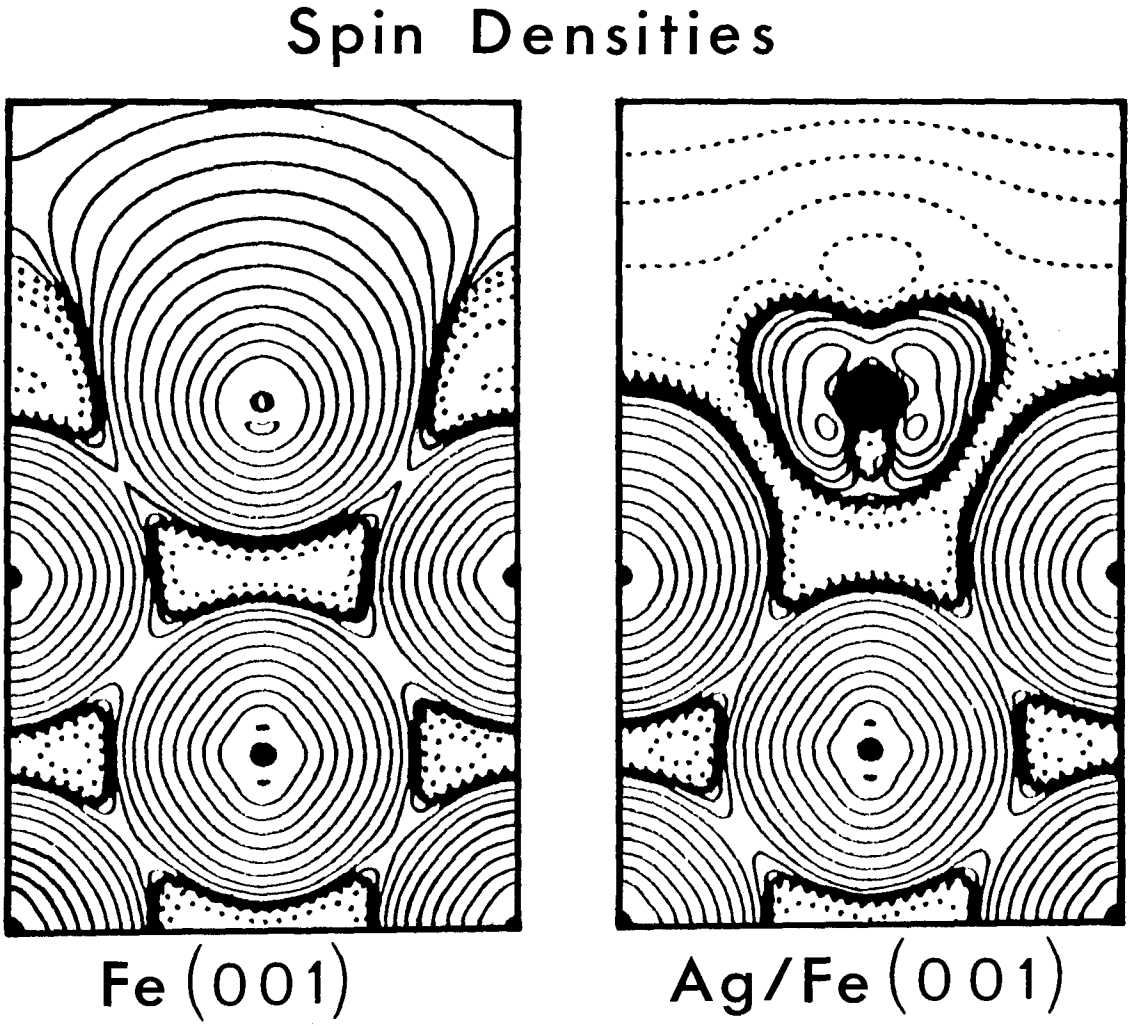

Fig. 3.5: Self-consistent spin-density map of seven-layer Fe (001) on the (110) plane. Full lines indicate positive spin density, while dashed lines indicate negative spin density. Left: clean Fe (001) surface. Right: Topmost Fe atom replaced by an Ag atom (taken from [33]).

valence contribution at the interface, a reduction of only ~7% is predicted for the H_{int} of the interface Fe atoms.

Most of the Mössbauer studies of surface magnetism have been made using thin films of α-Fe in UHV, and covered by different metallic or insulating materials. These effects have been reviewed by Shinjo [34], Topsøe *et al* [35], Walker [36], and Korecki [37]. As can be seen from Table (3.1,2), the magnitude of the surface hyperfine field depends on the nature of the covering material. In many of the film studies, the surface layer was prepared in such a way that all the surface atoms have identical environments. In small particles, however, a large number of different surface sites will exist, so a distribution in surface hyperfine fields is usually observed.

III.7 Mössbauer Studies of Superparamagnetism

Since the first observation of superparamagnetic relaxation using Mössbauer spectroscopy over 30 years ago [50], the technique of Mössbauer spectroscopy has been widely used in studies of superparamagnetism to give information on magnetic fluctuations, and thereby on magnetic anisotropy and particle size. Superparamagnetic behaviour has been observed in a variety of materials, ranging from biological systems [51] and corrosion products [52], to geological [53] and lunar samples [54]. A number of excellent reviews have been written and the interested reader is referred to these [55-58].

Table 3.1

Surface Magnetic Hyperfine Fields
Observed For Fe° Films at 4.2°K

Reference	Morphology	Surface Fe Environment	$\langle H_{surface} \rangle$[a]
Keune *et al* [38]	2-10Å thick Fe film	Fe/Cu interface	290kG
	18Å thick Fe film	Fe/Cu interface	306kG
Lauer *et al* [39]	105Å thick Fe film	Fe/Cu interface	290kG
Keune *et al* [38]	5Å thick Fe film	Fe/Ag interface	358kG
Owens *et al* [40]	60Å thick Fe film	Fe/Ag interface (2nd layer)	349kG
Korecki *et al* [41]	21 layer Fe (110) film	Fe/Ag interface	350kG
		(2nd layer)	347kG
		(3rd layer)	345kG
Hine *et al* [42]	8Å thick Fe (111) film	Fe/Sb interface	320kG
Stern *et al* [43]	50 layer Fe (110) film	Fe/MnF_2 interface (1st 2 layers)	369kG
		(1st 3 layers)	362kG
Droste *et al* [44]	50 layer Fe (110) film	Fe/MgF_2 interface (1st 2 layers)	358kG
	50 layer Fe (110) film	Fe/MgO interface (1st 2 layers)	330kG
		(1st 3 layers)	338kG
Shinjo *et al* [45]	SP 8Å thick Fe film	Fe/MgO interface	380kG

[a]Reported w.r.t α-Fe at RT.

Table 3.2

Surface Magnetic Hyperfine Fields
Observed For Fe° Particles at 4.2°K

Reference	Morphology	Surface Fe Environment	$\langle H_{surface} \rangle$[a]
Dormann *et al* [46]	15-200Å granular Fe in amorphous Al_2O_3 matrix	Fe/Al_2O_3 interface	370kG
	15-200Å granular Fe in amorphous ZrO_3 matrix	Fe/ZrO_2 interface	410kG
Dormann *et al* [47]	60-75Å granular Fe in amorphous SiO_2 matrix	Fe/SiO_2 interface	380kG
	60-75Å micro-crystalline Fe in amorphous SiO_2 matrix	Fe/SiO_2 interface	367kG
Furubayashi *et al* [48]	colloid of 20Å Fe with oil and amino radicals[b]	Fe/amino radical, oil interface	404kG
Ziethen *et al* [49]	13±2, 16±3Å microclusters in Faujasite-X zeolite	Fe/zeolite interface	380kG

[a]Reported w.r.t α-Fe at RT.

[b]Alkylnapthalene containing polybutenylsuccinopolyamine.

III.8 Particle Size Determination

Studies of superparamagnetic particles in the presence of applied magnetic fields can be very useful since particle-size information can be obtained directly. Above the blocking

temperature, magnetic saturation can be obtained in moderate magnetic fields even at room temperature (Fig. 3.6). According to eqs. (32,37) the hyperfine splitting of a superparamagnetic particle is restored for $\mu B/kT > 1$.

$$\left| H_{obs} - B_{appl} \right| \simeq H_{hf} \left[1 - \frac{kT}{\mu B_{appl}} \right] \qquad (39)$$

A plot of $\left|H_{obs} - B_{appl}\right|$ as a function of B_{appl}^{-1} should give a straight line with slope $H_{hf}(kT/\mu)$ and intercept H_{hf}. If the saturation magnetization is known (equal for example, to the value for the bulk compound), then the average particle volume can be obtained ($\mu=M_S V$). Such an approach for determination of the average particle volume has been used for samples of Fe_3O_4 [60], silica-supported Ni particles doped with ^{57}Co [61], amorphous frozen ferrofluids [62], carbon-supported α-Fe particles [63], and FeOOH particles found in ion exchange membranes [64].

If collective magnetic excitations are present in the particles studied, then the particle size can be approximated using eqs. (26,27):

$$\frac{\text{measured splitting}}{\text{bulk splitting}} \simeq 1 - \frac{kT}{2KV} \qquad (40)$$

This method of particle-size determination has been used by

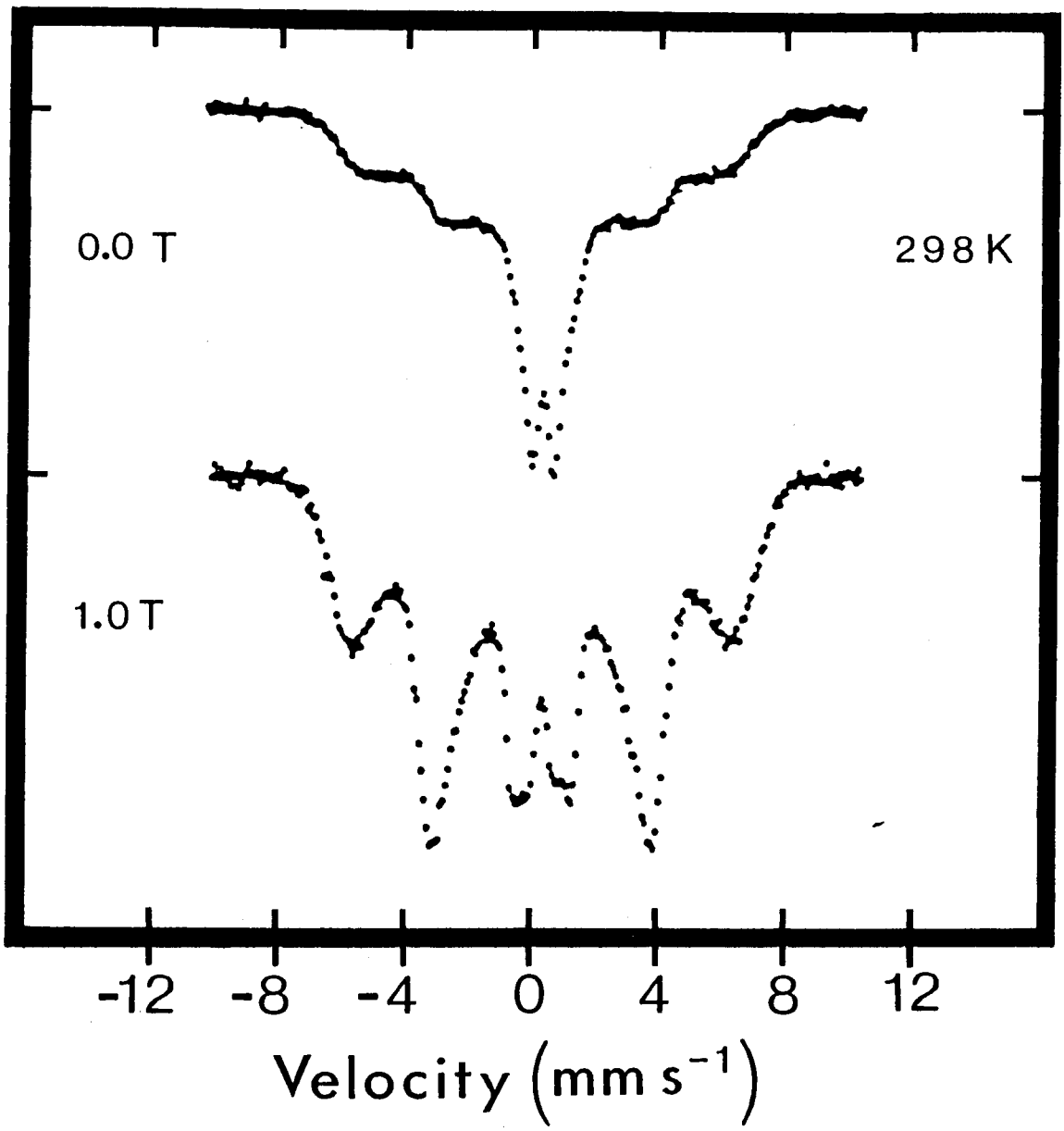

Fig. 3.6: Mössbauer spectra of synthetic feroxyhite (δ'-FeOOH) obtained at 298°K. The magnetic field was applied perpendicular to the γ-ray direction. (from [59])

Mørup and Topsøe [65,66] for MgO-supported and unsupported Fe_3O_4 particles, by Raupp and Delgass [67] for silica-supported Fe and NiFe catalysts, and by Phillips *et al* [68] for graphite-supported Fe particles.

The blocking temperature can be thought of as corresponding to that point at which the relaxation time due to fluctuations about the easy axis is equal to the nuclear Larmor precession time.

$$\tau_L = \frac{h}{\gamma_o \mu H_{obs,T_B}} = \tau_o \, e^{\{KV/kT_B\}} \qquad (41)$$

A value for T_B can be obtained experimentally by ^{57}Fe Mössbauer measurements at various temperatures, and is generally defined as the temperature at which the spectral area due to the superparamagnetic fraction is equal to the paramagnetic fraction. If a value for the magnetic anisotropy constant, K is available (from other experiments, or literature) then the average particle volume can be estimated. This of course is a crude estimate since the value of K itself is a function of many factors such as the nature of the particle-supported interface, and the actual particle volume. Johnson and Glasby [53] have estimated the average volume of FeOOH microcrystals found in geological samples from the ocean floor, and Dalton *et al* [69] also used this approach to determine the average size of Fe_2O_3 crystallites contained in high alumina cement.

Analysis of the lineshape using theoretical models and assumptions regarding values for K can yield mean values for particle-size distributions. Such analyses have been performed by a number of people with some success [68,70-74].

III.9 Superferromagnetism

If there is an exchange interaction between the micro-crystals (for example, if the particles are sufficiently close to each other), then in such a magnetically coupled system the nucleus will experience an additional hyperfine field. The two stable magnetic energy positions at $\theta=\pi$ and $\theta=0$ then have different energies. As a result, even in zero applied field, the magnetization relaxation frequencies between the two easy directions will not be equal ($\tau_+ \neq \tau_-$) and must be described by at least two dwell times. Magnetization fluctuations of such type have been named *superferromagnetism*. This concept was introduced independently by Mørup *et al* [75], and Rancourt *et al* [76] with different interpretations regarding the line broadening.

Brown [25] considered the situation of a small uniaxial ferromagnetic particle in the presence of an externally applied magnetic field B, applied along the uniaxial direction, and derived an expression for the relaxation time:

$$\left.\begin{matrix}\tau_{1\to 2}\\ \tau_{2\to 1}\end{matrix}\right\} \simeq A\,\alpha^{-\frac{1}{2}}\,(1-h_o^2)^{-1}\,(1\pm h_o)^{-1}\exp\left\{\alpha(1\pm h_o)^2\right\} \quad (42)$$

where $h_o=H_{eff}M_S/2K$, $\alpha=KV/kT$, and $A=M_S\pi^{\frac{1}{2}}/K\gamma_o$. The effective field H_{eff} will be the sum of any external applied field and fields from other contributions (e.g. interaction between particles, particle and support, stress and shape anisotropy, etc.), and for $h_o=0$, eq. (42) reduces to (25). The high-energy barrier approximation (37) is valid when $KV/kT>>1$, and $h_o<1$. According to Brown, the blocking temperature will be the temperature at which $\tau_+ \approx \tau_-$, and for ^{57}Fe Mössbauer, this occurs when the lines corresponding to the transitions $\pm\frac{3}{2} \to \pm\frac{1}{2}$ (lines 1 and 6) disappear.

Rancourt *et al* [76,77] defines a "Mössbauer window" to be a range of relaxation times $10^{-1}\tau_m \gtrsim \tau_{window} \gtrsim 10^{-3}\tau_m$, where τ_m is the Mössbauer measurement time ($\tau_m \sim 2 \times 10^{-8}$s), and is related to the lifetime of the $I=\frac{3}{2}$ nuclear spin state. At low temperatures ($\tau_\pm >> \tau_m$), the magnetization vector will be effectively stopped during the Mössbauer measurement time, and magnetic splitting is observed with a reduction in the hyperfine field.

$$H_{obs} = \frac{(\tau_+ - \tau_-)}{(\tau_+ + \tau_-)} H_{bulk} \quad (43)$$

At higher temperatures ($\tau_\pm << \tau_m$), a single line or a doublet will be observed due to the onset of fast superferromagnetic relaxation. It is still possible to see a hyperfine field at

these temperatures if the ratio τ_-/τ_+, is sufficiently different than 1. When the relaxation times fall within the Mössbauer window ($\tau_\pm \sim \tau_m$), then transitional type of spectra are observed. As pointed out by Rancourt, many authors have mistaken these transitional type of Mössbauer spectra at T_m as corresponding to the region of T_B. Calculations have shown that depending on the value of A, T_m can be quite a small fraction of T_B [76]. Using this model, Rancourt *et al* [77] were the first to determine the effective anisotropy field (h_o) for intra-zeolitic α-Fe_2O_3 particles.

Mørup [74], using a modified Weiss mean-field theory for interacting particles, obtained an expression for the observed hyperfine field as a function of temperature.

$$\langle H_{obs}(T)\rangle = H_{bulk}(T)\, L\left\{ \frac{3T_p}{T}\left[\frac{H_{bulk}(T)}{H_{bulk}(T_p)} \right]^2 \frac{\langle H_{obs}(T)\rangle}{H_{bulk}(T)} \right\} \quad (44)$$

The transition temperature T_p is the state at which $\langle M\rangle \to 0$, and is analagous to T_m in Rancourt's interpretation. Fits based on eq. (44) for the temperature dependence of the average magnetic hyperfine field of α-FeOOH particles, show a remarkable agreement with experimental results [75].

Mørup *et al* [78] have shown that for a system of magnetically interacting SP particles in the presence of an externally applied magnetic B field, the normalized hyperfine

field ($b(T,B) = (H_{obs})/H_{bulk}$) can be described by:

$$b(T,B) = 1 - \frac{kT}{\mu(T)[B + B_i(T,B)]} \qquad (45)$$

where $B_i(T,B)$ is the effective contribution from neighbouring interacting particles to the total internal hyperfine field of the particle. The magnetic coupling may be estimated from the field dependence of the magnetic hyperfine splitting above T_p if the magnetic anisotropy is negligible. This can be done by simply rewriting eq. (45).

$$[1 - b(T,B)]^{-1} = \frac{\mu(T)}{kT}[B + B_i(T,B)] \qquad (46)$$

A plot of $[1 - b(T,B)]^{-1}$ as a function of applied magnetic field B, will result in a straight line with slope $\mu(T)/kT$ allowing an estimate of the mean particle volume. The magnetic coupling can be calculated from the y-intercept $\mu(T)B_i(T,B)/kT$.

IV. ^{57}FE MÖSSBAUER SPECTROSCOPY OF THE LI/FES AND LI/FES_2 BATTERY SYSTEMS

^{57}Fe Mössbauer spectroscopy has the advantage that it is a non-destructive technique. Thus an *in situ* study of iron sulfide cathodes during discharge would in principle yield information concerning the change in the environment of the iron atoms with the extent of lithiation during battery discharge. The battery cells supplied by MoLi Energy shown in Figure (4.1), were specially designed so that such a study can be carried out.

IV.1 Previous Studies of Battery Cells Using Mössbauer Spectroscopy

The concept of Mössbauer spectroscopy as an analytical tool for battery research is not a new one, and has been applied before in the past. It has been used as early as 1974, when Kennedy and Sammells [79] used ^{57}Fe Mössbauer to study the reduction process in $Na|\beta\text{-alumina}|Na_2O\cdot 11(Fe_xAl_{2-x}O_3)$ cathodes where $0.9 < x < 1.2$. Later, Melendres and Tani [80] (ANL) obtained ^{57}Fe Mössbauer measurements of some solid state preparations of compounds which were previously found in discharged cathodes of high temperature Li/FeS_2 cells. This technique was also applied by Jacobson and McCandlish in 1979 [81], in an *in situ* study of the Li_xKFeS_2 ($0 \leq x \leq 1$) system, and in the following year by Eibschutz [82] (Bell Laboratories), to study Li/VS_2 cathodes. In this study, some Fe was substituted

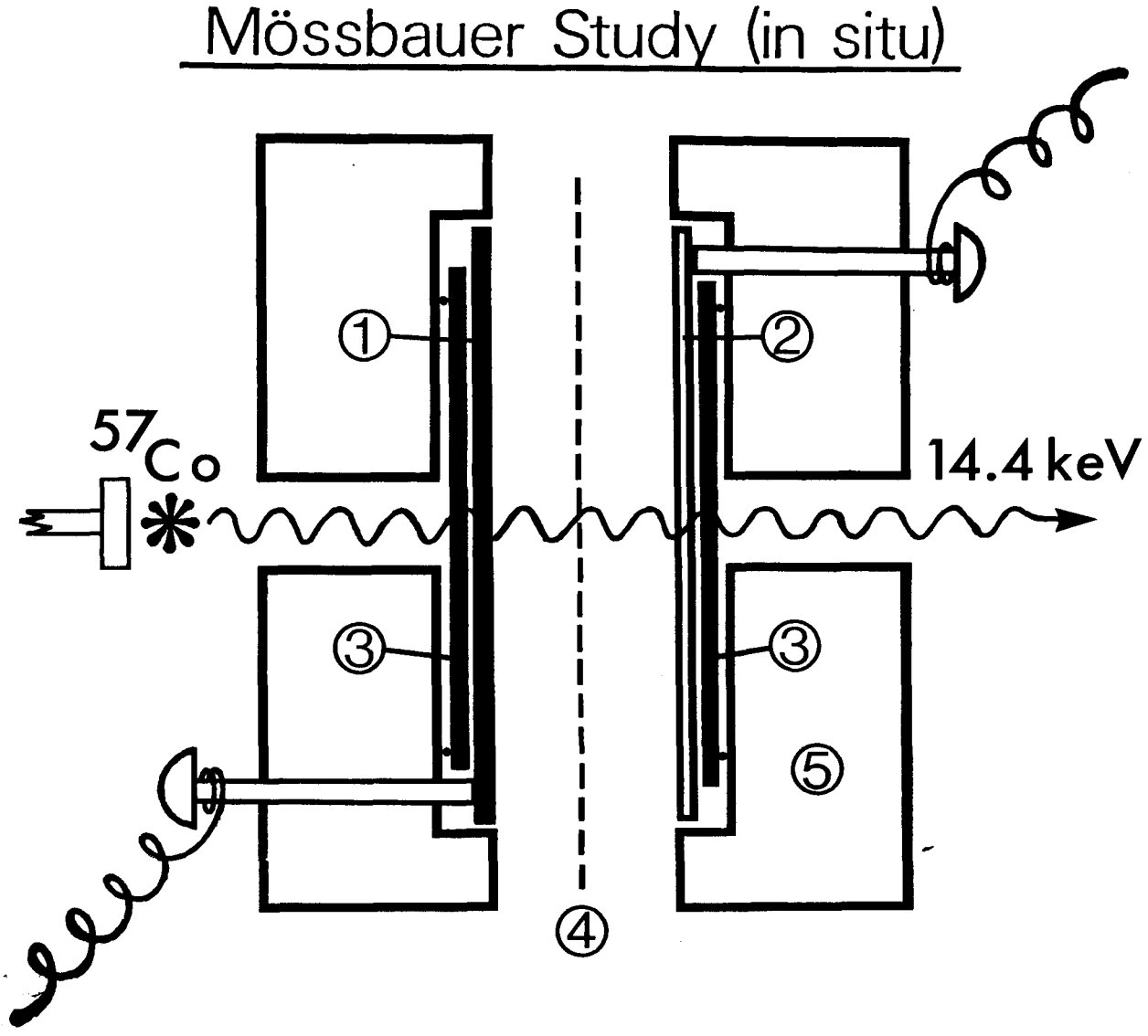

Fig. 4.1: Cross-section of a Li/FeS_2 cell designed for *in situ* ^{57}Fe Mössbauer experiments. (1) FeS_2 cathode pressure-wetted with $LiAsF_6$-PC or $LiClO_4$-PC electrolyte, on Al foil (2) Li metal anode (3) Be metal (low Z window) (4) Polypropylene separator (5) Polypropylene casing.

for V, and thus used as a probe to give indirect information about the valence state of V as a function of discharge. In a recent study, Morzilli and Scrosati [83] report the use of Mössbauer spectroscopy for studying Li$\left|LiClO_4\text{-}PC\right|Fe_2O_3$ cells. The Mössbauer spectra obtained for the cathode at various stages of discharge were quite helpful in clarifying the discharge mechanism.

IV.2 S.F.U. Research on Li/FeS and Li/FeS_2 Batteries

Preliminary investigations on the Li/FeS_2 cell used in this study, were first carried out by Dr. C.H.W.Jones, Dr. D.Sharma, and J.Aramini in the summer of 1983. The RT ^{57}Fe Mössbauer spectra was measured *in situ*, for a cell at various stages of discharge and recharge. A very broad absorption peak at near-zero velocity appeared in the spectra at early stages of discharge and in all the spectra for the duration of discharge. A phase exhibiting magnetic hfs appeared in the last 25% of discharge (Fig 4.2) with broad peak positions similar to that of elemental iron. During recharge of the cell, the presence of Fe° in the spectra decreased with rechargement, while the broad singlet remained in the spectra up to **full** recharge. It was concluded from the study, that ^{57}Fe Mössbauer could be used as a feasible monitor of phase changes occuring in the cathode during discharge, although low temperature measurements would be required in order to identify all the components in the cathode.

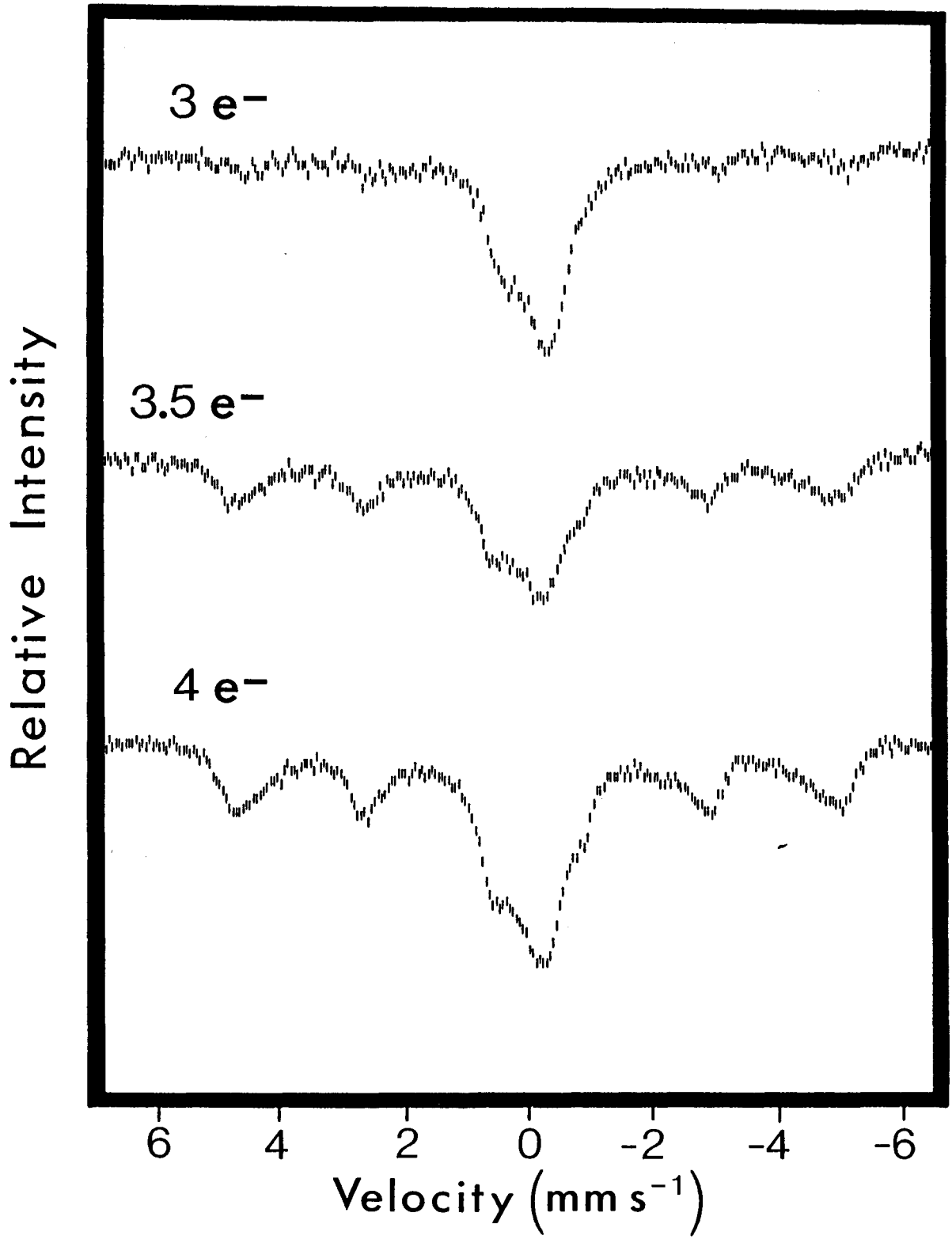

Fig. 4.2: *In situ* RT ^{57}Fe Mössbauer spectra of Li|$LiAsF_6$-PC|FeS_2 cell between stages of 75% and full discharge.

A similar observation has been reported by Clark and coworkers [84], who also tried using ^{57}Fe Mössbauer spectroscopy to determine the presence of metallic iron. They did note the change in the Mössbauer spectra of unreacted FeS_2 as the cathode became fully discharged, as was observed by the S.F.U. group, but could not detect any magnetic hyperfine structure. As a result, they felt that the technique was not a viable one, and did not pursue the use of Mössbauer spectroscopy any further. The presence of an appreciable amount of FeS_2 in their RT spectra for a cathode discharged to 75% of full discharge (Fig. 4.3) would indicate poor cell utilization.

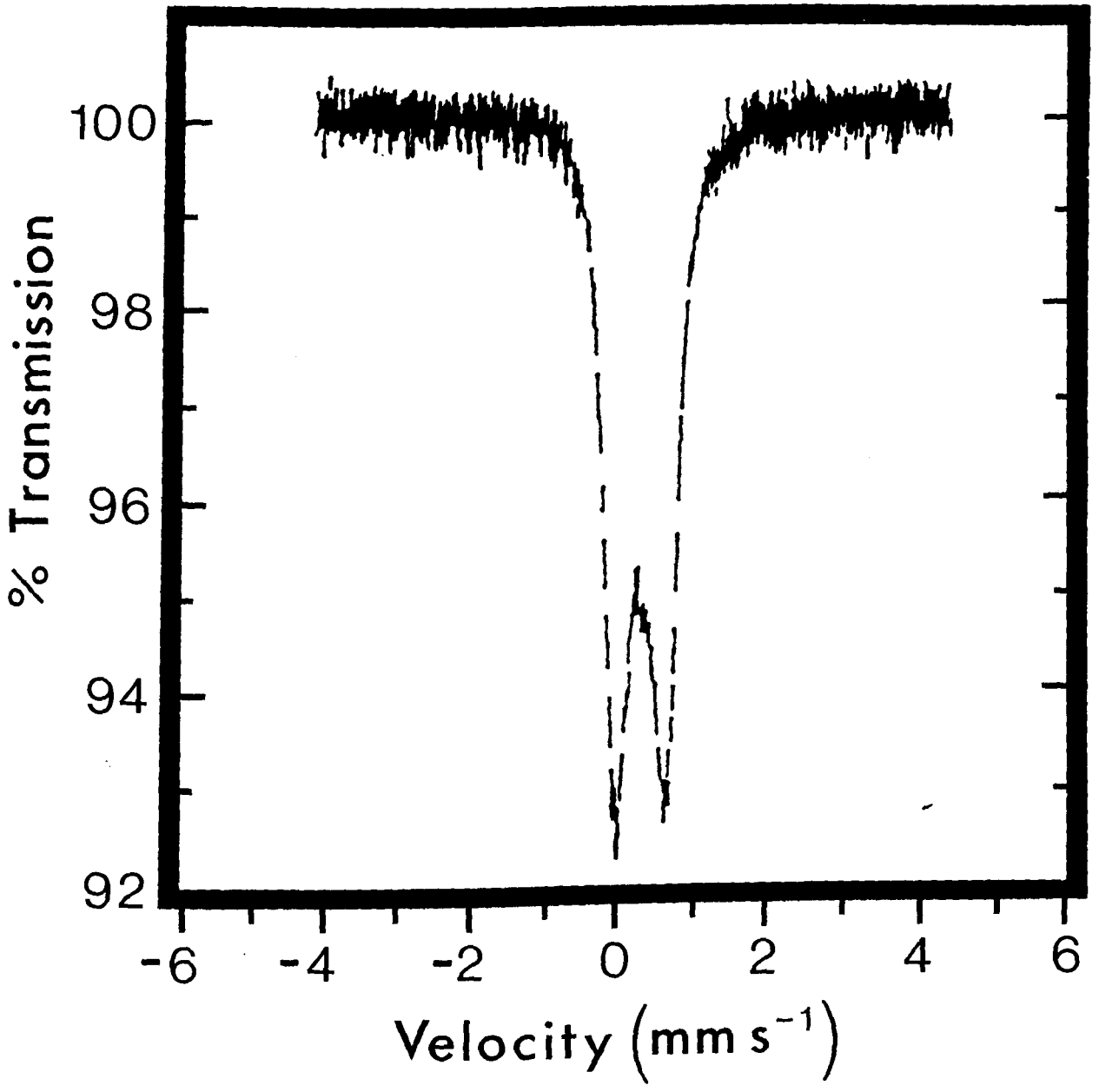

Fig. 4.3: RT ^{57}Fe Mössbauer spectrum of a FeS_2 cathode removed from a cell that was discharged to 75% of full discharge (taken from [84]).

V. EXPERIMENTAL

V.1 Mössbauer Spectroscopy

The schematic diagram for the Mössbauer experimental arrangement is shown in Figure (5.1). All Mössbauer equipment used for the duration of the study had been obtained from the Harwell Mössbauer group. The MWG 200 Waveform Generator simultaneously sends pulses to operate the multi-channel analyzer while providing a waveform to drive the servo-amplifier. The MSA 200 Servo-amplifier is an amplifier designed to suit the Vibrator MV 200. The output from the velocity transducer in the MV 200 is compared with a suitably attenuated signal from the waveform generator, and the amplified difference used to drive the vibrator. The waveform consists of a linear ramp, during which the vibrator executes a constant acceleration motion. Positive velocities correspond to the source moving towards the absorber.

The 14.4 keV γ-ray signals were detected using a Kr/CO_2 proportional counter (Reuter Stokes RSG-61 and RSG-61-M1) powered by a Fluke 413C dc supply. The detector signals were then fed through a Canberra 1406A preamplifier, amplified and shaped by an Ortec 440A amplifier and selected by an Ortec 406A timing single-channel analyzer (SCA). The drive and counting electronics were interfaced with the multi-channel analyzer (Nuclear Data 66 and 510). Data was collected in 256 channels of

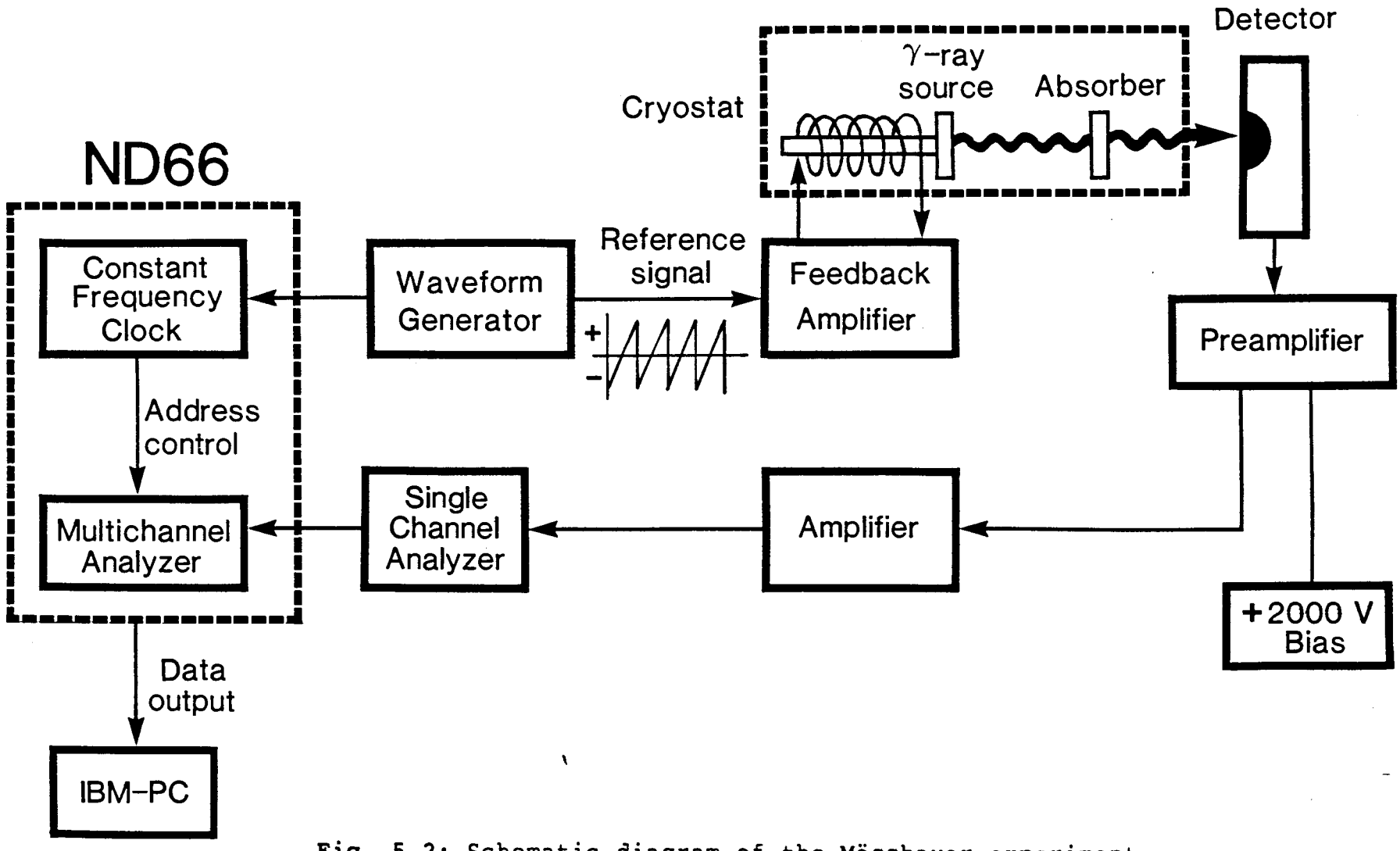

Fig. 5.2: Schematic diagram of the Mössbauer experiment.

the 4096 channels available in the MCA. An IBM PC which was interfaced with the MCA facilitated data manipulation and storage.

Throughout the duration of the experiments, sources of varying strength were used. The initial ^{57}Fe Mössbauer spectra were recorded using a 6.2 mCi ^{57}Co source. Later spectra were recorded using a 22.0 mCi and then a 27.4 mCi ^{57}Co source. All sources were diffused into 0.006 mm Rhodium foils, and were produced by the New England Nuclear Corporation.

The absorber sample thicknesses ranged from 32 to 48 mg cm^{-2}. Samples were sealed in teflon holders under an inert atmosphere and all openings on the sample holders were masked with vacuum grease. The sample holder was then wrapped in paraffin film, and covered with masking tape. A teflon holder employing an oil ring seal design was used in later experiments.

Low temperature ^{57}Fe Mössbauer measurements were carried out at 77.4K and 4.2K in a liquid helium cryostat (Harwell MHC 200). The PVC outer jacket of the cryostat (Fig. 5.2 and 5.3) was later replaced by a one-piece stainless steel jacket designed in our laboratory. The boil-off of the liquid He was sufficiently low, so that a single three litre filling would last three days.

A Varian V-3800 electromagnet was used for ^{57}Fe Mössbauer measurements in an external magnetic field. The homogeneity of the field across the $3\frac{1}{2}$" pole gap was better than 0.05%, and B values as high as 1.6T could be achieved. The externally applied

The figure shows an exploded section of the cryostat, which seals as follows:–
The N_2 Tank Assembly and the Lower Shell are sealed to the Outer Shell with "O" Rings.

The He Tank Assembly is sealed to the N_2 Tank Assembly by a piston "O" Ring Seal.

The He Tank Assembly and the N_2 Tank Assembly have a greased metal to metal contact.

The N_2 Tank Assembly, Outer Shield and Lower Shield have greased metal to metal contacts and are screwed together with twelve screws.

Insulation
The He Tank Assembly is super insulated on the outside with aluminized mylar.

The N_2 Tank Assembly and Shields are super insulated on the outside with Aluminium foil.

Windows
Mylar windows are fitted to He Tank Assembly and Lower Shell.

The Lower Shield has a greased-on aluminium foil window.

Vibration Suppression
Both the He Tank Assembly and N_2 Tank Assembly are braced to each other and also to the Outer Shell with a network of cotton threads to suppress vibration.

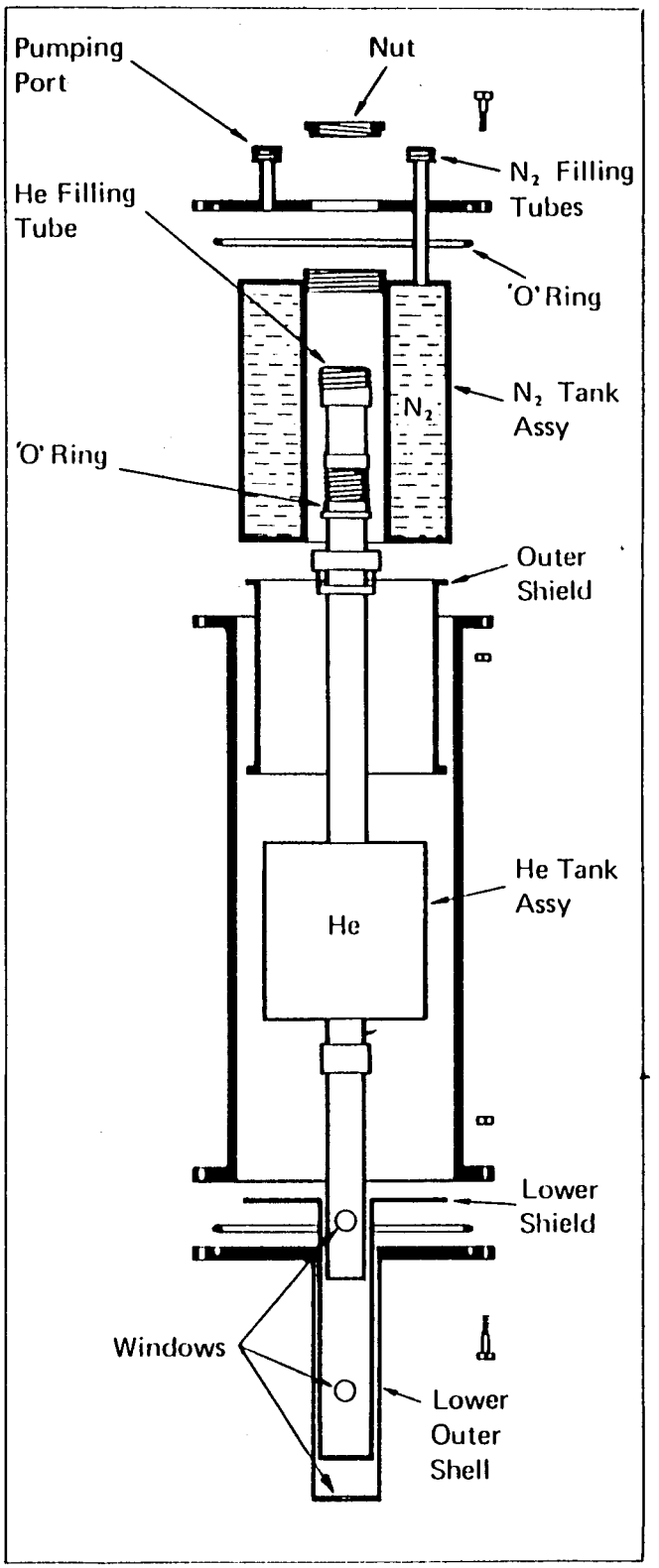

Fig. 5.2: Exploded section of the Harwell MHC 200 cryostat.

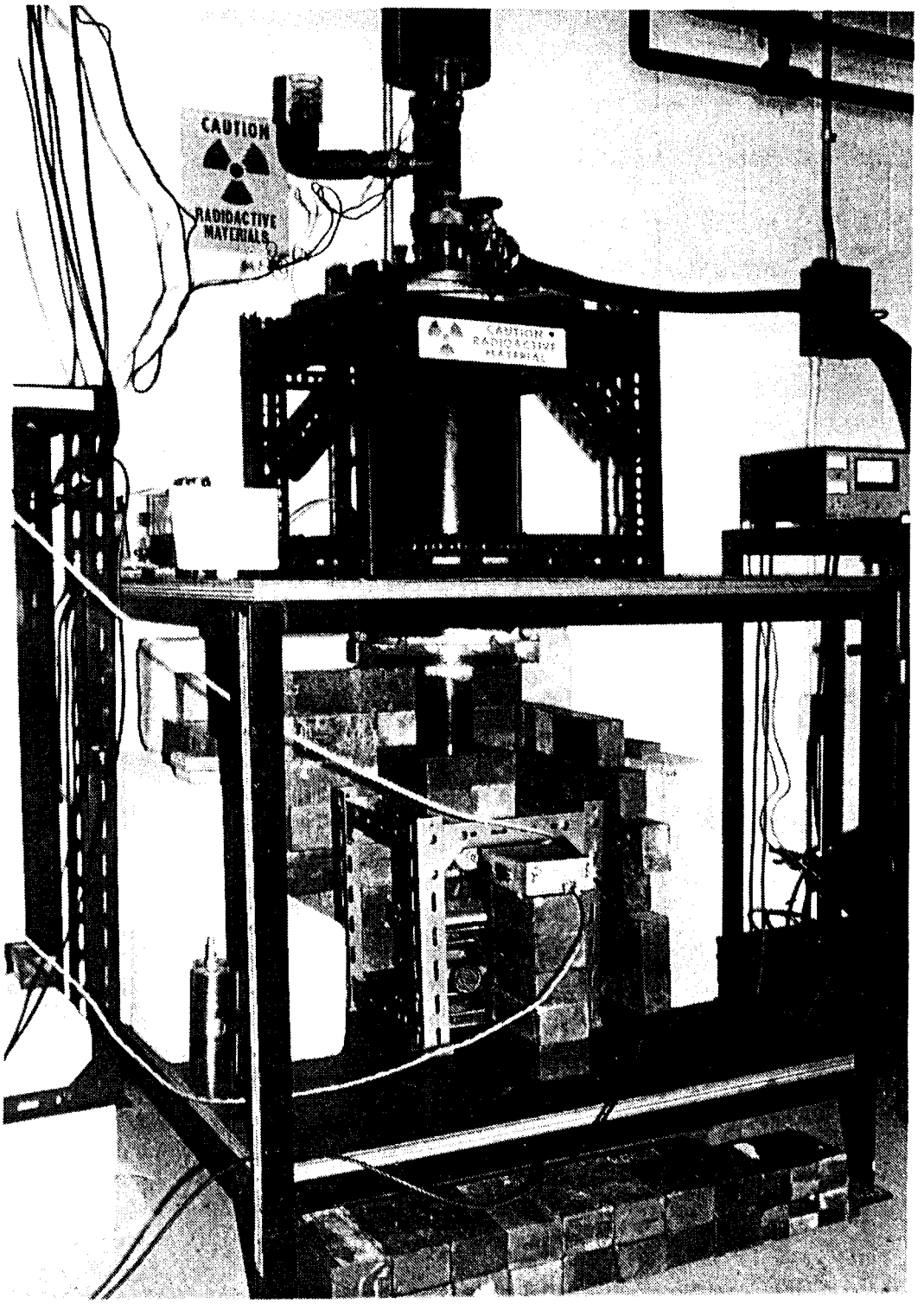

Fig. 5.3: Experimental arrangement for low temperature Mössbauer showing the transducer mounted in cryostat.

field was perpendicular to the direction of the γ-rays, and field values were measured using an nmr system. A small electromagnet with adjustable pole gap was also used to apply moderate magnetic fields in some of the experiments. The field values were measured using a gaussmeter.

V.2 Iron Pyrite Lithiation

Lithiation of iron pyrite was achieved by adding an appropriate amount of n-butyl lithium in hexane to a sample of FeS_2 (<40μm mesh pyrite), or FeS in a Schlenck tube, and stirring for several days at 25°C under purified dry Argon [85]. The supernatant solution was removed and analyzed for unreacted n-BuLi by either the Gilman double titration procedure [86], or by titration using a 1,3-diphenylacetone p-tosylhydrazone in THF as an indicator [87]. The solid was washed several times with dry hexane and dried under vacuum.

V.3 Synthesis of Li_2FeS_2

Li_2FeS_2 was prepared by heating a mixture of lithium sulfide and iron sulfide at 800°C [16,17,80]. An intimate mixture of

$$FeS + Li_2S \xrightarrow{800°C} Li_2FeS_2 \qquad (47)$$

5 mmoles of FeS and Li_2S (98% purity) was prepared in a glove

bag under prepurified Ar, and transferred to a graphite crucible contained in a quartz Carius tube. The quartz tube and graphite crucible had been previously heated to ≈950°C under high vacuum to remove any impurities. The Carius tube was evacuated (10^{-3} torr), sealed, heated slowly to 800 ± 5°C for 3 days in a tube furnace, and then slowly cooled. The heating and cooling steps were each carried out over a period of 4-5 days. The temperature was measured using an Al-Cr thermocouple which had been calibrated with a digital thermometer.

V.4 Synthesis of $Li_3Fe_2S_4$

$Li_3Fe_2S_4$ was prepared by two different methods. The first, involved heating a stoichiometric mixture of iron sulfide, iron disulfide, and lithium sulfide at 450°C [88].

$$3FeS + FeS_2 + 3Li_2S \xrightarrow{450°C} 2Li_3Fe_2S_4 \qquad (48)$$

An intimate mixture of 1.1482 g of FeS, 522.3 mg of FeS_2, and 600 mg of Li_2S was prepared and then pressed into a disc at a pressure of 280 MN/m_2 under Ar in a glove bag. The pellet was then placed into a graphite crucible inside a quartz Carius tube that had been previously heated to 950°C under a high vacuum for several hours. The Carius tube was evacuated, sealed, heated slowly to 450 ± 5°C for 140 hrs, and then slowly cooled. The heating and cooling steps were carried out over a period of 32

hrs, and 21 hrs. The pellet was then ground into a powder, pelletized and the procedure used in the first heating repeated, except that the temperature was maintained at 450°C for 112 hrs. A small sample of the mixture was removed after each heating step, and ^{57}Fe Mössbauer measurements used as a criterion as to whether the mixture would benefit from further heating.

The second preparation for $Li_3Fe_2S_4$ involved heating a mixture of lithium carbonate and sulfur (both in excess) with

$$\underset{\text{280 atm}}{4Fe + 4Li_2CO_3 + 9S} \xrightarrow{800°C} 2Li_3Fe_2S_4 + Li_2CO_3 + 4CO_2 \quad (49)$$

iron powder at 800°C. An intimate mixture of 1.0000 g of fine Fe powder, 6.0000 g of S powder, and 2.6732 g of Li_2CO_3 powder was prepared, and pelletized into 127 × 6 mm discs with a pressure of 280 MN/m^2. The pellets were then placed into a quartz tube. This was found to be the best vessel for holding the molten solution, in that minimal fusion to the walls occured during the cooling period. The quartz tube was placed into a graphite crucible contained in a quartz furnace tube and heated ≈50°C/hr under prepurified dry Ar to 805 ± 5°C for 1 hr, then cooled slowly. The quartz/graphite tube arrangement was pretreated as described earlier. The reaction was carried out in a single-zone vertical tube furnace while the heating and cooling steps were 16 and 19 hrs respective.

V.5 Sample Annealing

A sample of ~300mg of chemically lithiated FeS_2 was weighed out in an inert atmosphere, transferred to a pretreated graphite/quartz Carius tube, evacuated to 10^{-3} torr, and sealed. The arrangement was heated over a period of 3-4 days to 600-640°C, held at this temperature overnight, and then cooled to RT over the period of a day.

VI. EXPERIMENTAL RESULTS AND DISCUSSION

VI.1 ^{57}Fe Mössbauer Spectra of Li|$LiAsF_6$-PC|FeS_2 Cathodes at 295, 77.4, and 4.2°K

The RT ^{57}Fe Mössbauer spectra of FeS_2 cathodes removed from cells after various stages of discharge, are shown in Figure (6.1). These cells had been previously discharged at room temperature at a current of 400-500 $\mu A/cm^2$. The cathodes were sufficiently thin (12 mg cm^{-2}) that corrections for absorber thickness were not necessary. The absorption spectra show the presence of paramagnetic Fe in at least three different sites: a doublet due to FeS_2, a broad singlet at near zero velocity, and a shoulder on the singlet peak. As will be shown later, the broad line near zero velocity is the result of very small Fe° particles exhibiting fast superferromagnetic (SF) relaxation. The FeS_2/singlet intensity ratio varied with the degree of cell discharge, until at full dischargement there was very little FeS_2 remaining. The "shoulder" on the singlet at positive velocities, indicated another Fe species present as one of the final products in the cell reaction.

These spectra are at first glance rather disappointing and appear to provide little useful information about the nature of the intermediates or the final products formed during discharge. Indeed in earlier ^{57}Fe Mössbauer studies of this same system by Clark *et al* [84], they observed RT spectra similar to the 1e-

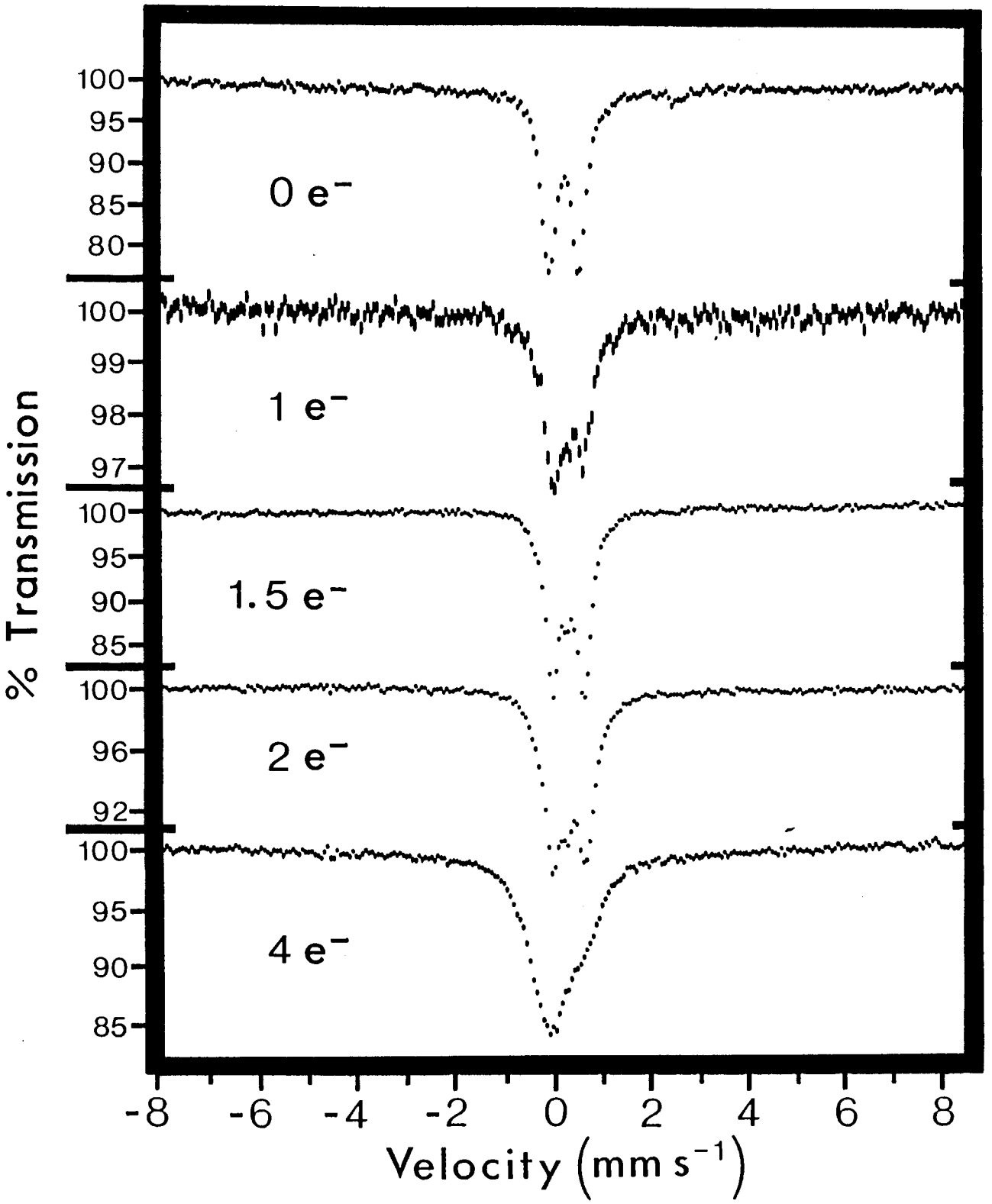

Fig. 6.1: RT ^{57}Fe Mössbauer spectra of Li|$LiAsF_6$-PC|FeS_2 cathodes at various stages of discharge. The cells were discharged at RT with a current of 400-500μA.

and 2e- discharge spectra reported here, and concluded that Mössbauer spectroscopy could not provide any useful information. They did not pursue their Mössbauer experiments. The fact that they did not observe spectra similar to the 4e- discharge spectrum of Fig. (6.1) suggests that they had only very poor cathode utilization in their experiments.

The Mössbauer spectra observed on cooling the discharged cathodes to 77.4°K or 4.2°K and illustrated in Figures (6.2) and (6.3) provide a much more detailed and informative picture. It is immediately apparent that magnetic hyperfine interactions are observed in the fully discharged cathode and also in partially discharged cathodes at 4.2°K.

VI.2 Studies of the Fully Discharged FeS_2 Cathode

The spectra of Figure (6.4) show the RT, 77.4°K and 4.2°K spectra of a fully discharged cathode. The appearance of the hfs on lowering the temperature could arise from the presence of a discharge product which is paramagnetic at RT, and which is ferromagnetic or anti-ferromagnetic at low temperature. However the low temperature spectra yield a hyperfine field very similar indeed to that of iron, although the spectra are complex and suggest the presence of more than one iron site. Since the anticipated final product in the cell is indeed iron, this suggests that the spectra of Figures (6.2) to (6.4) exhibit superparamagnetism, i.e. very small particles of iron are

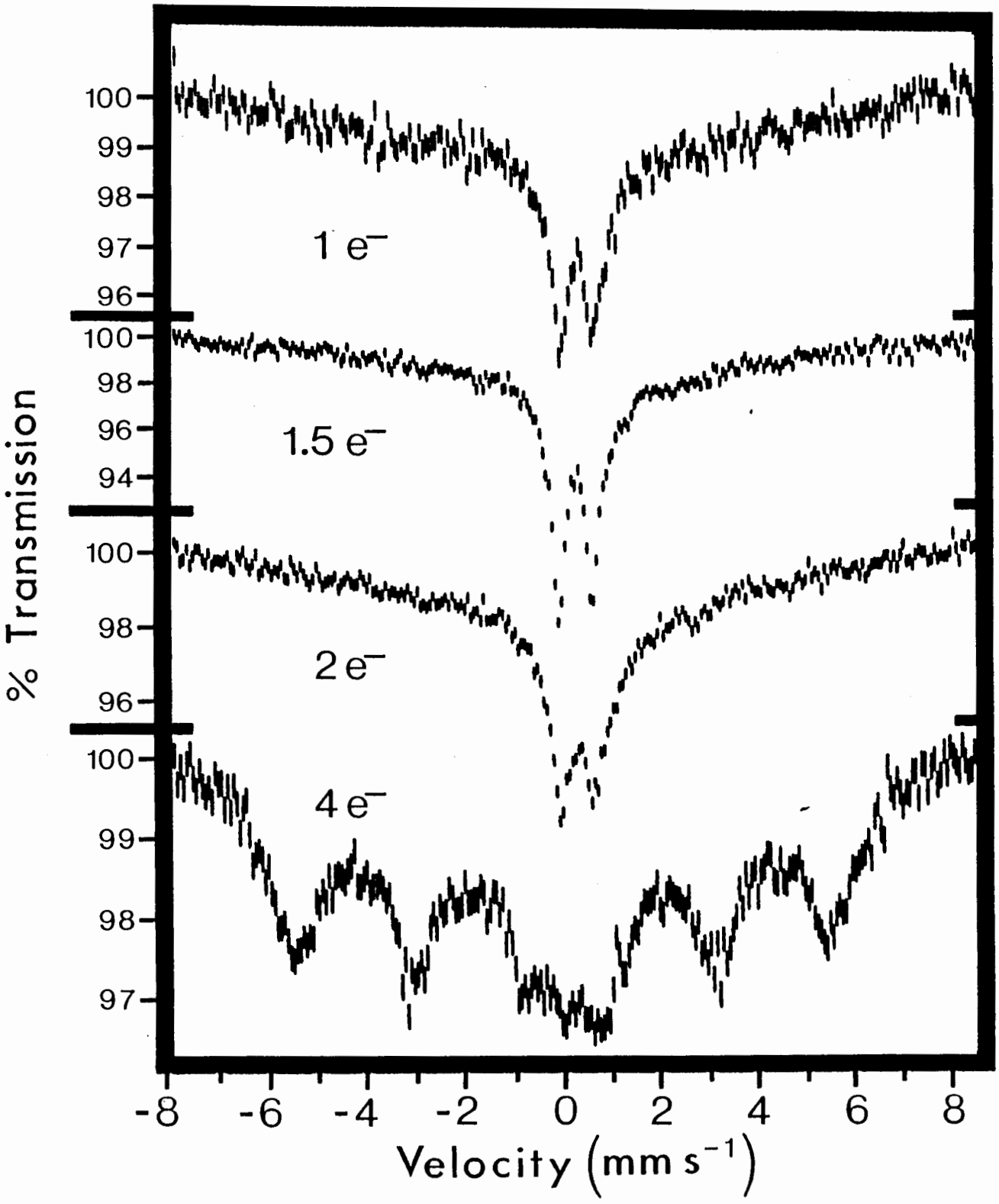

Fig. 6.2: 77.4°K ^{57}Fe Mössbauer spectra of Li|$LiAsF_6$-PC|FeS_2 cathodes at various stages of discharge. The cells were discharged at RT with a current of 400-500μA.

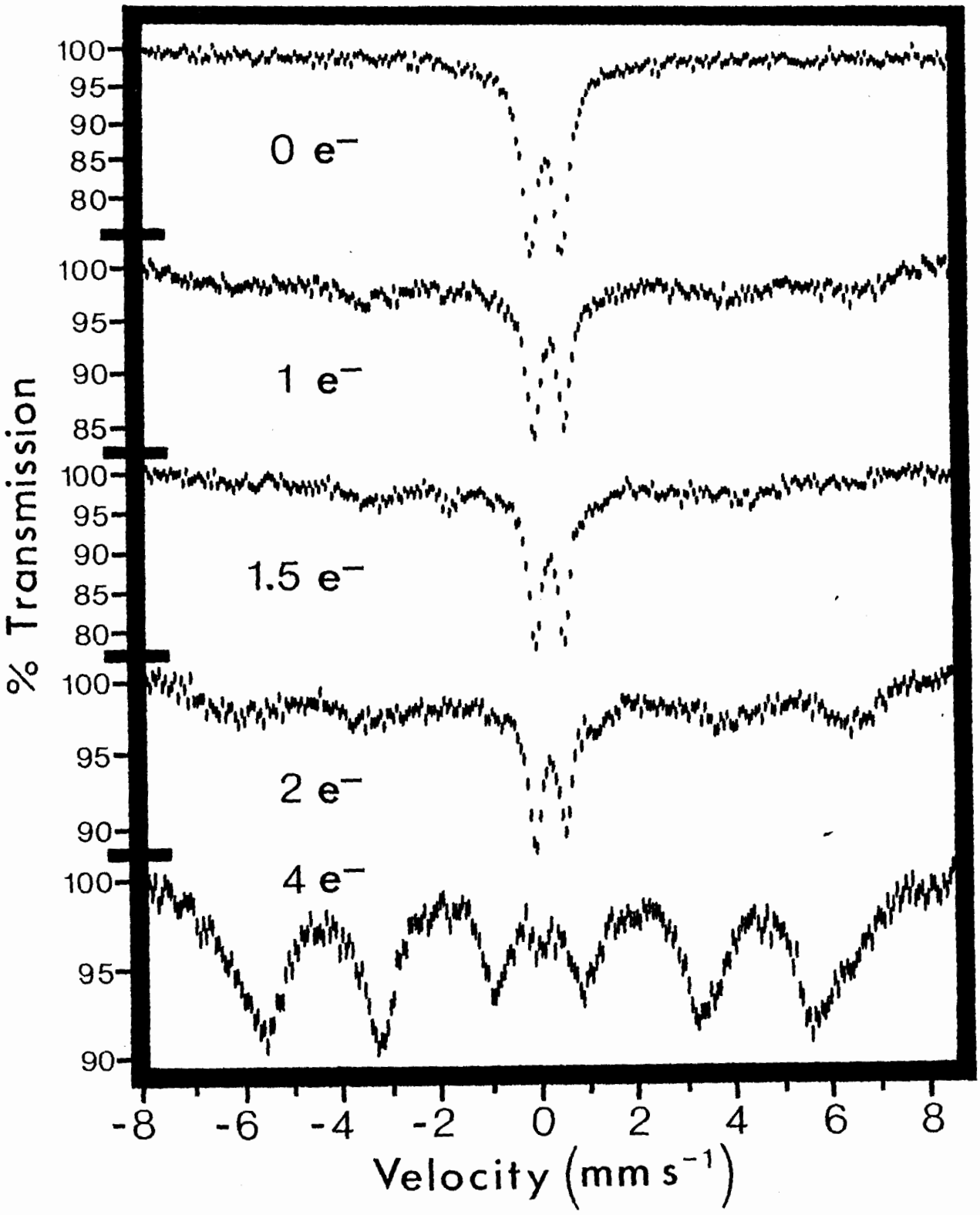

Fig. 6.3: 4.2°K ^{57}Fe Mössbauer spectra of Li|$LiAsF_6$-PC|FeS_2 cathodes at various stages of discharge. The cells were discharged at RT with a current of 400-500μA.

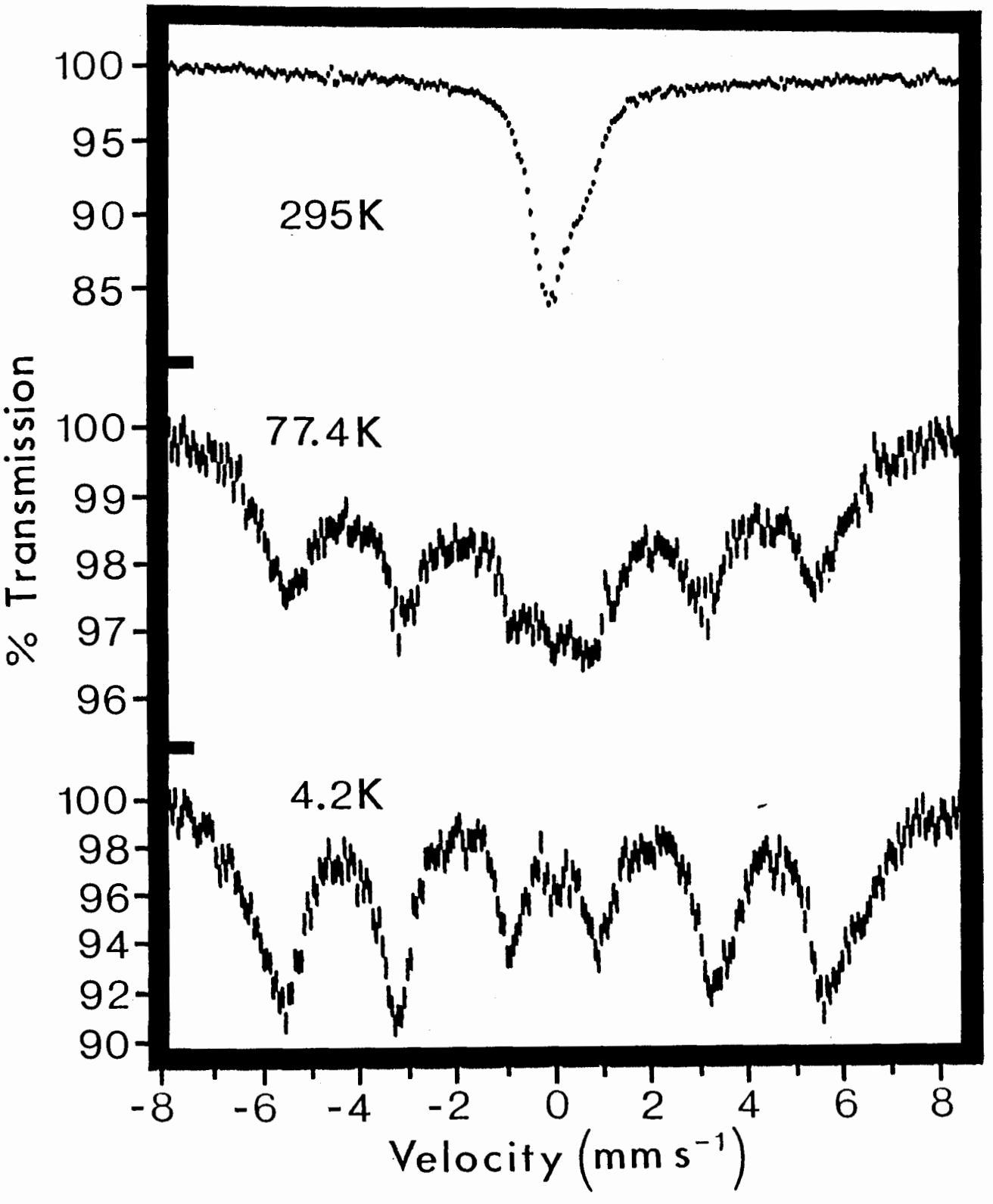

Fig. 6.4: ^{57}Fe Mössbauer spectra of a cathode removed from the fully discharged Li|$LiAsF_6$-PC|FeS_2 cell #R-1.

present which at room temperature do not exhibit hfs because the magnetization is fluctuating between the easy directions. On cooling below the blocking temperature the characteristic hfs is observed.

VI.2a ^{57}Fe Mössbauer of a Fully Discharged $Li|LiClO_4$-PC$|FeS_2$ Cathode at 295, 77.4, and 4.2°K

The Mössbauer spectra for a cathode from a fully discharged $Li|LiClO_4$-PC$|FeS_2$ cell are shown in Figure (6.5). The cathode had been previously discharged at room temperature with a drain current of 650μA (fast discharge). These spectra show some interesting features in comparison with the spectra of Figure (6.4) namely:

i) while in Figure (6.4) hfs was observed at 77.4°K this is not so in Figure (6.5).

ii) in Figure (6.4) the 4.2°K spectrum showed a hint of a shoulder to higher velocities for the higher velocity peaks and particularily for the absorption at 6.5 mm s^{-1}. In Figure (6.5) these shoulders are more clearly marked.

Both of these features are consistent with suggestion that in the $LiClO_4$ electrolyte cell, the iron particles formed are smaller in size. This leads to a lower blocking temperature below which hfs is observed in the case of the $LiClO_4$ cell. Moreover the shoulders on the absorption peaks, which are most

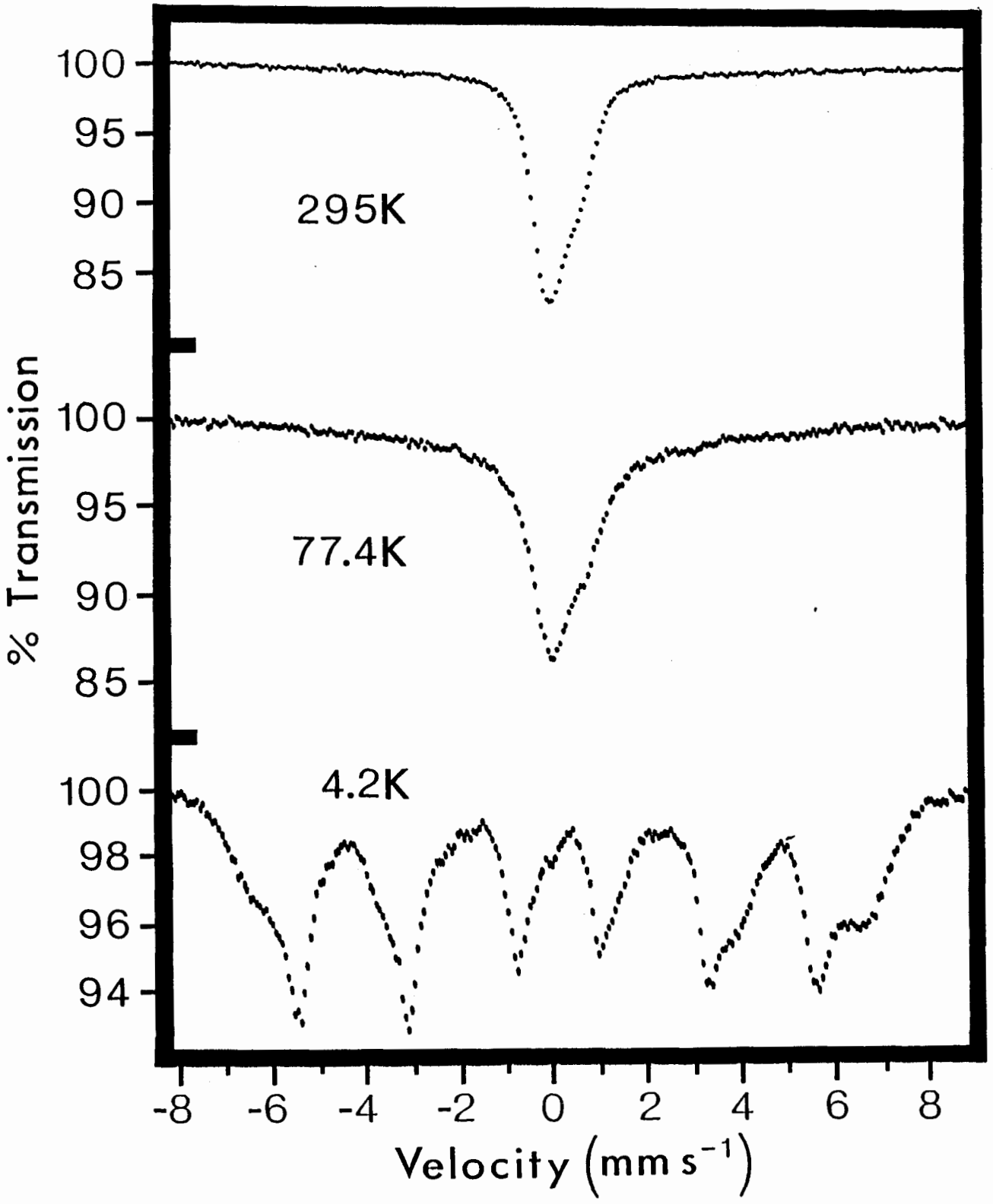

Fig. 6.5: ^{57}Fe Mössbauer spectra of a cathode removed from a fully discharged Li|$LiClO_4$-PC|FeS_2 cell #R-4. The cell had been discharged at RT with a current of 650μA (fast discharge).

pronounced in Figure (6.5), are precisely what one would expect for surface iron atoms in small particles and the smaller the particles the more clearly they should be resolved. This point will be returned to later.

VI.2b ^{57}Fe Mössbauer of a Fully Discharged Li|$LiClO_4$-PC|FeS_2 Cathode in an Externally Applied Magnetic Field

Confirmation that superparamagnetism arising from the presence of small particles was observed in these spectra is given by spectra in an externally applied weak magnetic field. Figure (6.6) elegantly illustrates the effect of an applied field on the spectrum of a fully discharged cathode. These spectra are characteristic of SP small particles in which the magnetization vector becomes aligned in the presence of a relatively weak external field. The relative intensities of the absorption lines in the magnetically split spectra are close to 3:4:1:1:4:3 as expected for a sample magnetized at right angles to the γ-ray beam. The broad line-widths and the asymmetry of the lines indicate a distribution in the hyperfine magnetic fields. The magnitude of the hfs shows a dependence on the applied field strength and this in turn allowed an estimate of the mean particle volume.

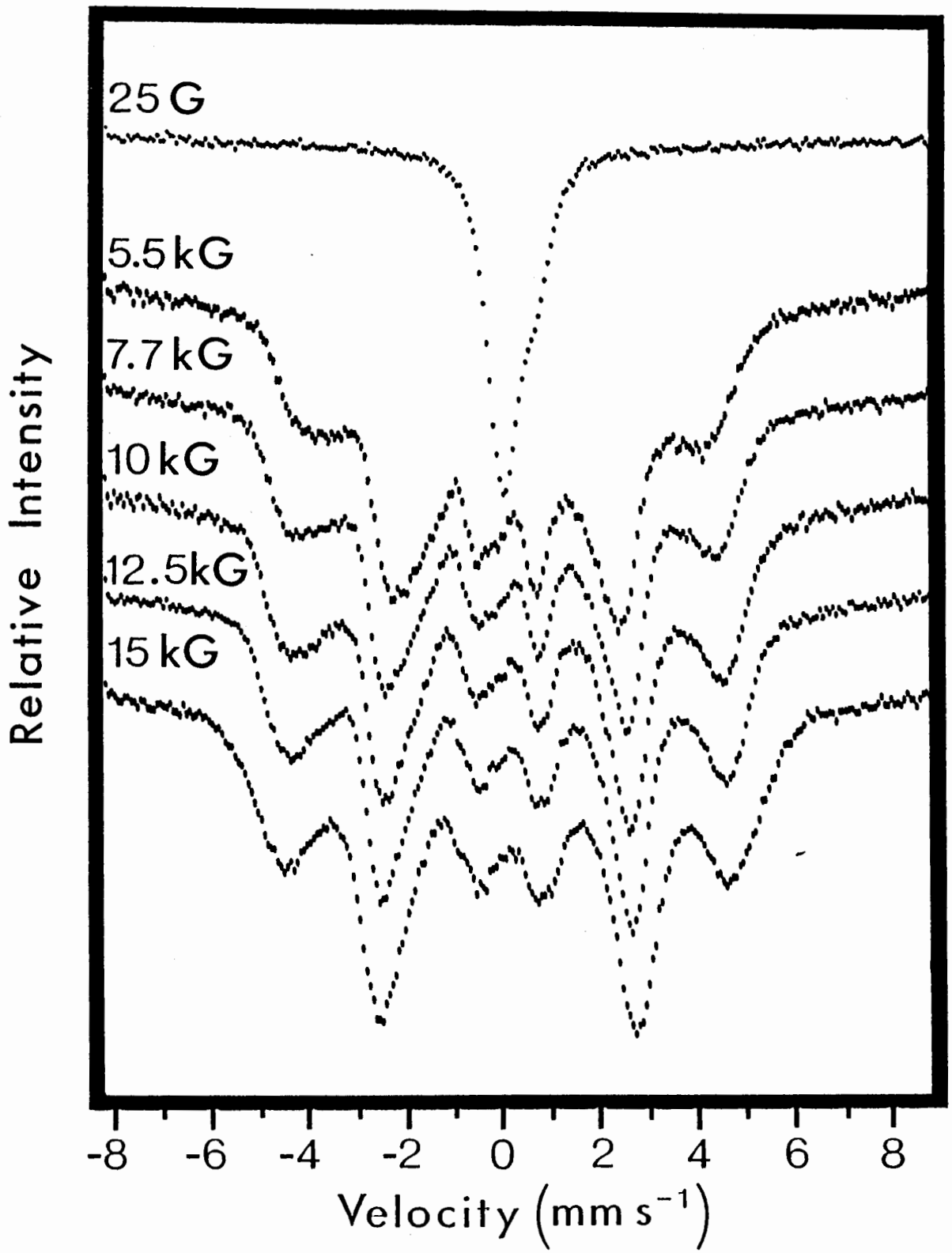

Fig. 6.6: RT ^{57}Fe Mössbauer spectra for the fully discharged Li|$LiClO_4$-PC|FeS_2 cathode #R-4 in externally applied magnetic fields. The spectra are normalized to the same height.

VI.2c Computer Analysis of the Spectra for Fully Discharged Cathodes

A detailed analysis of the spectra of the RT spectrum of a fully discharged cathode was not attempted. The broad irresolved absorption near zero velocity arises from the SP small particles and the shoulder to more positive velocity may reflect the surface atoms in these particles.

Two approaches were taken in the fitting of the 4.2°K hfs spectra:

i) Using a set of independent Lorentzians to represent the six-line magnetic components and the FeS_2 paramagnetic doublet, and applying the fitting program GMFP [89,90].

ii) Assuming a hyperfine field distribution (hfd) and applying the fitting program MCAL [91]. This latter approach yields a hfd plot rather than Mössbauer parameters.

The first approach yields only an estimate of the hyperfine field and the isomer shift. The spectral lines are in all probably not Lorentzian. The derived parameters for the fully discharged cathodes of Figures (6.4) and (6.5) are given in Table (6.1). The assumptions and approximations used in the fits are given in the footnotes of the table. In each case it was assumed that the spectra could be fitted to two sets of six-line

Table 6.1

Mössbauer Parameters for Fully Discharged FeS_2 Cathodes at 4.2°K

Component	Cell	Mössbauer Parameters			
		IS (mm/s)[a]	Γ (mm/s)	$\langle H_{int} \rangle$ (kG)[b]	A (%)
bulk Fe°	#R-1	-0.012(7)	0.74(3)	342(3)	68(3)
surface Fe°	#R-1	0.07(4)[c]	0.80(8)	385(4)[d]	27(4)
FeS_2[e]	#R-1	0.22214	0.42497	———	5(5)
bulk Fe°	#R-4	-0.056(5)[c]	0.36(1)[f]	340(3)[g]	22(1)
surface Fe°	#R-4	0.13(1)[c]	1.46(2)[f]	385(4)[g]	76(1)
FeS_2[e]	#R-4	0.21968	0.41926	———	2(1)

[a] IS reported w.r.t. α-Fe foil at 295°K.
[b] Each magnetic sextet was fitted assuming 3 sets of Lorentzian doublets with the same IS and Γ. The intensity of the inner doublet was constrained to be $\frac{1}{3}$ that of the outermost doublet.
[c] Average of IS determined for each doublet.
[d] Only the IS of the two innermost doublets constrained to be equal.
[e] Fixed using values from FeS_2 powder at 4.2°K.
[f] Average of Γ determined for each doublet.
[g] IS and Γ of doublets are independent w.r.t. one another.

magnetic hyperfine splittings and a quadrupole doublet due to a small fraction of undischarged FeS_2.

The component with H = 340 to 342kG is b.c.c. iron. The field observed is a little greater than that for α-Fe (H = 338(3)kG at 4.2°K [92]), and the difference appears to lie outside the error of the measurements.

The magnetic field observed at the Fe nucleus in a small particle can be written as:

$$H_{obs} = H_{bulk} + H_{dem} + H_{dip} \qquad (50)$$

Where H_{bulk} is the magnetic hyperfine field of nonmagnetized α-Fe bulk material, H_{dem} the demagnetizing field due to surface atoms, and H_{dip} the magnetic field of neighbouring particles. If we assume that the iron particles are approximately spherical and we use H_{dem} = 7kG and H_{bulk} = 338kG, then the $\langle H_{obs} \rangle$ values of 340 and 342kG would yield $\langle H_{dip} \rangle$ values of 3 and 5kG. The H_{dip} arises from interaction between neighbouring particles which are physically close together i.e. a weakly coupled SF system, and a H_{dip} of 3kG is not unexpected.

Rancourt *et al* [49] studied 25 ± 5Å α-Fe_2O_3 particles supported by zeolite-Y at temperatures above and below T_B. The two different SF dwell times (τ_+ and τ_-) were determined for spectra recorded below the blocking temperature from a detailed analysis of the lineshape through Voigt profiles [93]. Using eq. (42), they obtained a similar result for $\langle H_{dip} \rangle$ of 3.2kG.

The second magnetic component with $\langle H_{obs} \rangle$ = 385(4)kG may arise from atoms in the surface layers of the small particles. Such an enhancement in the field for surface layers is in accordance with predictions by Freeman *et al* [32,33] as mentioned earlier. The IS determined is slightly larger than that for bulk α-Fe but considerably smaller than values typical for Fe^{+2} or Fe^{+3}, thus indicating that these iron atoms have a slightly smaller s-electron density at the nuclei.

An analysis of the spectra of the fully discharged cathodes using MCAL resulted in the hyperfine field distributions shown in Figure (6.7). It has been noted by Williams *et al* [71] that the oscillations observed in the hfd plots at small fields are of no significance and usually result from the limit imposed on the distribution increment and from statistical fluctuations in the experimental data. Quadrupolar and SP contributions to the spectrum will also produce peaks in the low field regime of the hfd plots.

The hfd plots clearly show a sharp maximum at ca. 342kG and a distribution about this value. There is evidence for a small peak in the distribution at ca. 275-295kG which could arise from amorphous iron. The shoulder at 385kG may arise from surface iron. The broad distribution would be consistent with a wide distribution in surface H_{int} predicted by Ohnishi's calculations.

Xiao and Chien [94] measured H_{int} for various binary amorphous Fe-transition metal and Fe-metalloid alloys at 4.2°K, and determined the H_{int} of pure amorphous Fe by extrapolation to 100% Fe. The study revealed different states of amorphous Fe with $H_{int} \approx$ 250-280kG that could be related to the theoretically proposed γ_1 and γ_2 states of f.c.c. iron. Recently Pollard [95] has observed an Fe component resulting from high temperature reduction of fine γ-Fe_2O_3 particles with an H_{int} of 302kG at 4.2°. The IS of 0.08 mm/sec was close to the range of IS values determined by Xiao and Chien for pure amorphous Fe. Broad hfd's

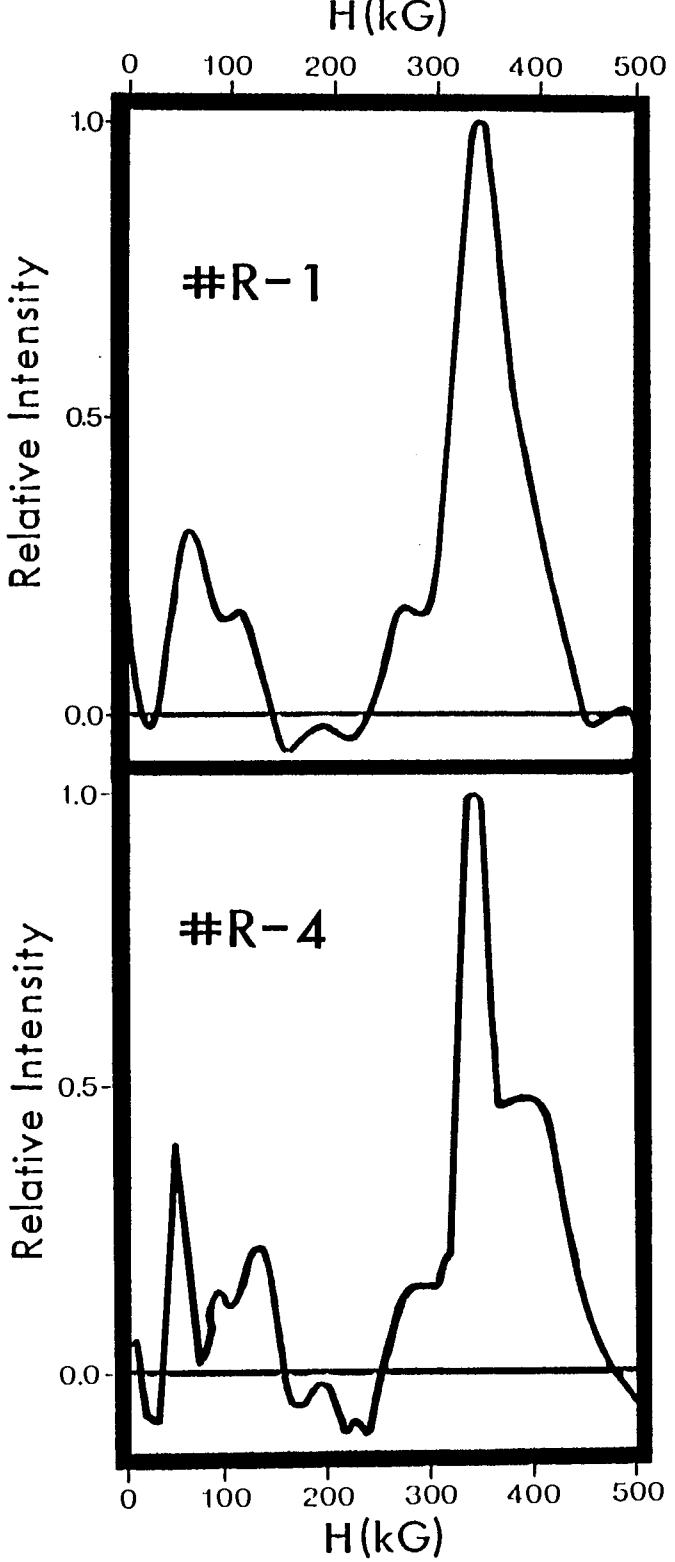

Fig. 6.7: Hyperfine field distribution plots for the 4.2°K spectra of fully discharged cathodes a) removed from a Li|$LiAsF_6$-PC|FeS_2 cell and b) removed from a Li|$LiClO_4$-PC|FeS_2 cell.

of 100-300kG have also been reported for non-crystalline Fe° clusters in zeolites [49,96], and sputtered non-crystalline Fe films [97].

The ratio of the spectral areas can give a rough indication of the actual ratio of surface atoms to bulk atoms in the particle, hence a crude estimate of the particle volume could be obtained. Assuming that 1) the particles were spherical, 2) the recoil-free fraction was the same for the surface and bulk atoms, and 3) the surface atoms were only the atoms in the first one or two layers, then the ratio of the "shell volume" of surface atoms over the total volume is:

$$\frac{n^3 - (n - (1 \text{ to } 2))^3}{n^3} = \frac{A_{surface}}{A_{surface} + A_{bulk}} \qquad (44)$$

The distance n, is in terms of inter-atomic nearest neighbor distances, while the thickness of the shell was assumed to be about 1 - 2 inter-atomic distances since surface effects are important for only one or two layers. The distance between an Fe atom and its nearest neighbor in a b.c.c. lattice at 300°K is ≈2.5Å as determined by x-ray diffraction. At 4.2°K, there will be a slight decrease in the lattice spacing due to thermal contraction. Using eq. (44), the mean diameter of the Fe° particles in the fully discharged $LiAsF_6$ electrolyte cathode is estimated to be 16 to 46 inter-atomic distances. This yields a range for the mean particle diameter of 32 - 115Å assuming an

Fe-Fe distance of 2 - 2.5Å. For the 4.2°K spectrum of the fully discharged $LiClO_4$ electrolyte cathode, the area of the surface contribution to the total spectrum resulted in a crude estimate for the mean particle diameter of 10 - 26Å.

The Mössbauer spectra in Figure (6.6) were fit to six independent Lorentzian lines with varying linewidth and intensity, and since only the positions of the lines were of interest for determination of the mean hfs, the error in this gross over-simplification was assumed to be minor.

According to eqn. (32), if the particles are purely superparamagnetic, then a plot of $\left|\langle H_{obs}\rangle - B_{applied}\right|$ vs $B_{applied}^{-1}$ should give a straight line with slope equal to $H_o kT/\mu(T)$ and intercept H_o. The results of such a plot shown in Figure (6.8), yielded an intercept of 280 ± 3kG, which after subtraction of the 7kG demagnetizing field for spherical particles, resulted in a saturation field of 273 ± 3kG. This value is far below the literature value of 330kG that would be expected for α-Fe, and further suggested that the Fe° particles present in the fully discharged $LiClO_4$ electrolyte cathode #R-4 were most likely superferromagnetic in nature.

If the dipole-dipole interactions between the particles are taken into consideration, then according to the more precise expression (40), a plot of $\{1 - b(B,T)\}^{-1}$ as a function of B is a straight line with slope $\mu(T)/kT$ and intercept $\mu(T)B_i(T,B)/kT$. The mean magnetic moment $\mu(300°K)$ of the particles was

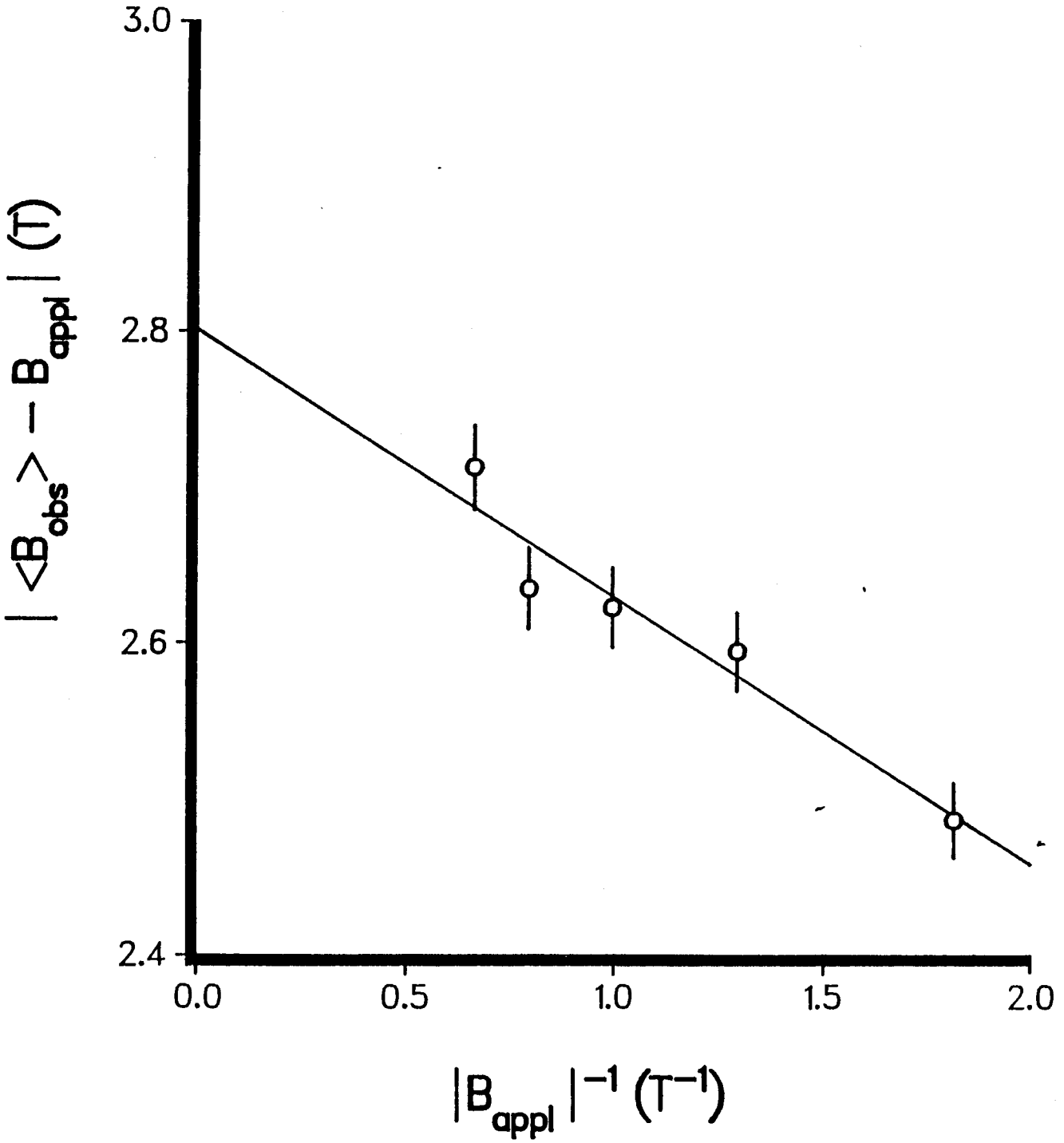

Fig. 6.8: A plot of $|(H_{obs}) - B_{applied}|$ vs $B_{applied}^{-1}$ based on the spectra shown in Figure (6.6).

determined to be 1.8(2) × 10^{-20} JT^{-1} from a least squares fit of the plot shown in Figure (6.9). Assuming that the particles are spherically shaped and that the saturation magnetization is equal to that of bulk metallic iron, the magnetic moment corresponded to a mean particle diameter of 27 ± 1Å. The effective magnetic field due to particle-particle interactions B_i(B=0,300°K), was determined from the y-intercept to be 5 ± 1kG, and is in agreement with the value estimated from the spectrum at 4.2°K.

Christensen *et al* [63] obtained a value of 1.6(3) × 10^{-20} JT^{-1} for the μ(300°K) of 25 ± 2Å SP α-Fe particles supported on carbon. Since the mean particle sizes are similar, the small difference in the mean magnetic moments can be attributed to particle-support (Li_2S matrix in this study), and magnetic dipolar interactions which were negligible in the aforementioned study because the particles were well separated.

VI.3 Studies on Partially Discharged FeS_2 Cathodes

VI.3a ^{57}Fe Mössbauer of Partially Discharged Li|$LiClO_4$-PC|FeS_2 Cathodes at 295, 77.4°, and 4.2°K

While cells utilizing $LiAsF_6$ as an electrolyte did not yield significant evidence for intermediates in the discharge, when $LiClO_4$ was the electrolyte for slow discharge at drain currents of 470 to 520μA, intermediates were indeed observed for spectra

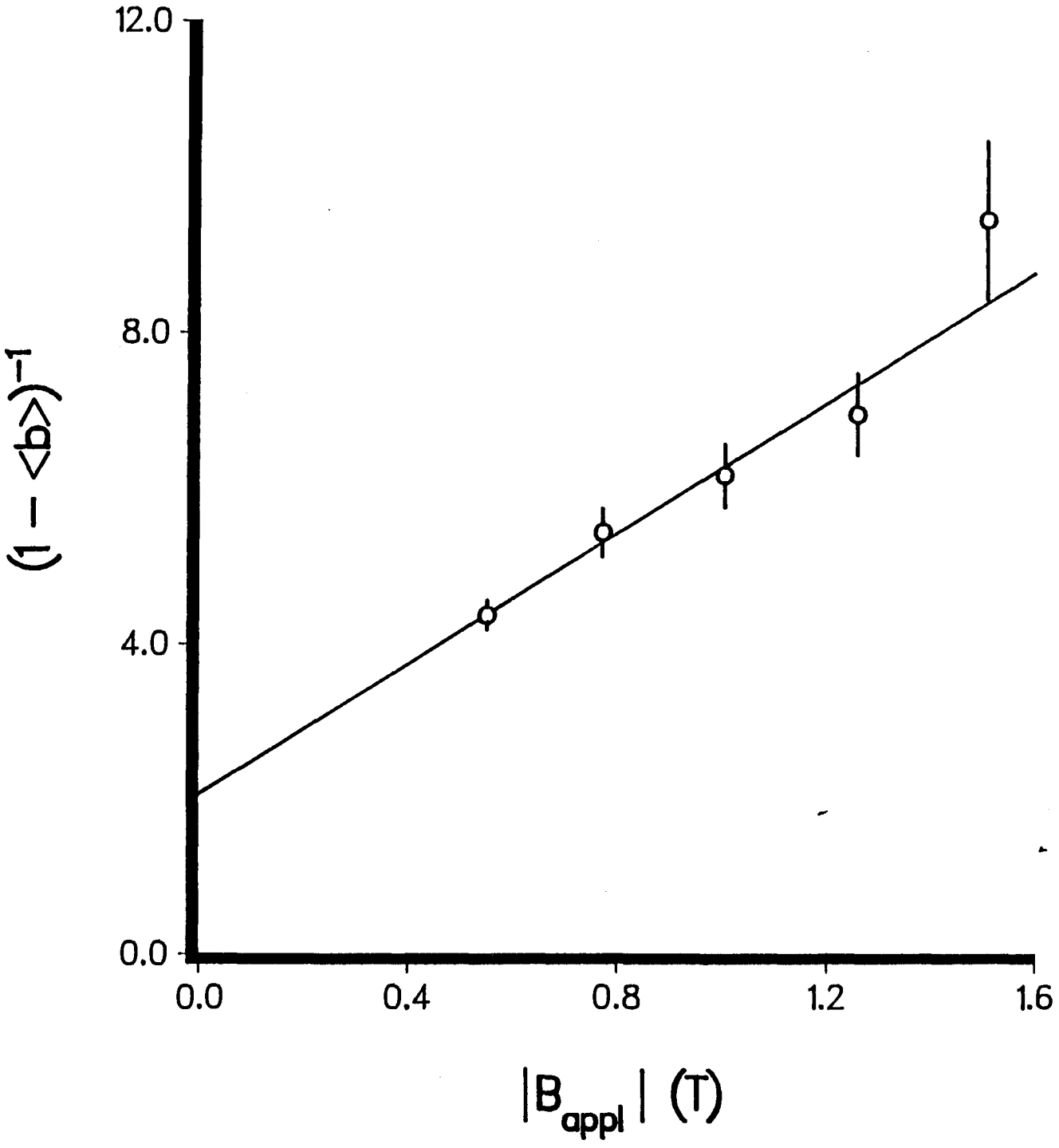

Fig. 6.9: A plot of $\{1 - b(B,T)\}^{-1}$ as a function of applied magnetic field where b(B,T) is the reduced hyperfine magnetic field for the spectra of Figure (6.6).

recorded at low temperature.

The RT Mössbauer spectra for a $LiClO_4$ electrolyte cell discharged at 470μA are shown in Figure (6.10). The fully discharged cathode shows the presence of a magnetic component even at RT. This would be consistent with the formation in this case of larger iron particles than those observed in the other batteries studied.

In the 77.4°K spectra (Fig. 6.11) and particularily in the 4.2°K spectra (Fig. 6.12) there is clear evidence for the formation of an intermediate or a group of intermediates with a magnetic field of $\gtrsim$ 240kG at 4.2°K. The question immediately arises as to the identity of the intermediate(s). It has been proposed by Nardi *et al* [84] that lithiated intermediates Li_xFeS_2 should be formed during discharge. From the Li-Fe-S phase diagram (Fig. 4.1), Li_2FeS_2 would appear to be a very likely candidate. This compound was synthesized in our laboratory and its x-ray crystal structure determined [98]. The Mössbauer parameters for the RT and 77.4°K spectra are compared with the results of Melendres and Tani [80] in Table (6.2).

The Mössbauer spectrum of Li_2FeS_2 at RT (Fig. 6.13) shows the presence of two quadrupole split doublets. On cooling to 4.2°K an exceedingly complex magnetic hyperfine split spectrum is observed. There appears to be a range of sites which are magnetically inequivalent at 4.2°K. This spectrum is compared with that of partially discharged cathodes in Figure (6.14).

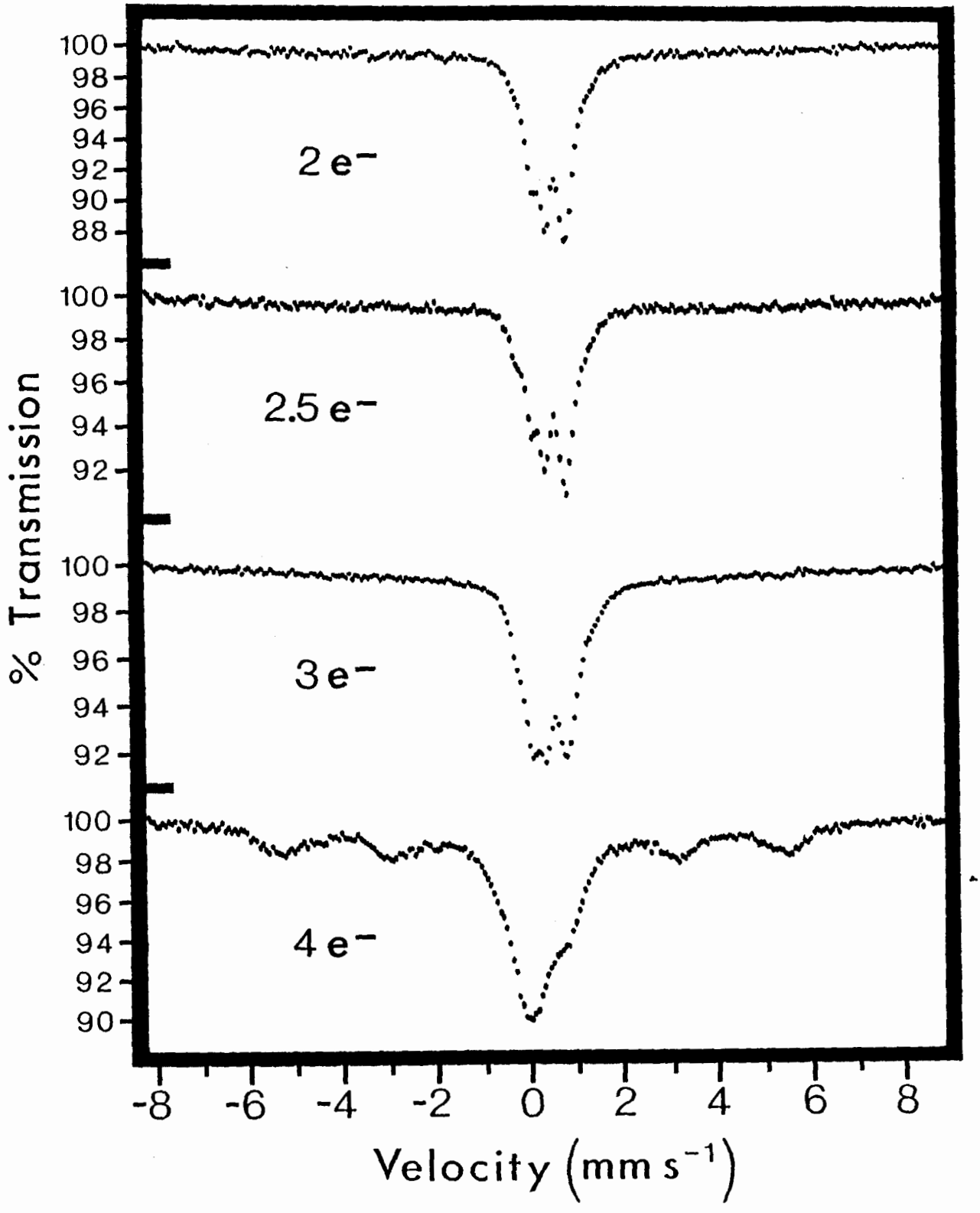

Fig. 6.10: RT ^{57}Fe Mössbauer spectra of $Li|LiClO_4\text{-}PC|FeS_2$ cathodes at various stages of discharge. The cells were slowly discharged at RT with a drain current of 470-520μA.

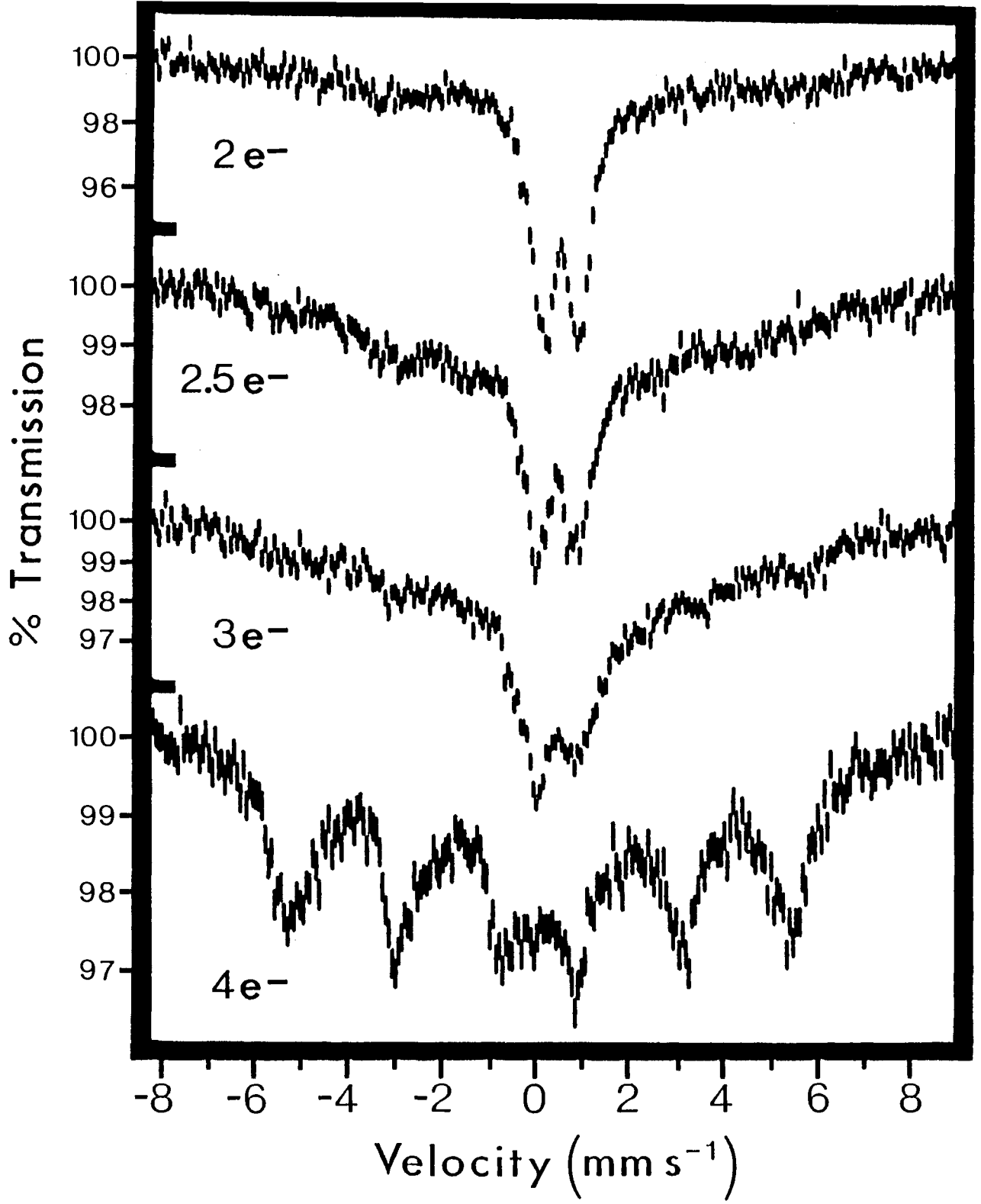

Fig. 6.11: 77.4°K ^{57}Fe Mössbauer spectra of Li|$LiClO_4$-PC|FeS_2 cathodes at various stages of discharge. The cells were slowly discharged at RT with a drain current of 470-520μA.

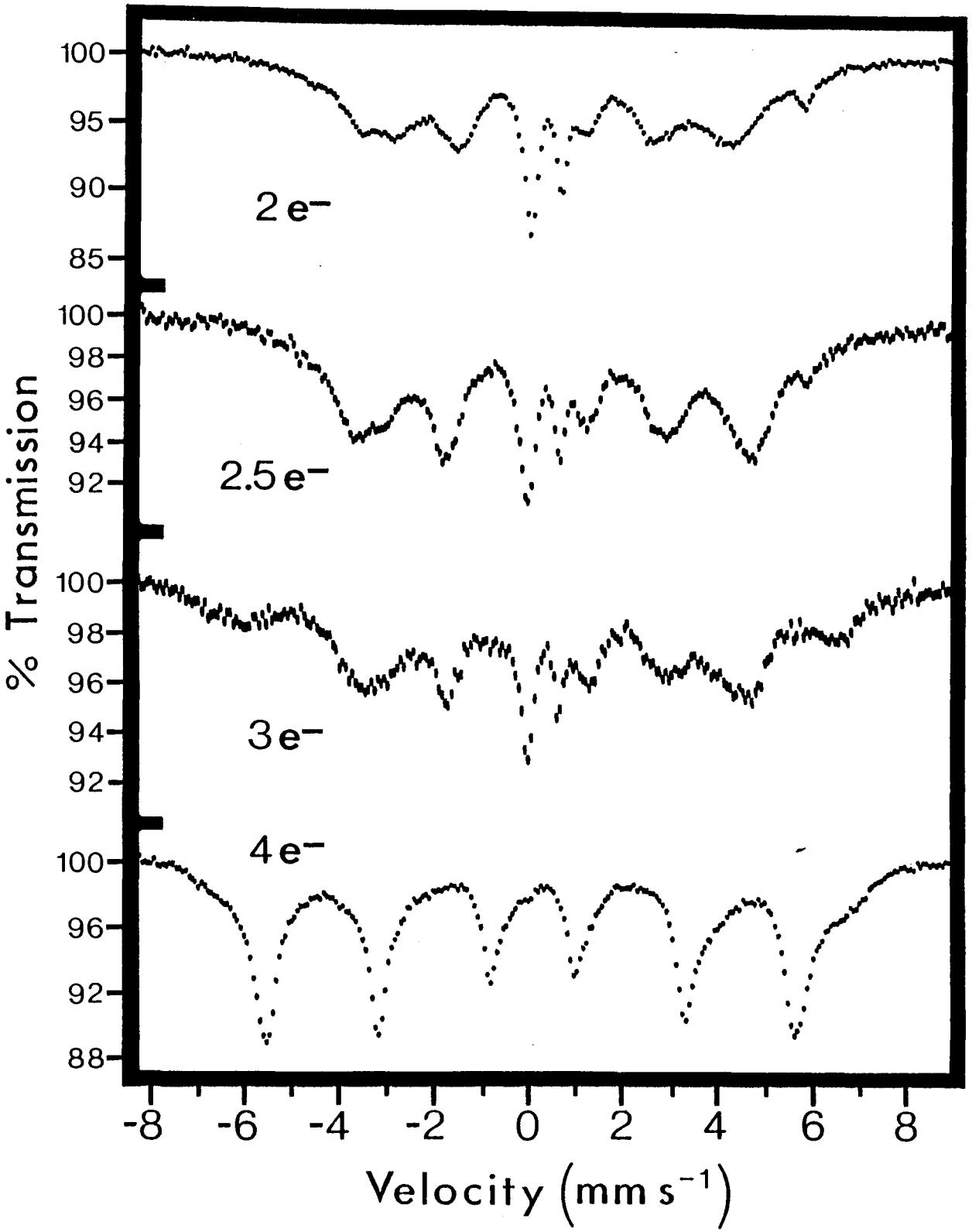

Fig. 6.12: 4.2°K ^{57}Fe Mössbauer spectra of $Li|LiClO_4\text{-}PC|FeS_2$ cathodes at various stages of discharge. The cells were slowly discharged at RT with a drain current of 470-520μA.

Table 6.2

Mössbauer Parameters for Li_2FeS_2 at 295 and 77.4°K

Component	T (°K)	Mössbauer Parameters			
		IS (mm/s)[a]	Γ (mm/s)	QS (mm/s)[a]	A (%)
Doublet 1	RT	0.698(2)	0.513(2)[b]	0.990(3)	83.9(3)
Doublet 2	RT	0.648(3)	0.276(4)[c]	1.779(5)	16.1(2)
Doublet 1[d]	RT	0.50(2)	———	0.62(2)	———
Doublet 2[d]	RT	0.49(1)	———	1.46(2)	———
Doublet 1	77.4	0.57(2)	0.476(8)[b]	1.08(1)	67(2)
Doublet 2	77.4	0.52(2)	0.360(12)[b]	1.73(1)	33(1)
Doublet 1[d]	77.4	0.61(2)	———	1.06(2)	———
Doublet 2[d]	77.4	0.61(1)	———	1.68(2)	———

[a]IS reported w.r.t. α-Fe foil at 295 °K.
[b]Constrained to be equal.
[c]Average of Γ for two peaks.
[d]From Melandres and Tani [80].

There appears to be a very poor correspondence between the two spectra.

Another lithiated phase reported in the literature is that of "$Li_3Fe_2S_4$". Samples of this phase were prepared in our laboratory but we have been unable to characterize the material by chemical analysis because of the presence of impurities (e.g. FeS_2 and Li_2S). Nevertheless a relatively pure sample containing traces of FeS_2 yielded the 4.2°K spectrum shown in Figure (6.15a). There is some similarity between this spectrum and that of the discharged (2e-) cathode although they are certainly not identical. In particular the absorption at 5.63 mm/s corresponds

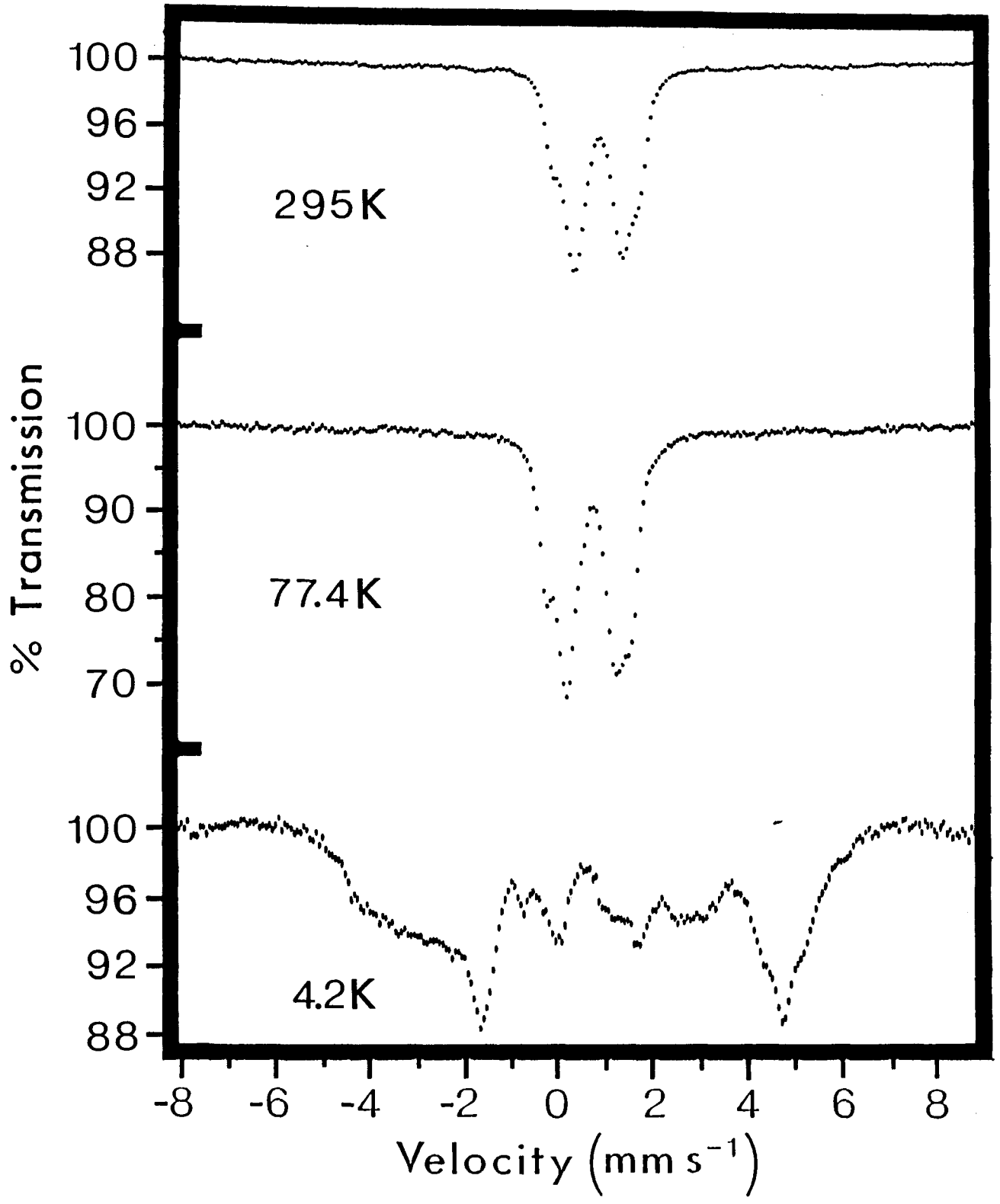

Fig. 6.13: ^{57}Fe Mössbauer spectra of Li_2FeS_2 at 295, 77.4, and 4.2°K.

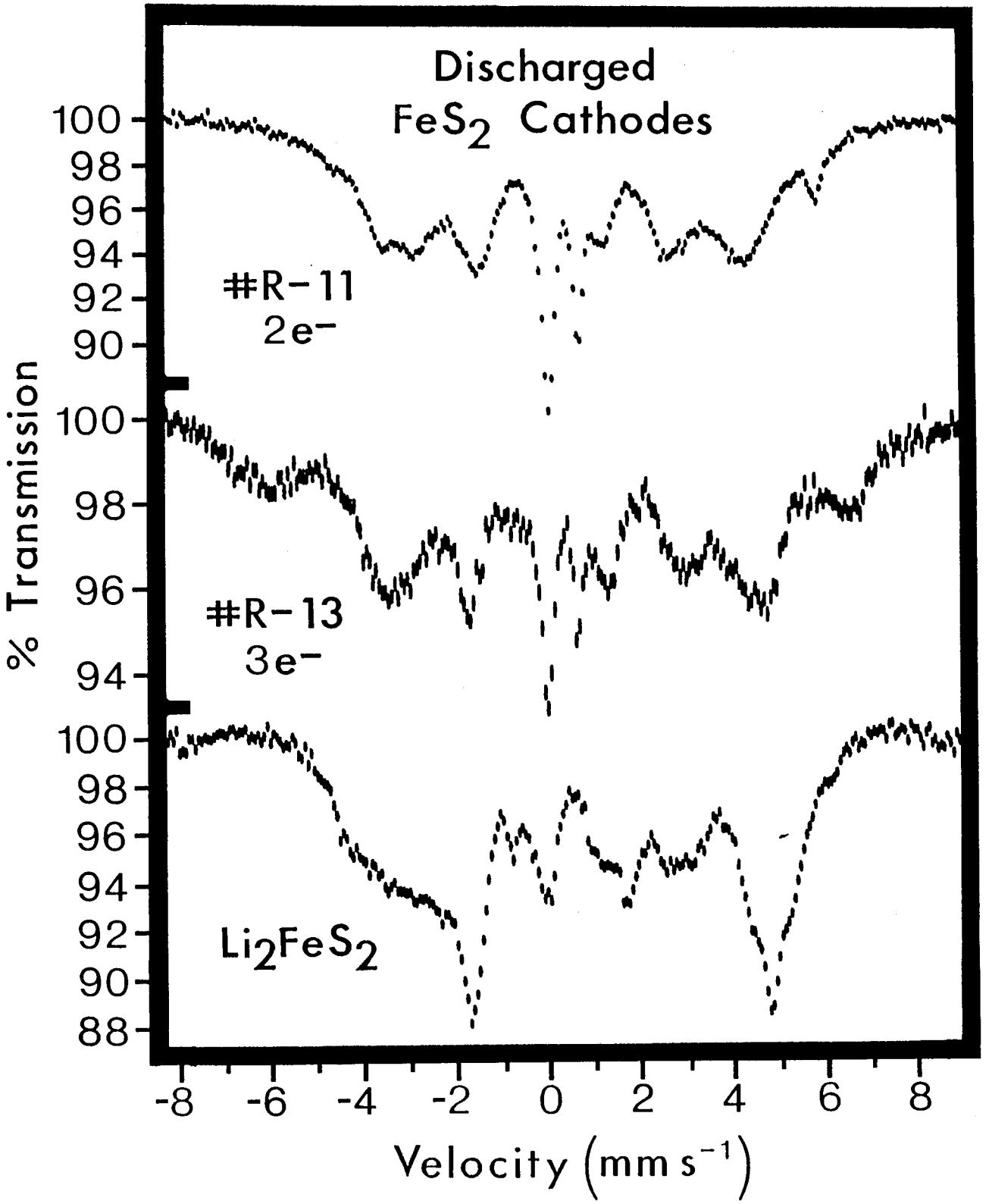

Fig. 6.14: 4.2°K ^{57}Fe Mössbauer spectra of Li|$LiClO_4$-PC|FeS_2 cathodes #R-11 (2e-) and #R-13 (3e-) compared with the spectrum for chemically synthesized Li_2FeS_2 recorded at the same temperature and velocity.

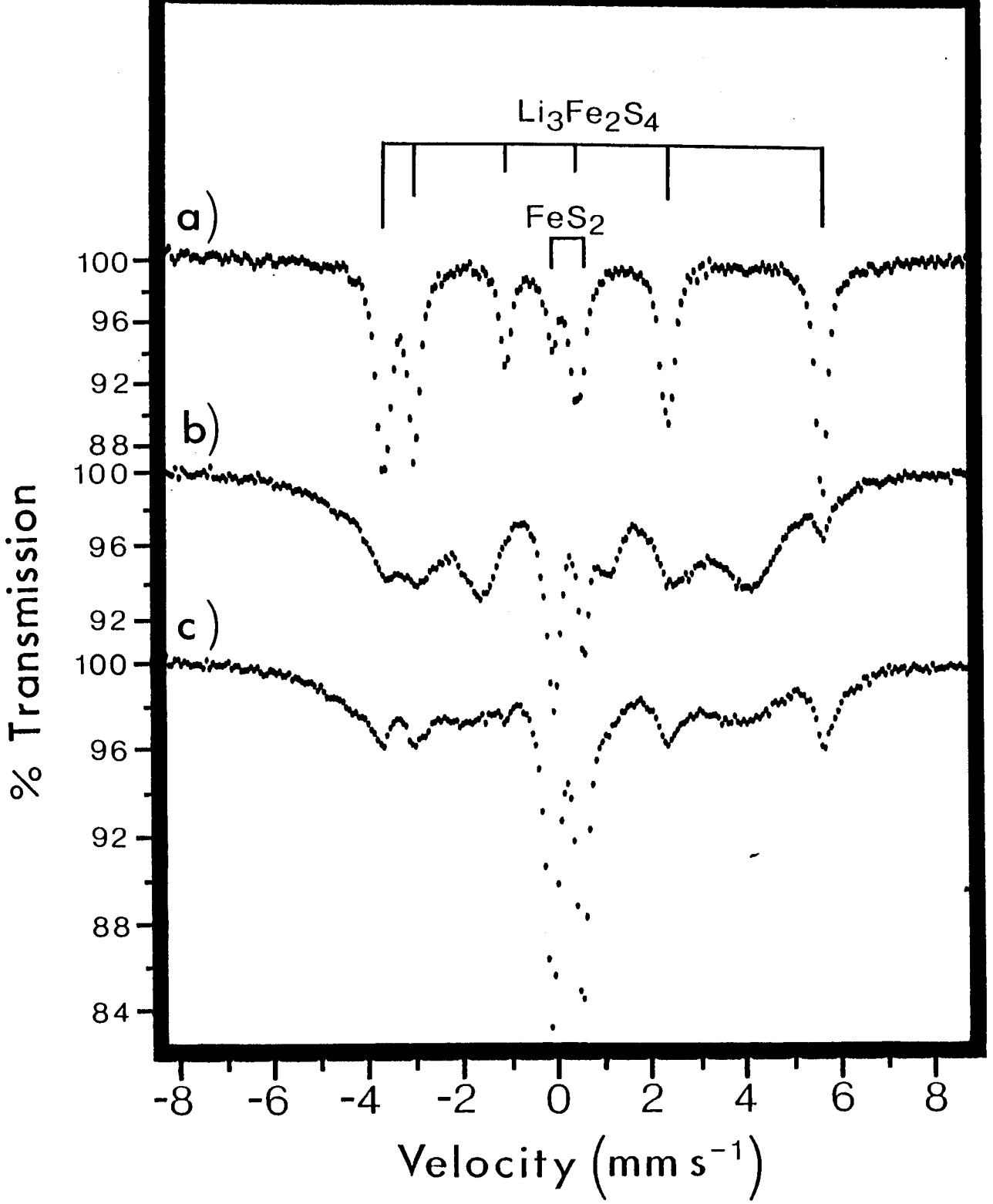

Fig. 6.15: 4.2°K ^{57}Fe Mössbauer spectra of a) chemically synthesized $Li_3Fe_2S_4$ compared with spectra of partially discharged (2e-) $Li|LiClO_4\text{-}PC|FeS_2$ cathodes discharged at b) RT and c) 55°C, recorded at the same temperature and velocity.

exactly, as do the absorptions at -3.02 mm/s and -3.66 mm/s. This points to the probable presence of $Li_3Fe_2S_4$ in the discharge process, along with other lithiated phases.

It has been pointed out that on discharge at 55°C, the FeS_2 cell may approach thermodynamic equilibrium and formation of one intermediate phase, Li_2FeS_2, has been postulated [99].

The Mössbauer spectrum of a cell which had been discharged at 55°C is compared in Figure (6.15) with one discharged at RT. There are clearly similarities between the two but the 55°C spectrum is cleaner and perhaps simpler. Indeed it corresponds very closely to the $Li_3Fe_2S_4$ phase.

From this evidence it would appear that, for a cell which approaches thermodynamic equilibrium, $Li_3Fe_2S_4$ is formed during the discharge. However there is no definitive evidence for the formation of Li_2FeS_2.

For cells discharged at RT it would appear that a mixture of lithiated species are present including a small amount of $Li_3Fe_2S_4$. It would appear that the dominant intermediate is another discrete lithiated FeS_2 species which the present time remains unidentified (Y-phase).

The nature of these spectra and also those of chemically lithiated FeS_2, which will be discussed later, suggest that the lithiation proceeds in fairly discrete steps. If Li_xFeS_2 phases with continuously variable x were formed then the spectra would

in all probability be even more complex than they are. The observed spectrum of Li_2FeS_2 is evidence of the complexity of such a system.

VI.3b Collective Magnetic Excitations

One further point deserves attention. The magnetic field observed at 77.4°K (Fig. 6.13) is significantly less (332(3)kG) than that of bulk material. This diminuition in the field at the iron nucleus is in all probability due to collective magnetic excitations where the magnetization vector fluctuates about the easy axis leading to a reduced field.

VI.4 Studies on Chemically Lithiated FeS_2

VI.4a ^{57}Fe Mössbauer of Chemically Lithiated FeS_2 at 295 and 4.2°K

The electrochemical reactions occuring inside the cathode were mimicked by reacting samples of the same FeS_2 powder used in cathode preparation with n-BuLi in hexane. The ^{57}Fe Mössbauer spectra of FeS_2 after reaction with various stoichiometric amounts of n-Buli had been recorded at 295°K (Fig. 6.16) and 4.2°K (Fig. 6.17). The low temperature Mössbauer spectra indicated a mixture of different Fe phases, each having a distribution in hyperfine magnetic fields. This was better shown by the asymmetry in the peak shapes of the Fe component with the

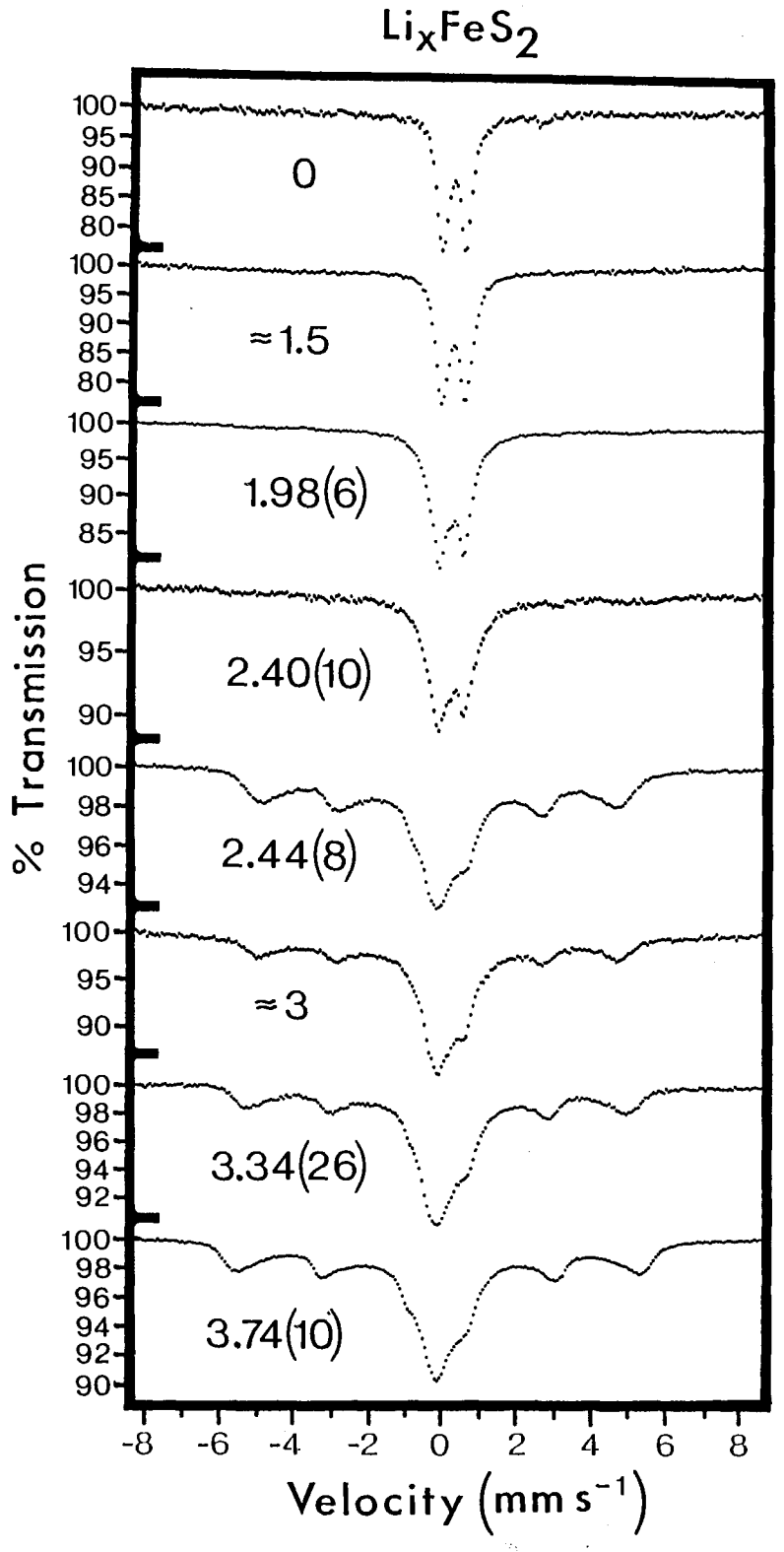

Fig. 6.16: RT ^{57}Fe Mössbauer spectra of chemically lithiated Li_xFeS_2 (x=0 ⇒ 3.74) samples.

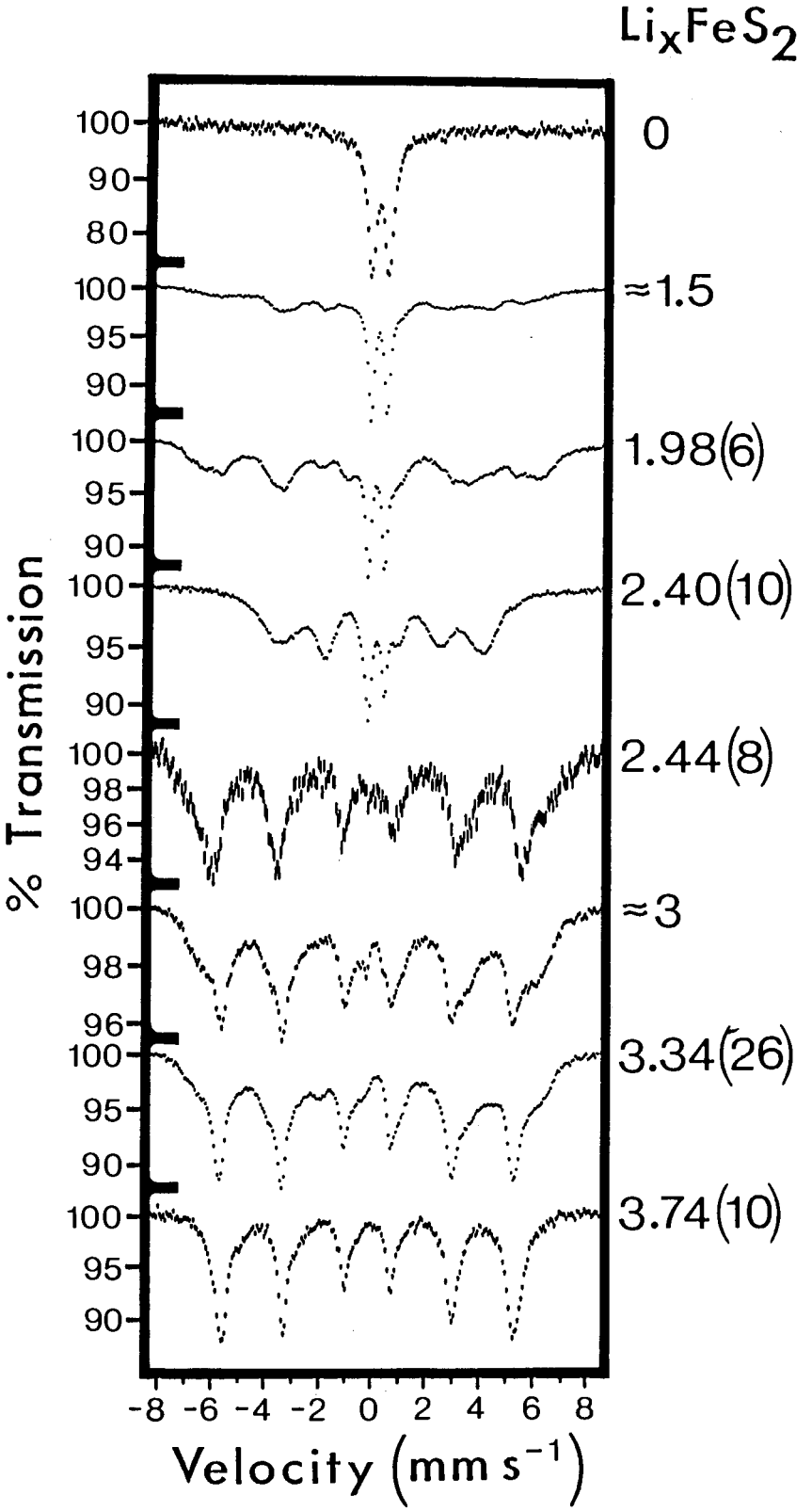

Fig. 6.17: 4.2°K ^{57}Fe Mössbauer spectra of chemically lithiated Li_xFeS_2 (x=0 ⇒ 3.74) samples.

observable hyperfine field at 295°K. As a result, a Lorentzian analysis was not attempted and a qualitative analysis will have to suffice.

The absorption spectra recorded at RT displayed a similar pattern to that seen in partially discharged FeS_2 cathodes. The appearance of a broad absorption peak at near-zero velocity which increases in intensity as the extent of lithiation also increases is consistent with previous observations. After the stoichiometry of intercalated Li to FeS_2 had exceeded 2:1, there was evidence of an appreciable amount of some magnetic compound present; the magnitude of $\langle H_{int} \rangle$ increasing with further lithiation from ≈ 290kG to ≈ 320kG w.r.t. α-Fe at RT. The pronounced asymmetry in the peaks of this magnetic component is clearly indicative of a hfd.

It is apparent upon comparing the ^{57}Fe Mössbauer spectra recorded at RT and 4.2°K, that the single absorption present at near-zero velocity in the RT spectra, was actually comprised of at least 1 - 3 magnetic components which became resolved at 4.2°K. Two of the magnetic components could be identified from the peak positions, and IS as corresponding to SP or SF Fe° particles, and the hyperfine magnetic field due to the surface atoms. The other magnetic component had an $\langle H_{int} \rangle$ of ≈ 240kG, and a more positive IS. The peak positions of this Fe phase were very similar to that of the "Y-phase" that was observed in FeS_2 cathodes discharged to about the same extent. The Y-phase is most apparent in the low temperature spectrum for the sample

Li_xFeS_2 x = 2.4 and the similarity between the Mössbauer spectrum for this particular chemically lithiated sample, and the cathode electrochemically lithiated to the same extent (Fig. 6.18) is remarkable.

It can be seen from Figure (6.17), that the Y-phase, and small particles of Fe° were formed after a small amount of Li intercalation had occurred, with the ratio of each component dependent on the extent of lithiation in each sample. Although there are some irregularities, the general trend displayed in the spectra seems to be that as the extent of lithiation increases, the relative amount of Y-phase and FeS_2 decreases, while the portions due to Fe° increase until by $x \geq 3$, there was only a small amount of Y-phase and FeS_2 left. Further lithiation results in the mean Fe° particle volume getting larger so that the contribution from the surface Fe atoms to the total spectra becomes less and less significant.

The Fe phase with the observable $\langle H_{int} \rangle$ at RT, was not observed at 4.2°K, hence this phase must also be α-Fe with a particle-size distribution corresponding to values of $T_B > 295°K$. This volume dependence is also reflected by the approach of $\langle H_{obs} \rangle$ to the saturation value of 330kG with a corresponding increase in lithiation. The reduced but still observable $\langle H_{int} \rangle$ is a consequence of collective magnetic excitations. Reduced hyperfine fields for small particles of Fe° have been observed at RT before in the past by other workers [67,68,100].

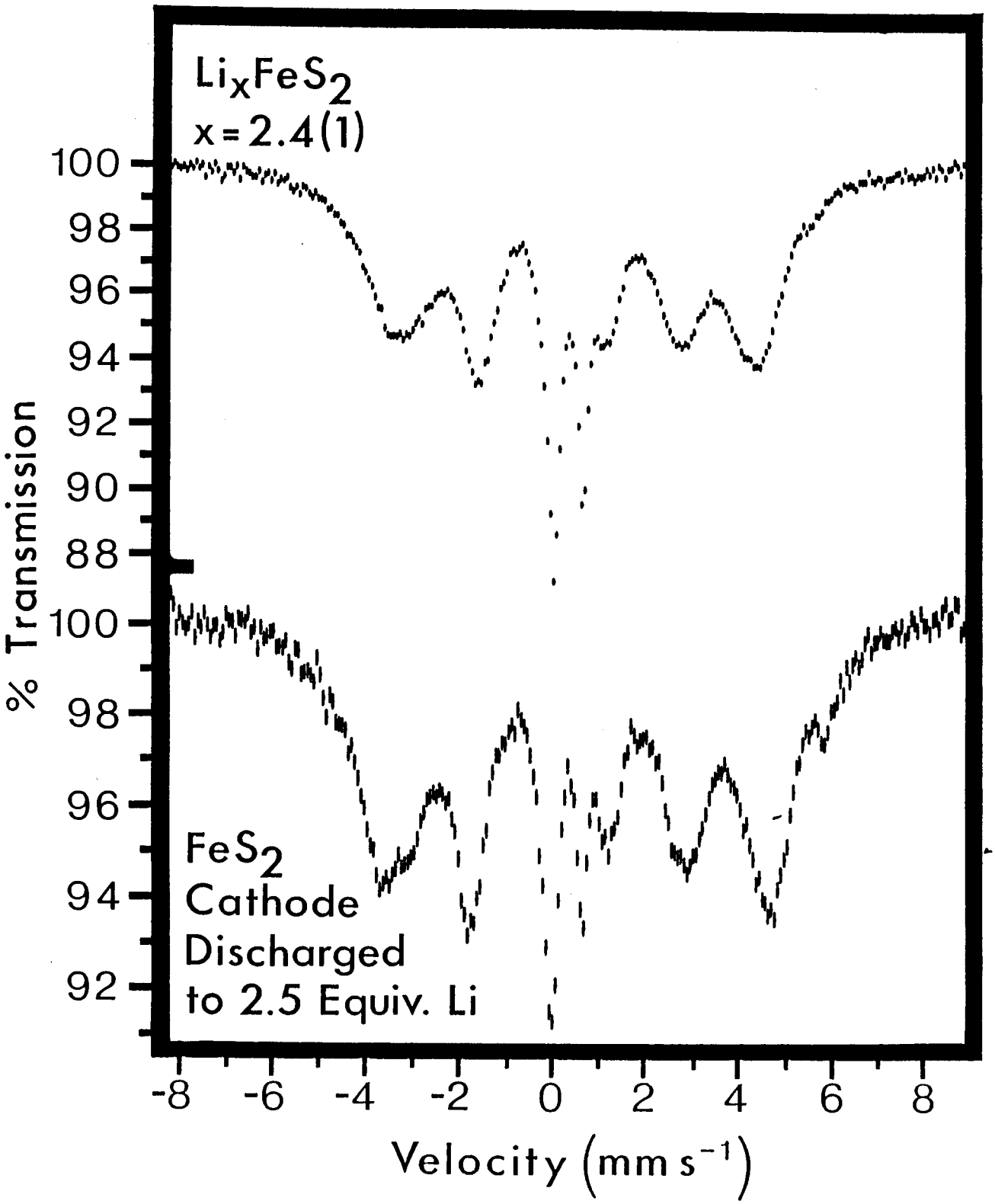

Fig. 6.18: 4.2°K Mössbauer spectra of a) chemically lithiated $Li_{2.4}FeS_2$ and b) electrochemically lithiated $Li_{2.5}FeS_2$.

VI.4b ^{57}Fe Mössbauer of Chemically Lithiated FeS_2 in an Externally Applied Magnetic Field

The room temperature ^{57}Fe Mössbauer of some lithiated samples before and after application of an external magnetic field is shown in Figure (6.19). After application of the magnetic field, it can be seen from the spectra that the broad singlet peak at near-zero velocity became resolved into a six-line hyperfine spectrum with the magnitude of the observed hfs close to the saturation value of 330kG for bulk Fe°. The results are consistent with the interpretation that SP or SF Fe° particles were present in most of the lithiated FeS_2 samples. A particle-size determination through Mössbauer measurements with various external B fields was not possible since many of the samples contained particles below their respective blocking temperatures.

VI.4c ^{57}Fe Mössbauer of Chemically Lithiated FeS_2 After Annealing

The RT ^{57}Fe Mössbauer of some chemically lithiated FeS_2 samples after annealing, is shown along with the spectrum for Fe° foil in Figure (6.20). The major component in the two samples was bulk Fe° with a much narrower hyperfine field distribution than what was previously observed in the unannealed sample at 4.2 and 295°K. Annealing the sample had the effect of fusing all the SP Fe° particles into larger sizes exhibiting an

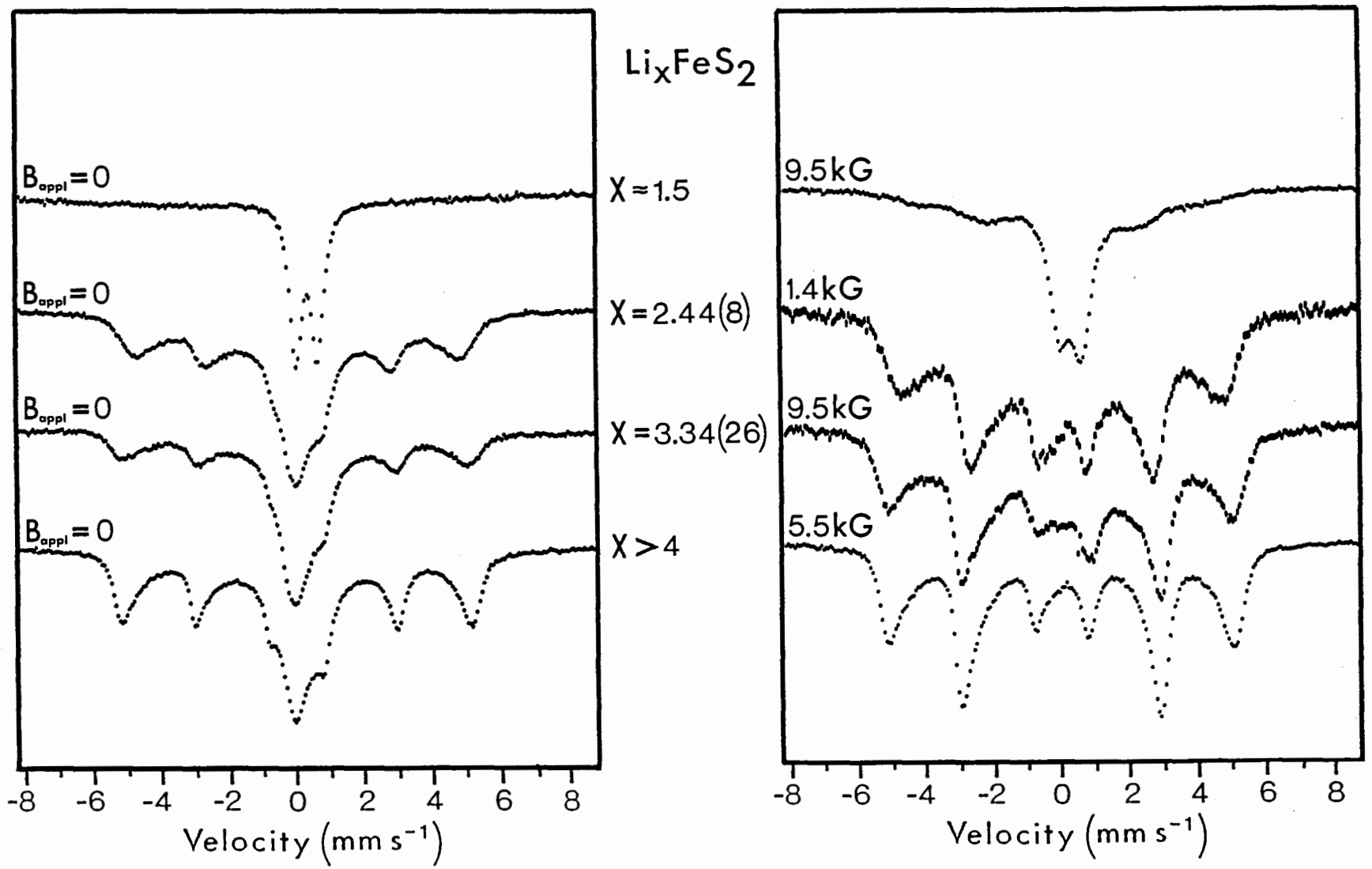

Fig. 6.19: RT ^{57}Fe Mössbauer spectra of chemically lithiated FeS_2 (Li_xFeS_2) samples with and without an externally applied magnetic field. The spectra are normalized to the same height.

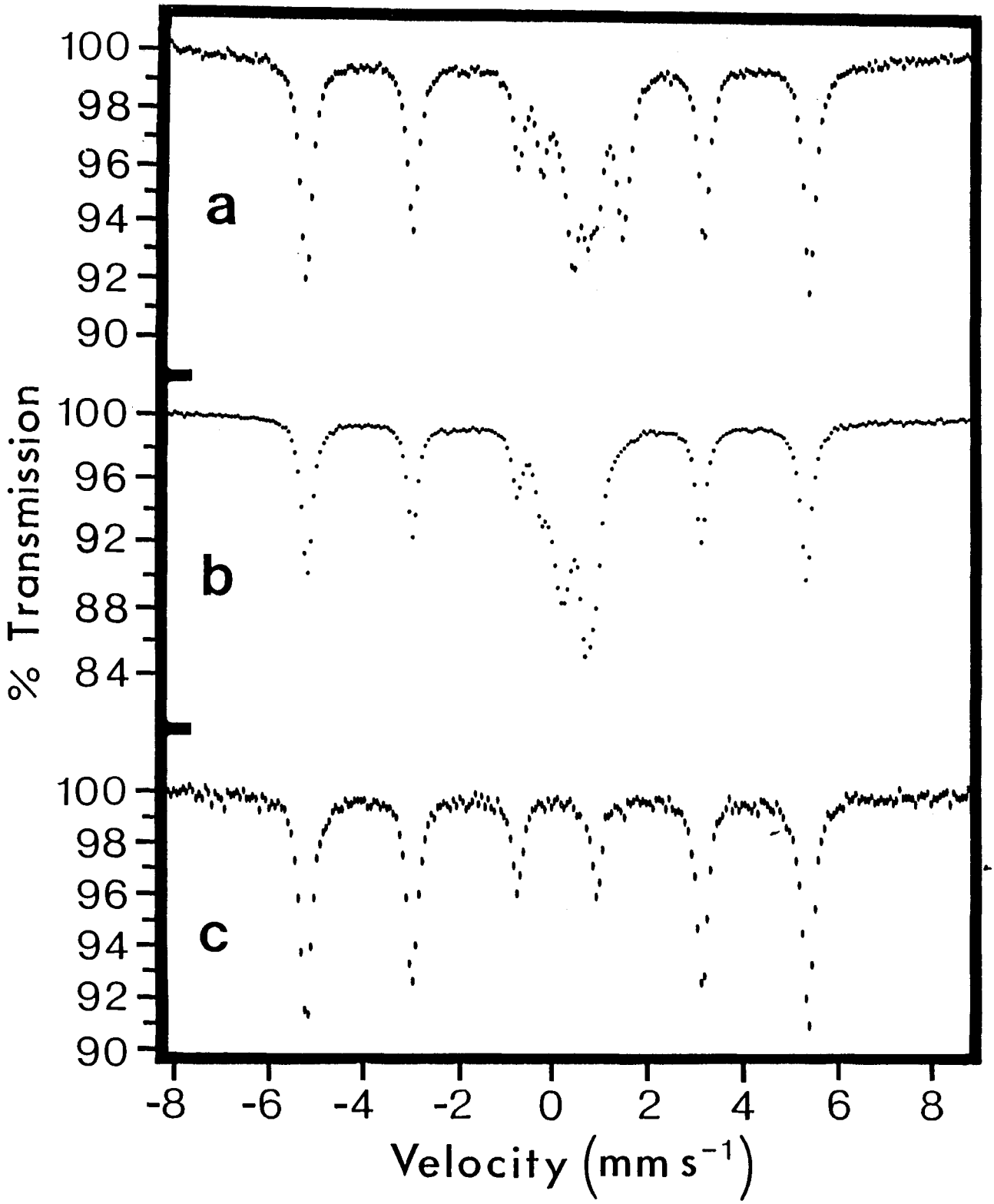

Fig. 6.20: RT ^{57}Fe Mössbauer spectra of Li_xFeS_2 a)x = 3.74, annealed at 640°C and b)x > 4, annealed at 600°C. A spectrum for Fe° foil is also shown for comparison in (c).

observable H_{int}. The samples were chosen because the low temperature spectra indicated that they were the cleanest, however annealing the samples had resulted in other paramagnetic Fe species being formed such as FeS_2.

VI.4d X-Ray Powder Diffraction of Chemically Lithiated FeS_2

X-ray powder diffraction was carried out on some of the lithiated FeS_2 samples, and the powder patterns are shown in Figure (6.21). As the extent of lithiation increases, the intensities of the peaks due to FeS_2 decreases with a corresponding increase in the Li_2S peak intensities. The (110) diffraction peak due to Fe metal was just barely discernable and the broadened peak would also indicate that the particles are very small, or non-crystalline. The presence of the Y-phase could not be detected in the Li_xFeS_2 ($x = 2.40$) sample or in the $x = 3.34$ sample.

VI.4e Computer Analysis of the Spectra for Chemically Lithiated FeS_2

The hfd plots of the 4.2°K spectra for the lithiated Li_xFeS_2 ($x \approx 3$ to 3.74) samples, are shown in Figure (6.22). The high field regime of the hfd plots exhibits the same features displayed in the hfd plots of the fully discharged cathodes (Fig. 6.18) i.e. hfd's for amorphous, b.c.c., and surface Fe°. The hfd for the bulk component was centered at c.a. 347kG and

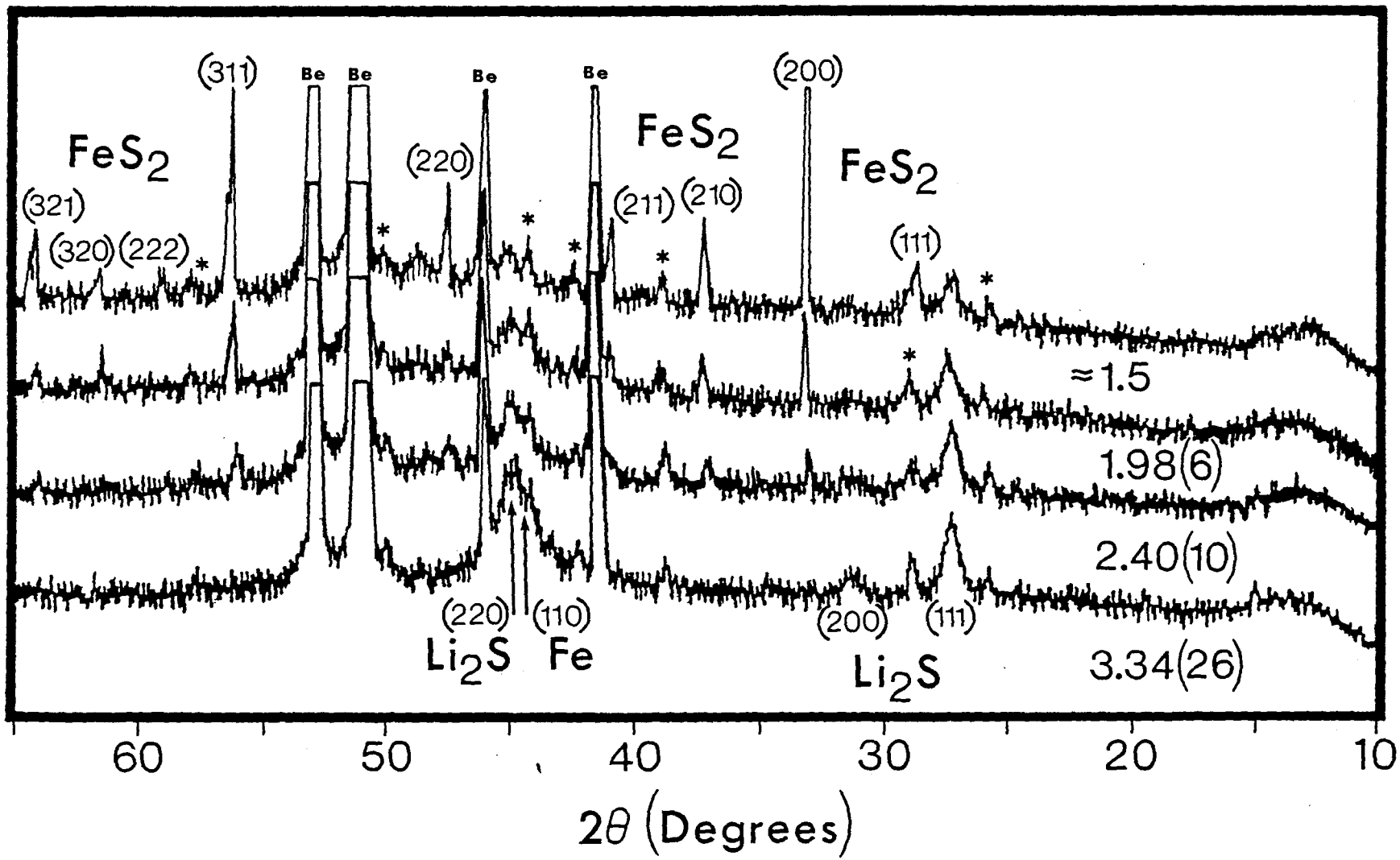

Fig. 6.21: X-ray powder diffraction spectra of chemically lithiated FeS_2 (Li_xFeS_2) samples.

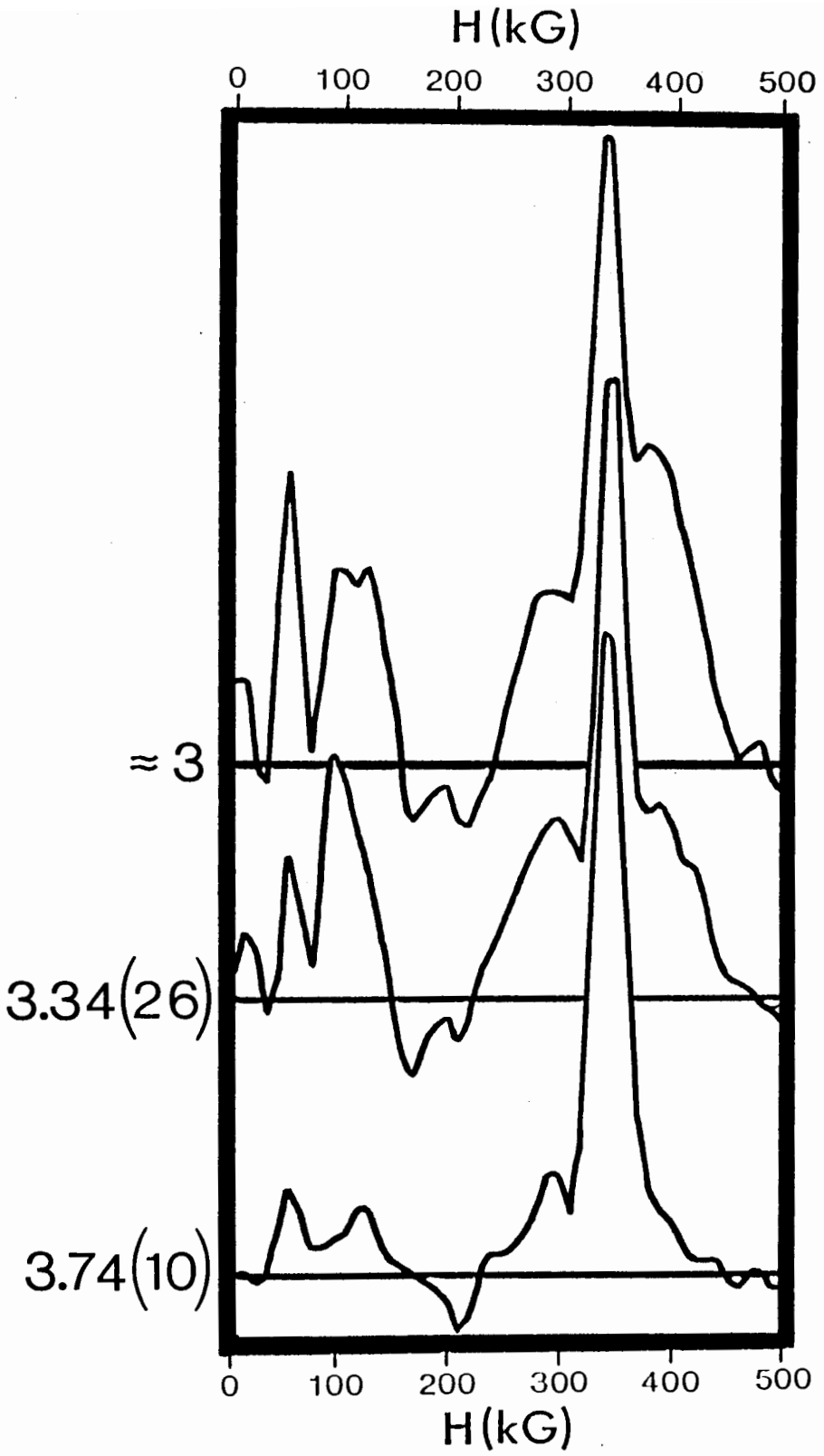

Fig. 6.22: Hyperfine magnetic field distribution plots for 4.2°K spectra of the chemically lithiated Li_xFeS_2 ($x \approx 3 \Rightarrow 3.74$) samples.

from (50), would indicate that $\langle H_{dip} \rangle \approx 0$ (i.e. the particles are superparamagnetic with negligible dipole-dipole interactions.

The hfd plots clearly show that an increase in lithiation results in a decrease in the amount of amorphous Fe° present, as well as a decrease in the contribution of surface Fe° attributed to the formation of larger Fe° particles.

VI.5 Studies of Partially and Fully Discharged FeS Cathodes.

VI.5a In situ ^{57}Fe Mössbauer of Li|$LiAsF_6$-PC|FeS Cells

Two Li|$LiAsF_6$-PC|FeS cells were discharged (500μA) to various extents at RT, afterwhich the ^{57}Fe Mössbauer absorption spectrum was recorded *in situ*. The series of spectra shown in Figure (6.23), is actually a combination of spectra obtained for the two cells #FeS-1, and #FeS-2.

Before discharge (0e-), the Mössbauer spectrum consisted of a six-line hfs due to antiferromagnetic FeS. At 75% discharge (1.5e-), essentially all of the FeS had been consumed, and the appearance of the Mössbauer spectrum was very similar to the RT ^{57}Fe Mössbauer spectra of fully discharged FeS_2 cathodes (Figs. 6.4 and 6.5). The spectrum consisted of a magnetic sextet with very broad linewidths responsible for the slope in the baseline, a broad singlet at near-zero velocity and a shoulder towards positive velocities, which had been observed in fully discharged

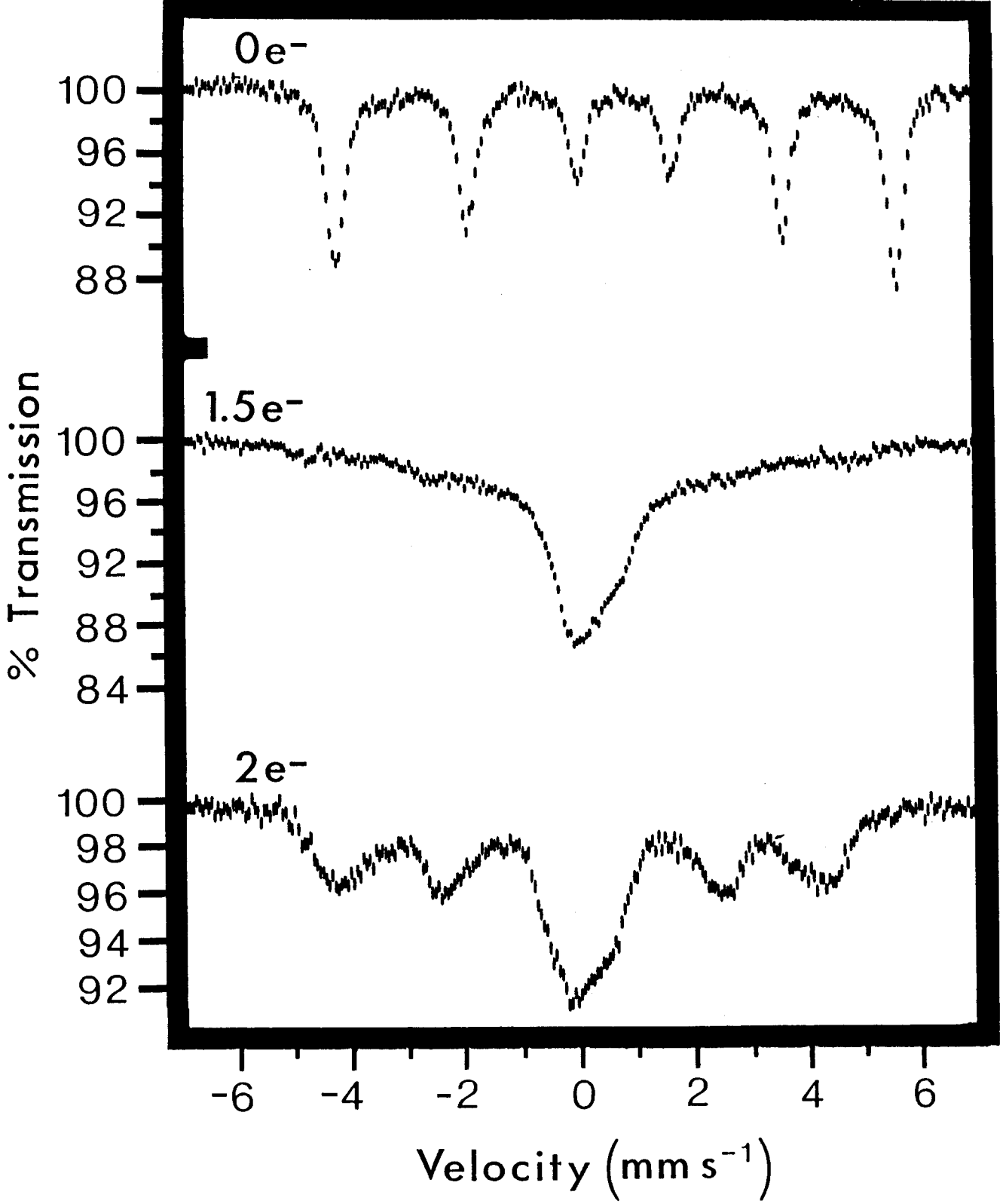

Fig. 6.23: RT *in situ* ^{57}Fe Mössbauer spectra of Li|$LiAsF_6$-PC|FeS cells #FeS-1 and #FeS-2 at various stages of discharge. The cells were discharged at RT with a drain current of 500μA.

FeS_2 cathodes.

The Mössbauer spectrum for the fully discharged cell (2e-) was similar to the RT Mössbauer spectrum of the fully discharged FeS_2 cathode #R-14 (Fig. 6.10), and some of the RT spectra of lithiated FeS_2 (Fig. 6.16). The magnetic Fe-phase is due to α-Fe particles that are too large to exhibit fast SP relaxation, but yet are not large enough to exhibit an $\langle H_{int} \rangle$ equal to H_{bulk}. This is born out by the experiments to be described below.

VI.5b ^{57}Fe Mössbauer of a Fully Discharged Li|$LiAsF_6$-PC|FeS Cathode at 295, 77.4 and 4.2°K

A cathode was removed from the fully discharged #FeS-1 cell used in the *in situ* study, and the ^{57}Fe Mössbauer spectra recorded at low temperatures (Fig. 6.24). It can be seen from the spectra at low temperatures that the only Fe-phase present in the cathode appears to be Fe° exhibiting a distribution in hfs. The absence of an appreciable hfs component due to surface Fe° would indicate that the mean particle size is greater than the particles observed in fully discharged FeS_2 cathodes.

VI.5c In Situ ^{57}Fe Mössbauer of a Li|$LiAsF_6$-PC|FeS Cell in Externally Applied Magnetic Fields

A Li|$LiAsF_6$-PC|FeS cell was discharged using a drain current of 500μA to 1 equiv. Li and then to 1.5 equiv. Li at 400μA. The

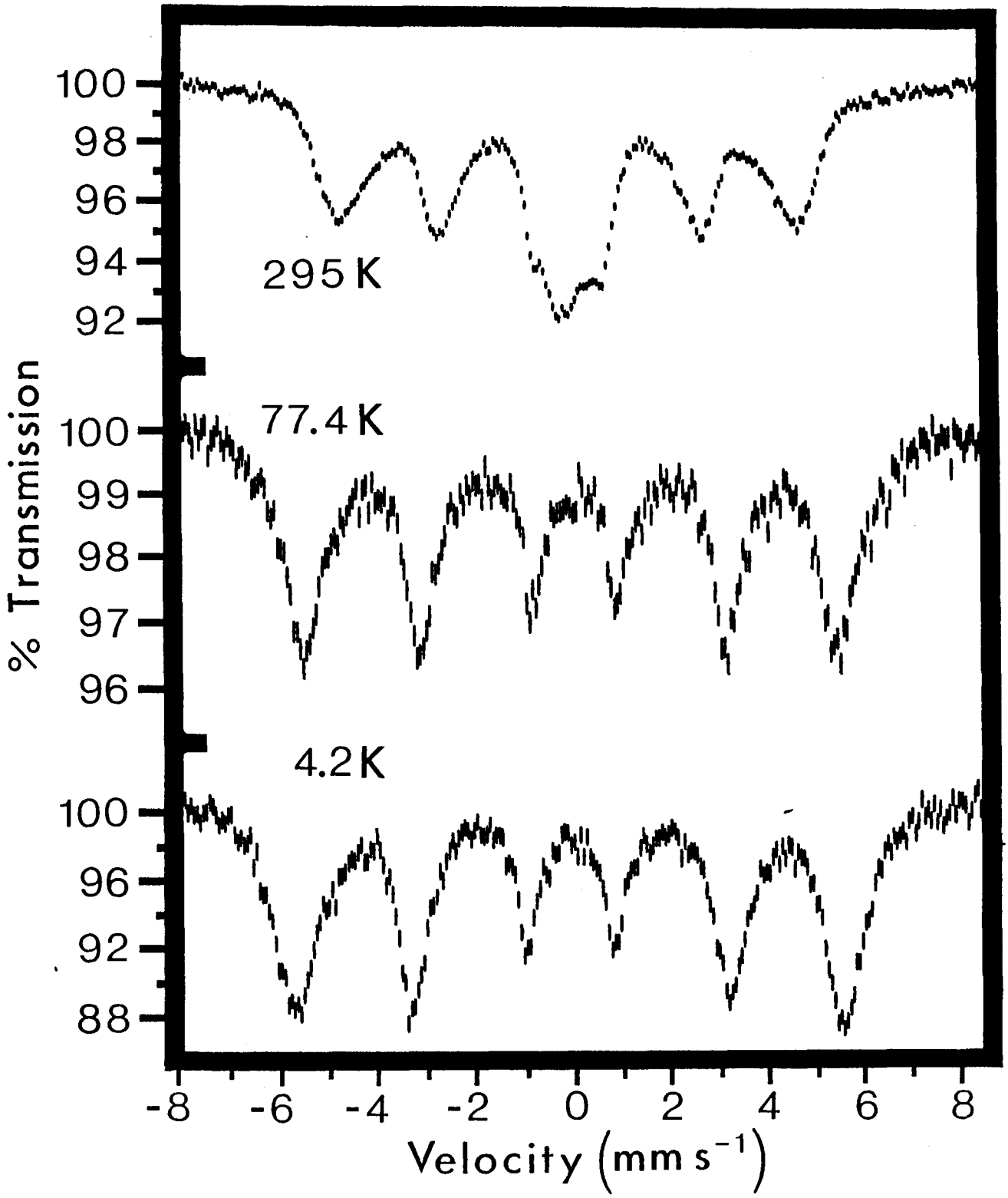

Fig. 6.24: ^{57}Fe Mössbauer spectra of the Li|LiAsF$_6$-PC|FeS cathode #FeS-1 at 295, 77.4, and 4.2°K.

^{57}Fe Mössbauer spectra were recorded *in situ* for the cell #FeS-3 in externally applied fields of various strengths at each of the steps. The direction of the external field was perpendicular to the direction of the γ-ray beam. Unfortunately the dimensions of the cell, and the voltage of the power supply limited the strength of the field produced by the small electromagnet used in these experiments to 1500G.

It can be seen from the spectra, shown in Figure (6.25), that application of a magnetic field results in partial resolution of the broad SP fraction into a magnetic hyperfine spectrum. The strength of the applied field was insufficient to allow the determination of the mean particle volume, and so the experiments merely confirmed the presence of superparamagnetism in the cathode. This is more readily seen in the spectra for the fully discharged cathode removed from the #FeS-2 cell (Fig. 6.26) before, and after the application of a stronger external field.

VI.5d Computer Analysis of the Spectra for Partially and Fully Discharged FeS Cathodes

A simple Lorentzian fit for the *in situ* hyperfine spectrum (0e-) of the Li|$LiAsF_6$-PC|FeS cathode #FeS-1 resulted in an H_{int} and an IS close to the literature parameters for pyrrhotite, or non-stoichiometric $Fe_{1-x}S$ [101]. The low-temperature spectra of the fully discharged cathode were fitted to six independent

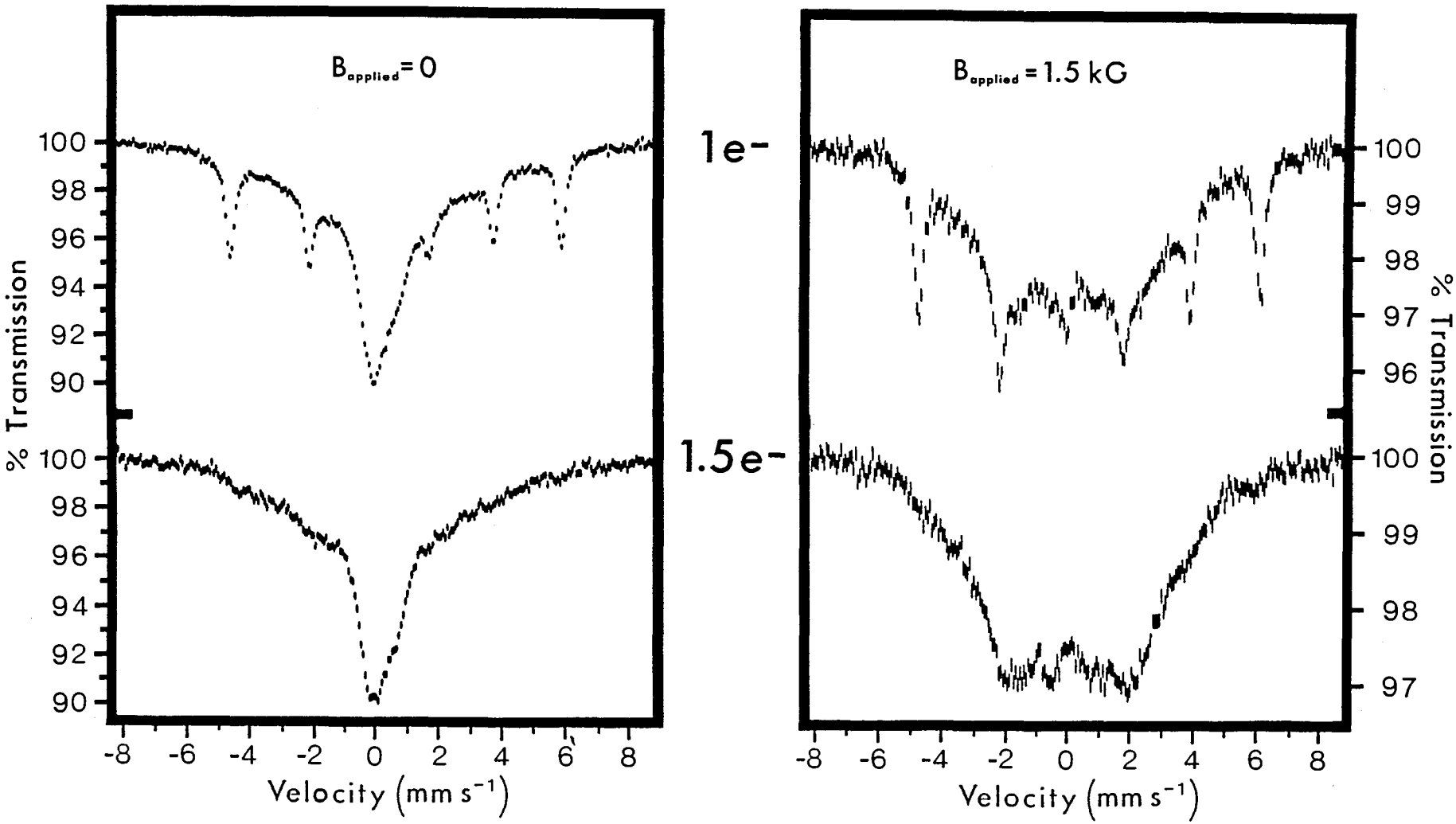

Fig. 6.25: RT *in situ* ^{57}Fe Mössbauer spectra of partially discharged Li|$LiAsF_6$-PC|FeS cell #FeS-3 with and without an applied external B of 1500G.

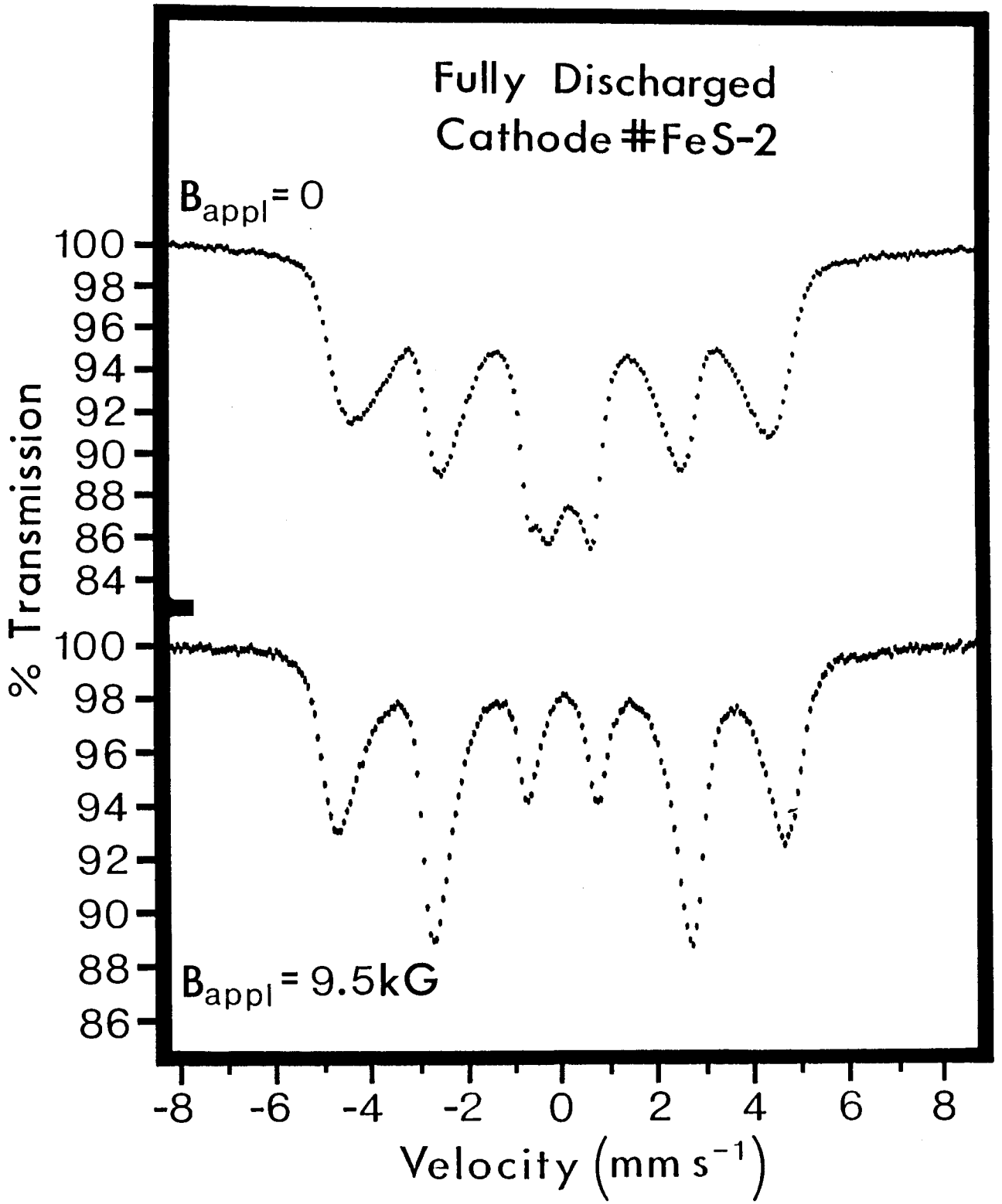

Fig. 6.26: RT ^{57}Fe Mössbauer spectra of fully discharged Li|$LiAsF_6$-PC|FeS cathode #FeS-2 with and without the application of an external B of 9500G.

Table 6.3

Mössbauer Parameters for Fully Discharged Li|$LiAsF_6$-PC|FeS Cathode #FeS-1

Component	T (°K)	Mössbauer Parameters		
		IS (mm/s)[a]	Γ (mm/s)	$\langle H_{int} \rangle$ (kG)[b]
bulk Fe°	77.4	0.06(1)	0.74(2)[c]	338(3)
bulk Fe°	4.2	0.02(1)	0.77(2)[c]	346(3)

[a]IS reported w.r.t. α-Fe foil at 295 °K.
[b]Magnetic sextet fitted as six independent Lorentzian peaks.
[c]Average of Γ for all six peaks.

Lorentzian peaks using the program MOSSFIT [102] and the results are shown in Table (6.3). At 77.4°K, the particles exhibit an $\langle H_{int} \rangle$ equal to that of the bulk material within experimental error. The $\langle H_{obs} \rangle$ measured at 4.2°K is 346(3)kG and as discussed earlier, is characteristic of SP iron.

The hfd plot for the spectrum of the fully discharged #FeS-1 cathode at 4.2°K (Fig. 6.27a) does not show an appreciable amount of amorphous Fe° or surface Fe° present. The maxima of the bulk hfd are similar to the values obtained from a Lorentzian analysis.

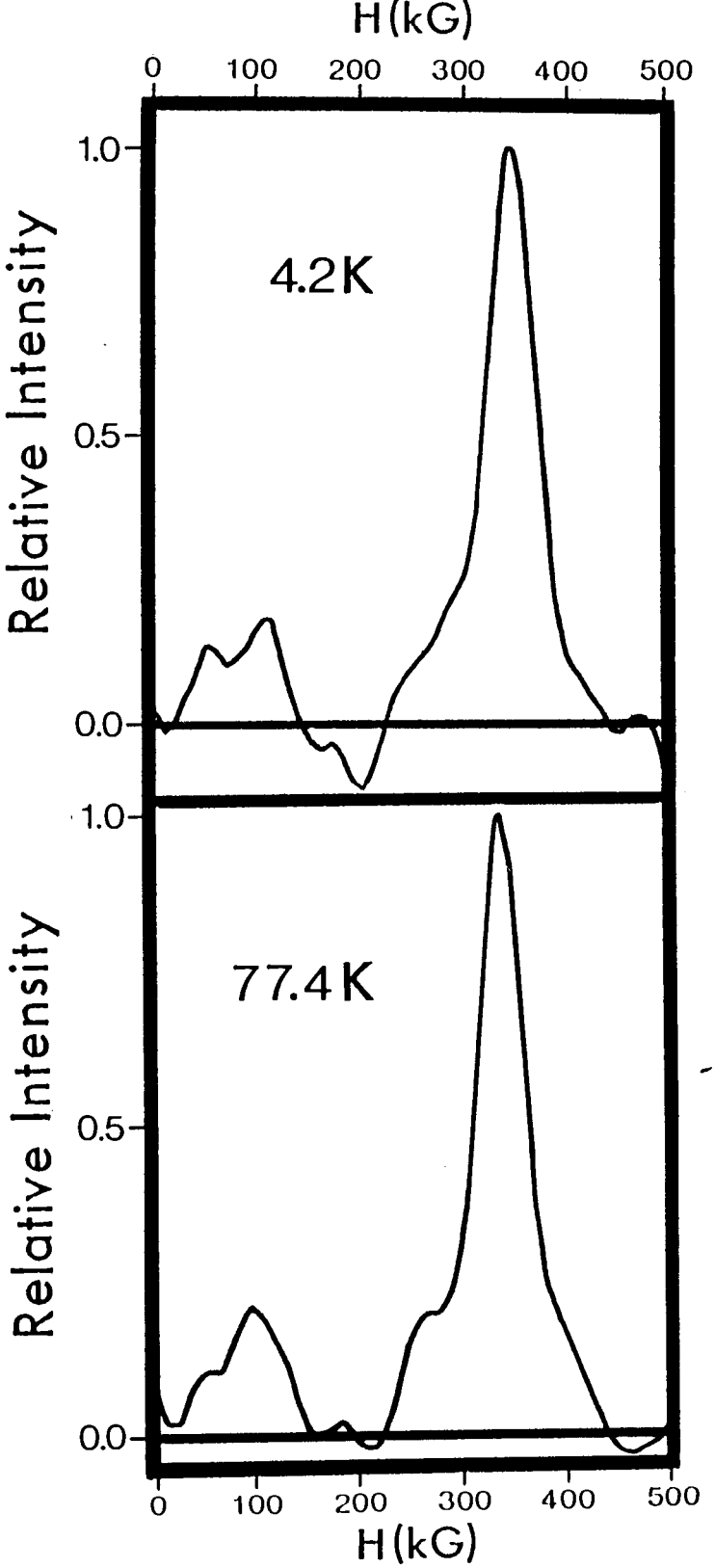

Fig. 6.27: Hyperfine field distributions plots for the low temperature spectra (Fig. 6.24) of the fully discharged Li|$LiAsF_6$-PC|FeS cathode.

VI.6 Studies on Chemically Lithiated FeS

VI.6a ^{57}Fe Mössbauer of Chemically Lithiated FeS at 295, 77.4, and 4.2°K

As in the FeS_2 study, the same FeS powder used in the cathode preparations was lithiated with n-BuLi in the ratios 1:1, 1.5 and 2 to mimic 50%, 75% and full discharge of the $Li|LiAsF_6$-PC$|FeS$ cell.

The RT ^{57}Fe Mössbauer spectrum of lithiated Li_xFeS ($x \approx 1$) (Fig. 6.28a) shows two magnetic sextets. The phase with sharp line-widths is unreacted FeS, while the other phase with broadened line-widths can be attributed to α-Fe particles with reduced H_{int}. The absorption in the centroid of the spectrum for $Li_{1.8}FeS$ is indicative of a SP fraction.

In contrast with the RT Mössbauer spectra of a discharged cell, the majority of the Fe° particles have $\tau >> \tau_L$, with only a small fraction being superparamagnetic at RT. The increase in $\langle H_{int} \rangle$ with a corresponding increase in lithiation is not as pronounced as was observed in the chemically lithiated FeS_2 samples.

In FeS_2 which has the NaCl structure, the Fe-Fe nearest neighbour distance (3.82Å) is almost 30% greater than the Fe-Fe distance in FeS (2.99Å) which has a structure closely related to that of NiAs. The closer proximity of the Fe° atoms formed upon

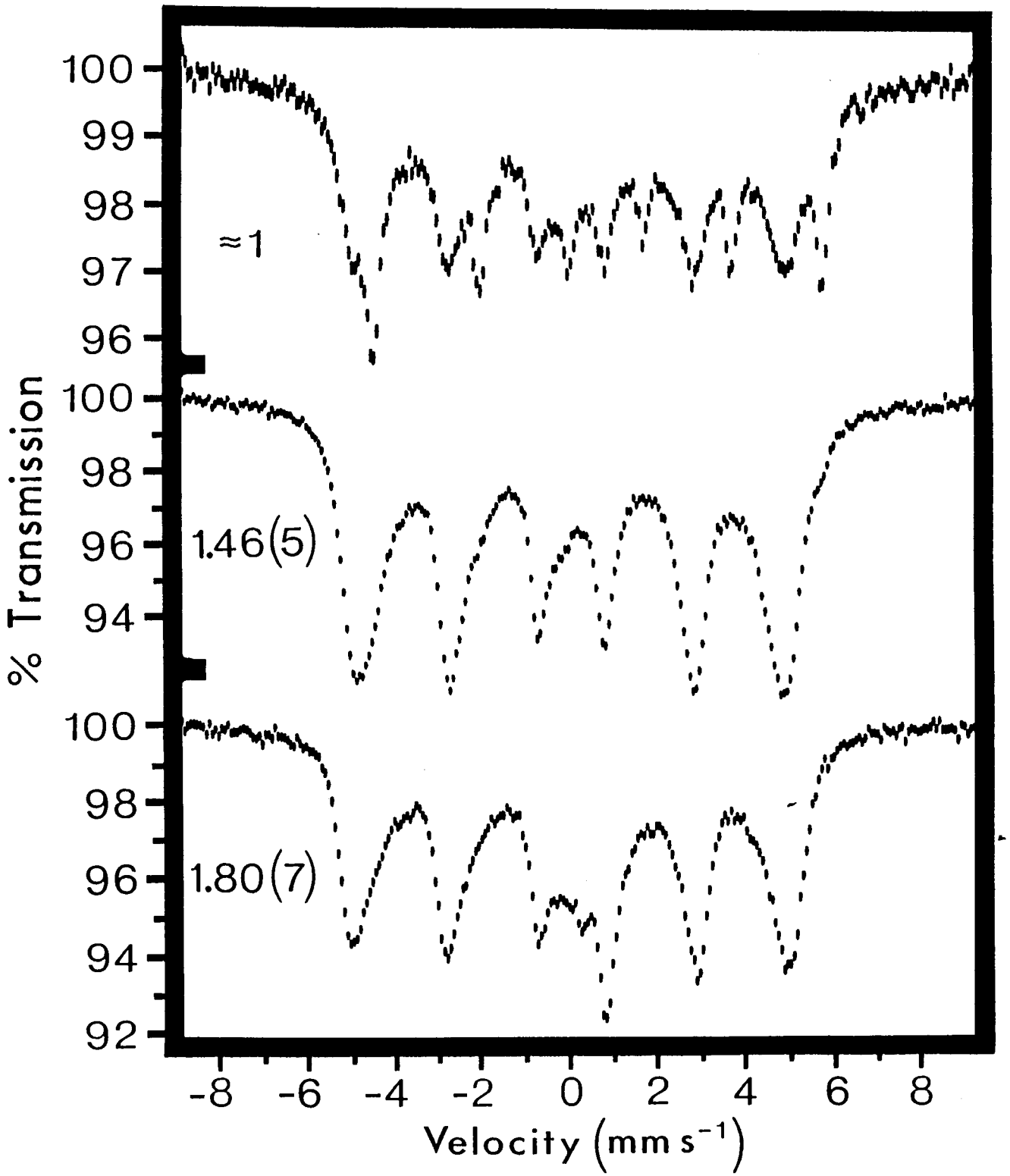

Fig. 6.28: RT ^{57}Fe Mössbauer spectra of chemically lithiated Li_xFeS ($x \approx 1 \Rightarrow 1.8$) samples.

reduction in FeS will thus favor formation of larger Fe° particles compared with FeS_2.

In the FeS_2 study, the trend which was observed in chemically lithiated FeS_2 samples was very similar to that observed in the cathodes at various stages of discharge. However, the RT Mössbauer spectra of the lithiated Li_xFeS samples (x = 1,1.46) are quite different from the analogous spectra for 50% and 75% discharged FeS cathodes (Fig. 6.23,25).

Various experimental problems involving the cryostat, and discharge of Li/FeS cells occurred during this study. As a result, no low temperature ^{57}Fe Mössbauer measurements could be obtained for FeS cathodes at intermediate stages of discharge. It is difficult therefore, to draw conclusions regarding the Fe-phases formed in the cathode since the most interesting information is usually obtained from 4.2°K measurements on partially discharged cells. It is certain, however, that the Fe° particles formed by electrochemical lithiation of FeS are much smaller than those produced through chemical lithiation.

The low temperature ^{57}Fe Mössbauer spectra of the Li_xFeS samples at 77.4°K (Fig. 6.29) and 4.2°K (Fig. 6.30) show that almost all of the FeS had been reduced to Fe° when the extent of lithiation had approached $\approx$ 1.5, and this is qualitatively similar to the results for lithiated FeS_2.

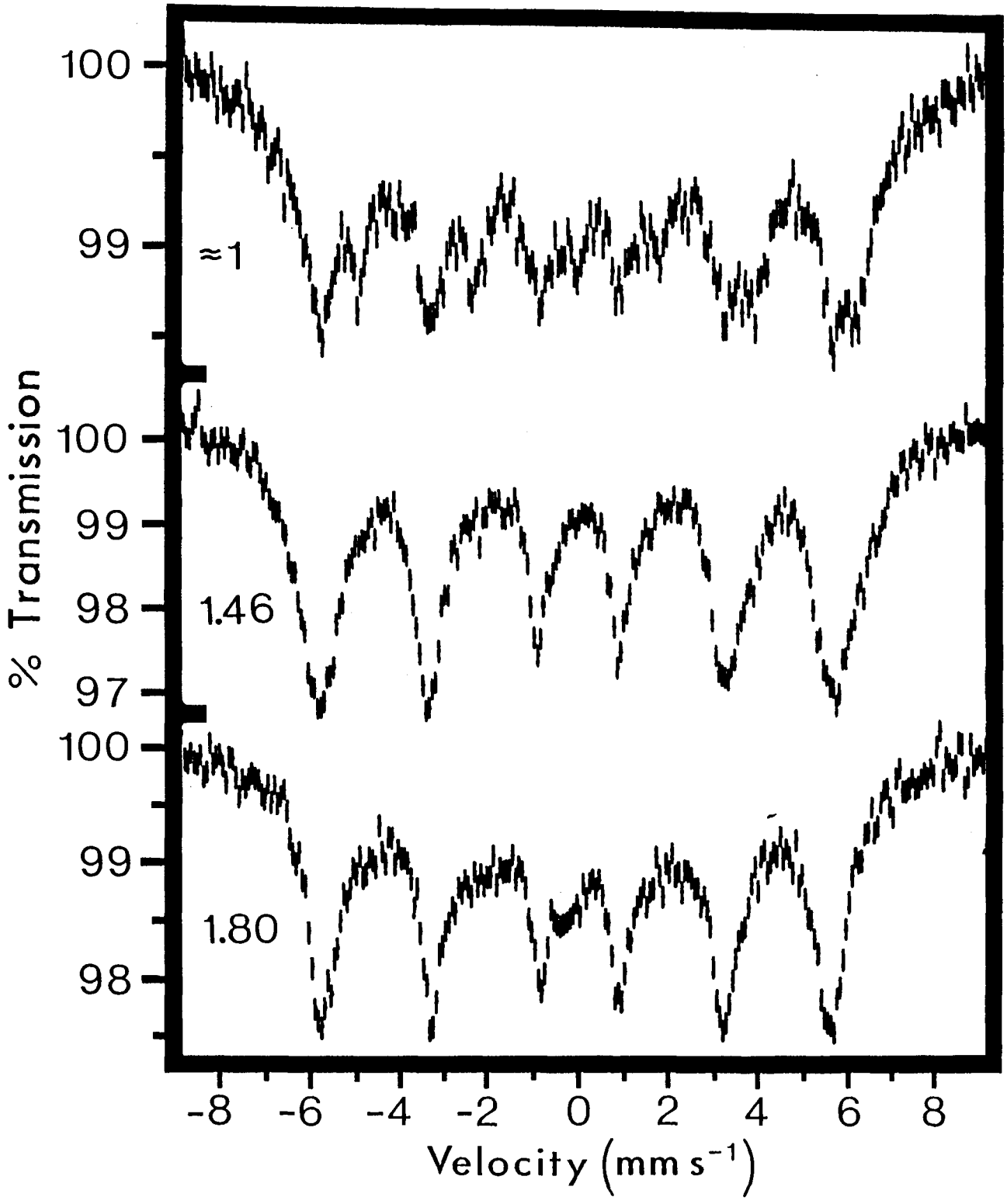

Fig. 6.29: 77.4°K ^{57}Fe Mössbauer spectra of chemically lithiated Li_xFeS ($x \approx 1 \Rightarrow 1.8$) samples.

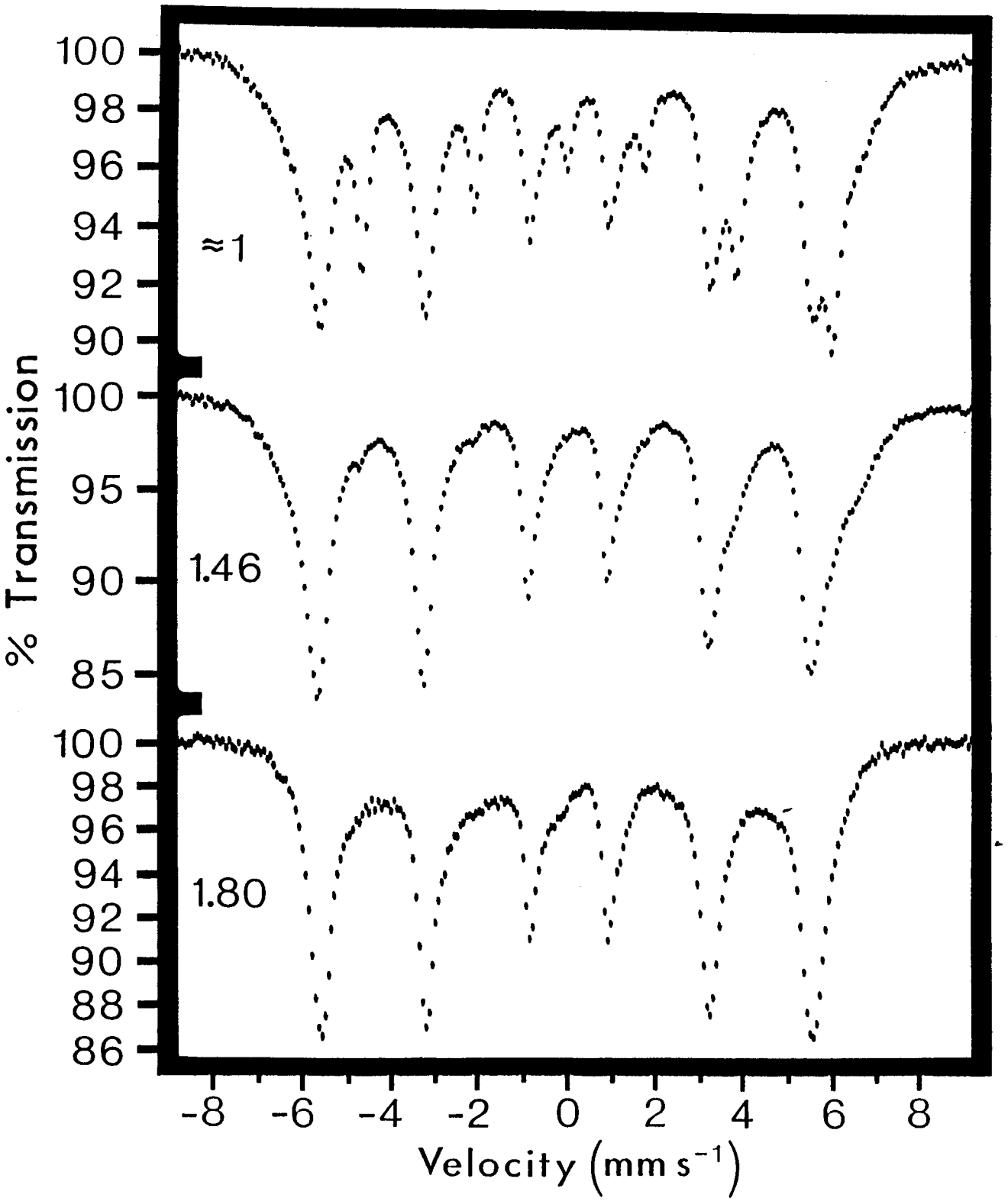

Fig. 6.30: 4.2°K ^{57}Fe Mössbauer spectra of chemically lithiated Li_xFeS ($x \approx 1 \Rightarrow 1.8$) samples.

VI.6b Computer Analysis of the Spectra for Chemically Lithiated FeS

The hfd plots for the Li_xFeS x = 1.46 and x = 1.80 RT Mössbauer spectra are shown in Figure (6.31). The maximum of the hfd is ca. 301-306kG and considerably lower than the value of 330kG for multi-domain α-Fe. As is observed in some of the chemically lithiated FeS_2 samples, the reduced hfs may arise from a small particle size.

The hfd plots for the Mössbauer spectra of the same lithiated samples at 77.4°K are shown in Figure (6.32). The x = 1.46 sample exhibits a broad symmetrical hfd centered at 357kG, while the x = 1.80 sample displayed a narrower hfd with a maximum centered at 352kG. These values are considerably higher than the H_{int} of bulk α-Fe at 77.4°K, even when the influence of the surface demagnetizing field is taken into consideration. As noted by Niemantsverdriet *et al* [103], the influence of the demagnetizing field would probably be obscured by thermal excitations at this temperature.

Recently Herr *et al* [104] have proposed a new solid state structure for nanocrystalline Fe (10-100Å polycrystals). An ^{57}Fe Mössbauer study on pure 60Å crystals of Fe° (pelletized into discs) was carried out over the temperature range of 10-300°K. At 77°K the spectra was interpreted as arising from two components: 1)20% due to bulk Fe and 2)80% due to the Fe atoms which are situated in the interphase boundaries between

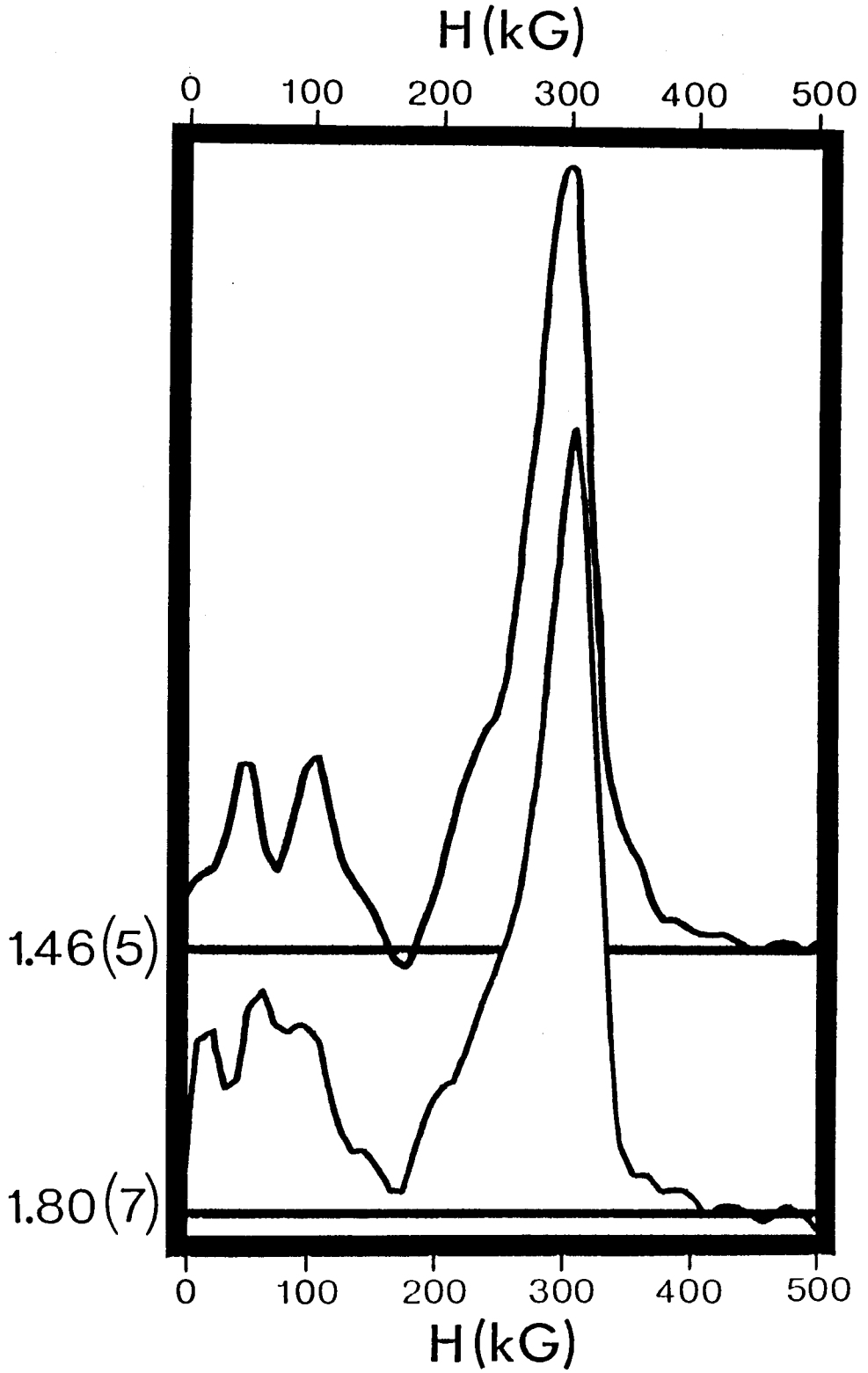

Fig. 6.31: Hyperfine magnetic field distribution plots for RT spectra of the chemically lithiated Li_xFeS (x = 1.46 and 1.80) samples.

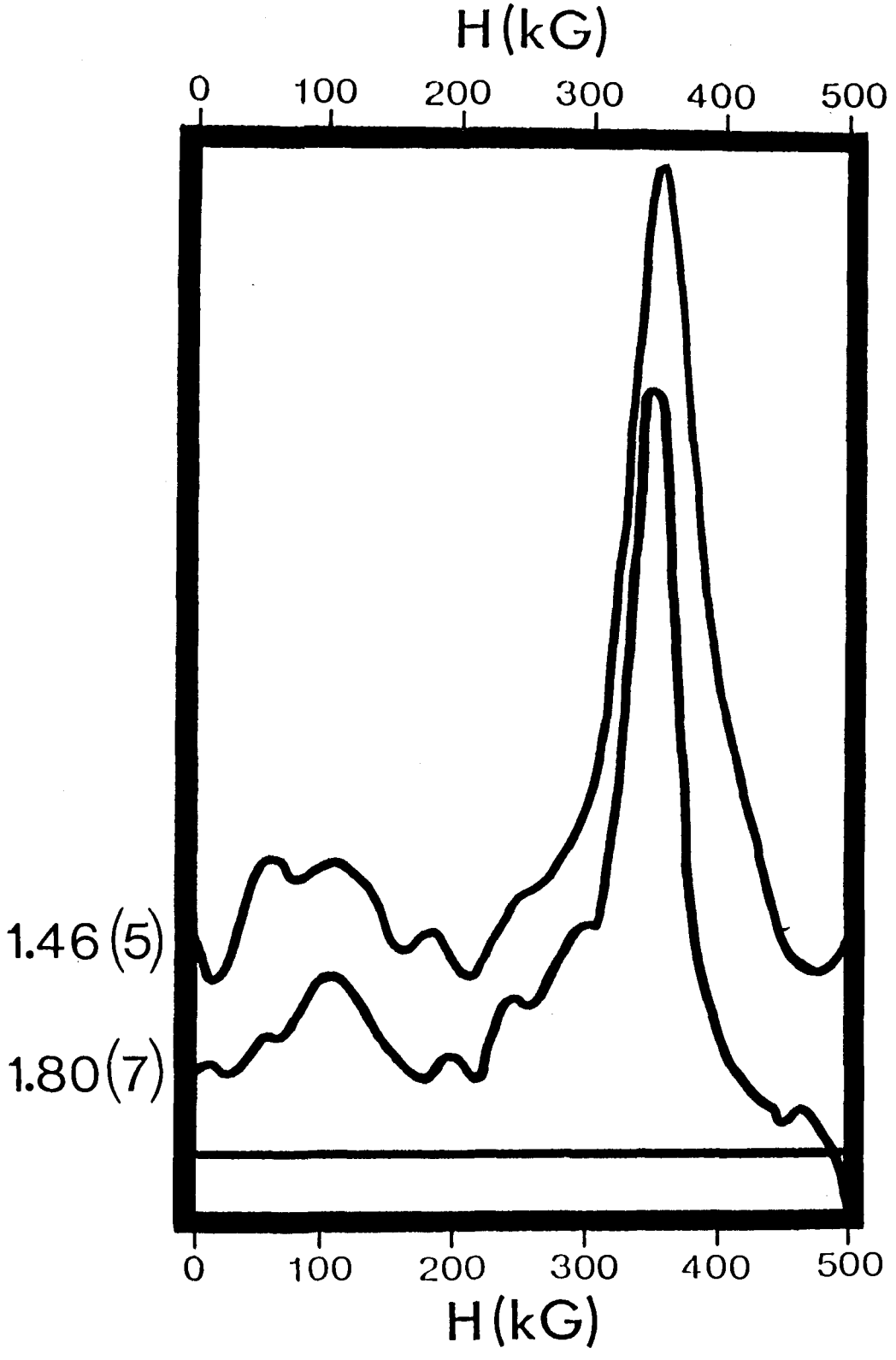

Fig. 6.32: Hyperfine magnetic field distribution plots for 77.4°K spectra of the chemically lithiated Li_xFeS (x = 1.46 and 1.80) samples.

crystallites. The results of a Lorentzian analysis on the 77°K spectrum indicated that the H_{int} of the bulk Fe° atoms was enhanced to 343kG from the influence of the interfacial component. The interfacial Fe° atoms exhibited a broad hfd with a mean $\langle H_{int} \rangle$ of 351kG. The enhancement in the H_{int} of ≈4% w.r.t. the H_{int} of iron in a b.c.c. lattice was attributed to the expansion of the nearest neighbour spacing in the interfacial component.

The Fe particles observed in our study can be thought of as clusters of Fe° microcrystallites, and hence there would also be interfacial Fe atoms throughout the cluster (Fig. 6.33). Thus the broad hfd observed for the x = 1.46 spectrum can be interpreted as the sum of hfd's arising from 1) bulk Fe° atoms with an enhanced $\langle H_{int} \rangle$ and 2) the interfacial Fe° atoms at the crystal boundaries. In the x = 1.80 sample, the mean size of the crystals must be greater resulting in a lower number of interfacial Fe° atoms, and a corresponding lower value for $\langle H_{bulk} \rangle$.

The analogous hfd plots for the 4.2°K spectra (Fig. 6.34) do not fully support this interpretation as the hfd for the bulk Fe° atoms exhibits a sharp maximum at 347kG. Thus at RT a field of 301-306kG is observed, at 77.4°K the field is 357(4)kG, and at 4.2°K the internal field is 347(4)kG. While the presence of interfacial iron can explain the greatly enhanced H_{int} at 77.4°K, the subsequent diminuition in H_{int} at 4.2°K is difficult to understand. The latter may in part be an artifact of the hfd

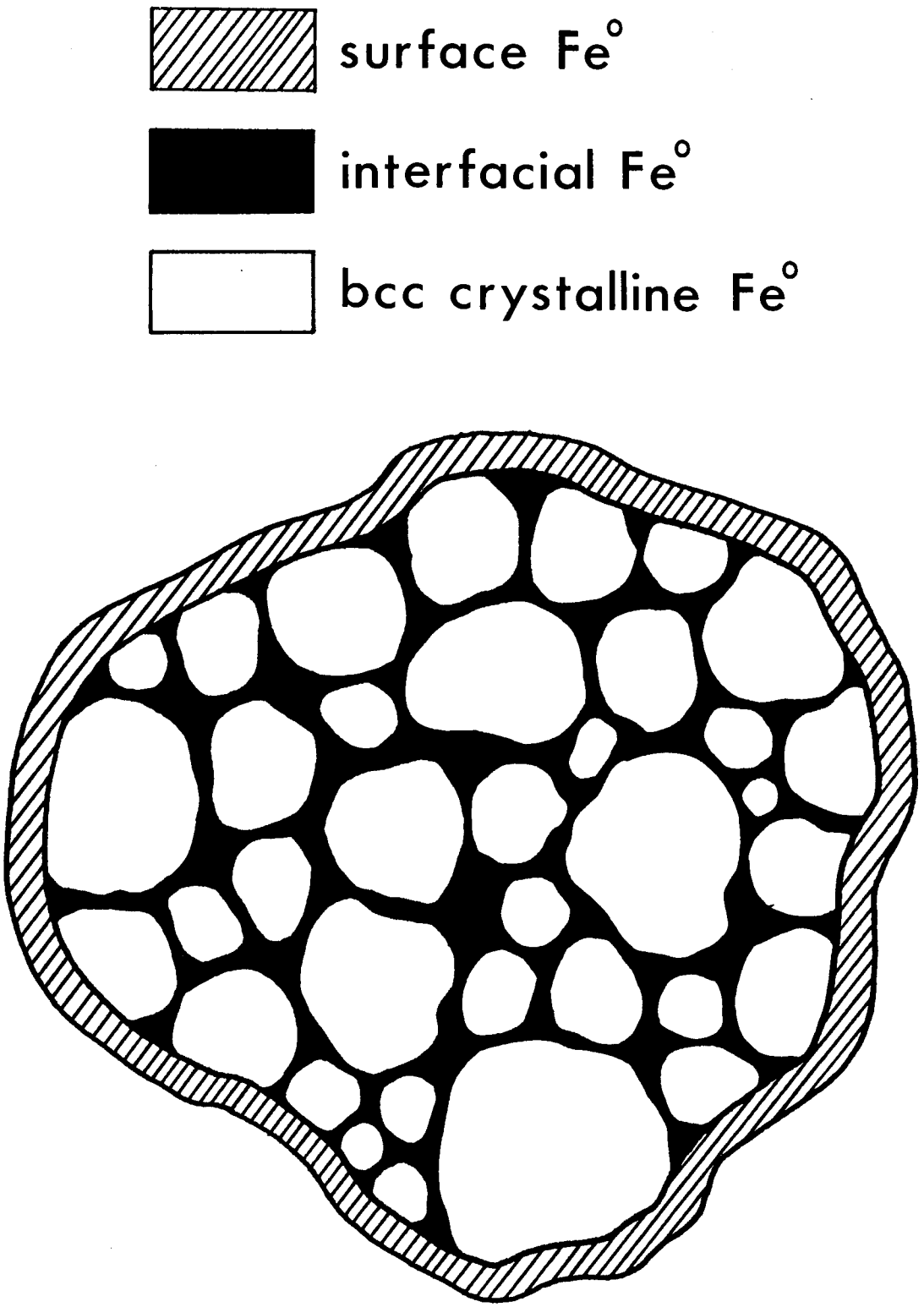

Fig. 6.33: Model of an iron microcluster showing the different phases that can be observed by Mössbauer spectroscopy at 4.2°K.

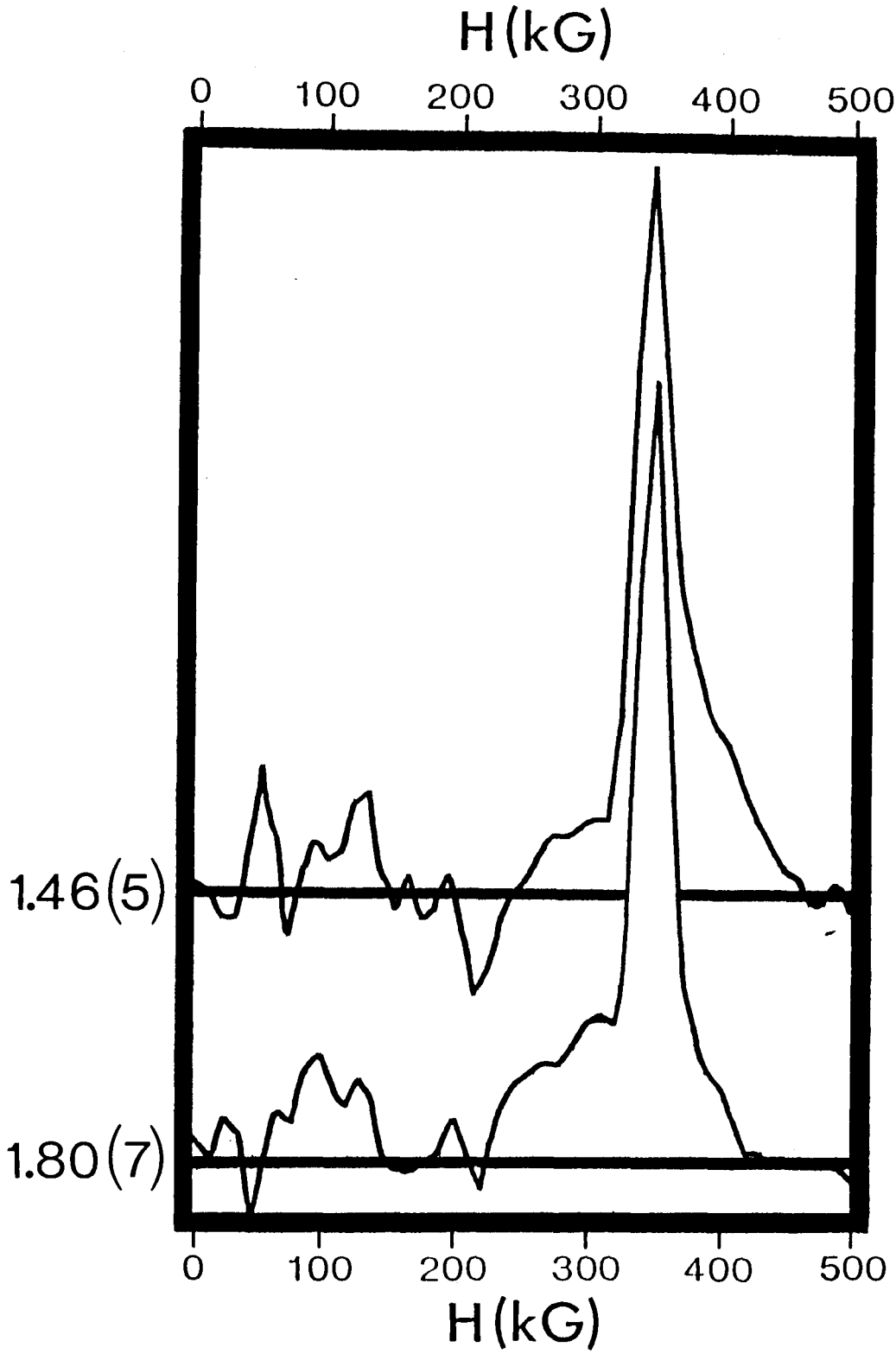

Fig. 6.34: Hyperfine magnetic field distribution plots for 4.2°K spectra of the chemically lithiated Li_xFeS (x = 1.46 and 1.80) samples.

fits. The spectra at 77.4°K exhibit broad asymmetric lines due to relaxation while those at 4.2°K are sharply resolved.

VI.7 ^{57}Fe Mössbauer of Chemically Lithiated $CuFeS_2$

VI.7a ^{57}Fe Mössbauer of Li_4CuFeS_2 at 295, 77.4 and 4.2°K

The ^{57}Fe Mössbauer spectra of chemically lithiated chalcopyrite Li_4CuFeS_2 were recorded at 295, 77.4, and 4.2°K (Fig. 6.35). The spectra are qualitatively similar to the spectra for the fully discharged $Li|LiClO_4$-PC$|FeS_2$ cathode #R-4 at the same temperatures. The 4.2°K spectrum can be attributed to SP α-Fe particles and contributions from surface atoms. The RT spectrum, and the 77.4°K spectrum, neither of which shows any hfs, indicate that the Fe° particles produced in this sample are considerably smaller than the Fe° particles produced in FeS_2 chemically lithiated to the same extent (Fig. 6.16).

VI.7b Variable Temperature ^{57}Fe Mössbauer of Li_4CuFeS_2

The ^{57}Fe Mössbauer spectra for the Li_xCuFeS_2 ($x = 4$) sample between ≈60° and 15°K are shown in Figure (6.36). This series of experiments was conducted using the variable temperature apparatus of the UBC Mössbauer group. The counting statistics were poor, the percent effect low and the linewidths broad. Nevertheless, this series of spectra showed that as the temperature was lowered the SP fraction decreased with an

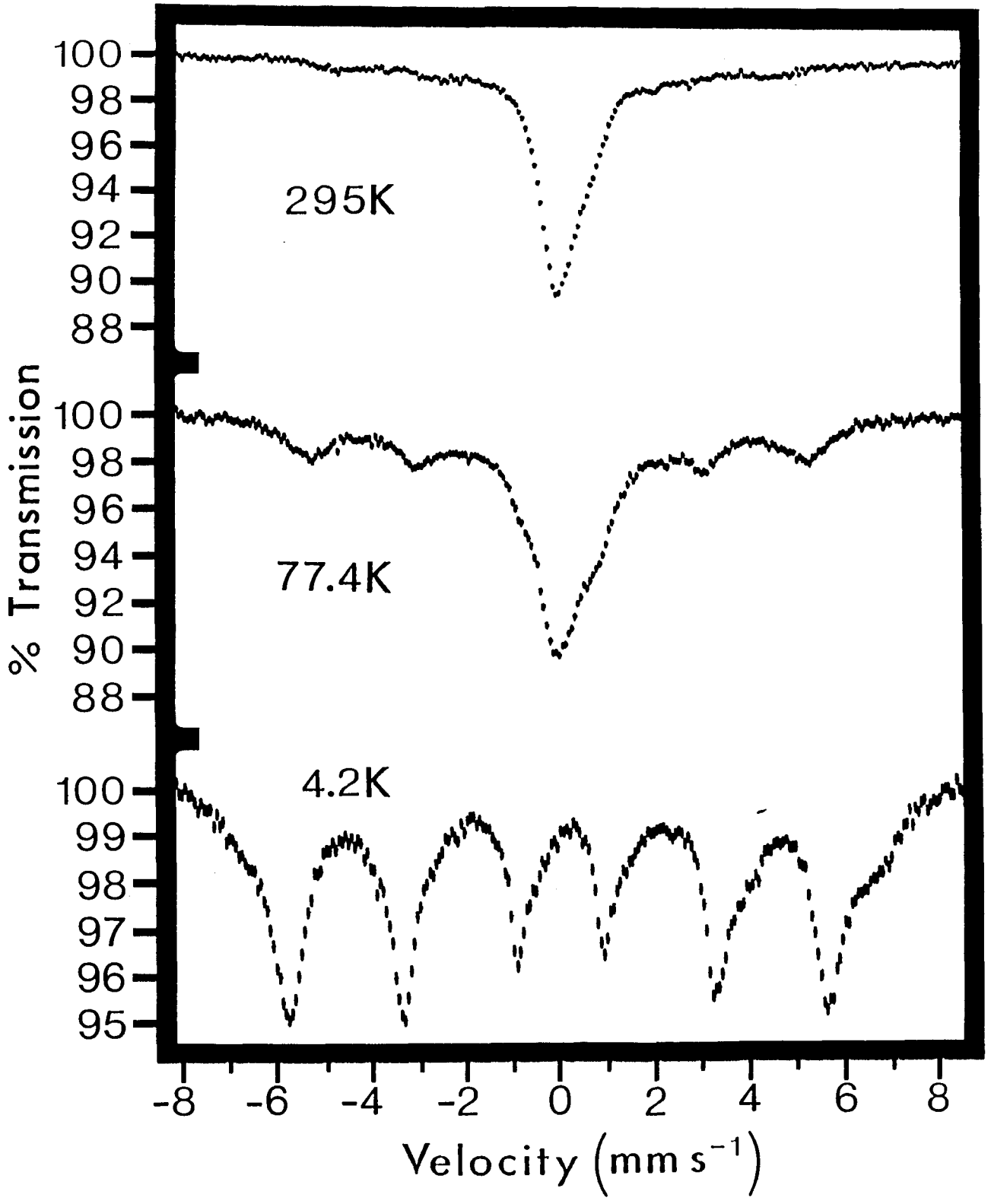

Fig. 6.35: ^{57}Fe Mössbauer spectra of Li_4CuFeS_2 at 295, 77.4, and 4.2°K.

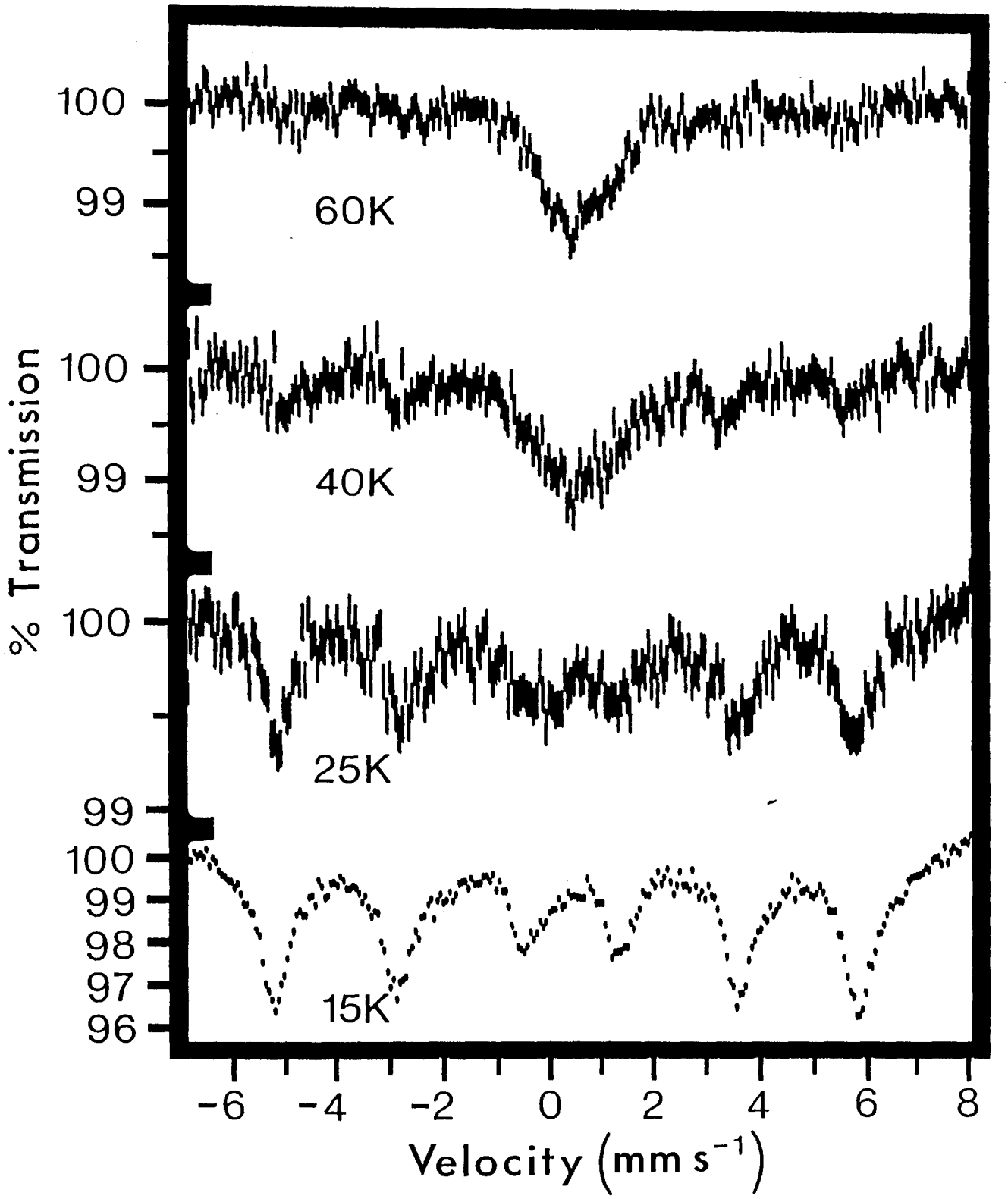

Fig. 6.36: ^{57}Fe Mössbauer spectra of Li_4CuFeS_2 between 60 and 15°K

associated increase in the magnetic component. From these spectra a value for the blocking temperature, T_B, was estimated to be $\approx 35 \pm 5°K$.

VI.7c ^{57}Fe Mössbauer of Li_4CuFeS_2 in Externally Applied Magnetic Fields

The RT ^{57}Fe Mössbauer spectra of the Li_4CuFeS_2 sample in an external magnetic field, applied perpendicular to the direction of the γ-ray beam, are shown in Figure (6.37). It can be seen from the spectra that some of the particles exhibit hfs in the presence of an external field as low as 1500G. As was discussed in VI.5c, the dimensions of the electromagnet and the limitations of the power supply were insufficient to produce the required field strength necessary in order to use the high field approximation, (37), for determination of the mean particle size. Thus while these experiments confirm the presence of superparamagnetism in the sample, they do not allow a determination of particle size.

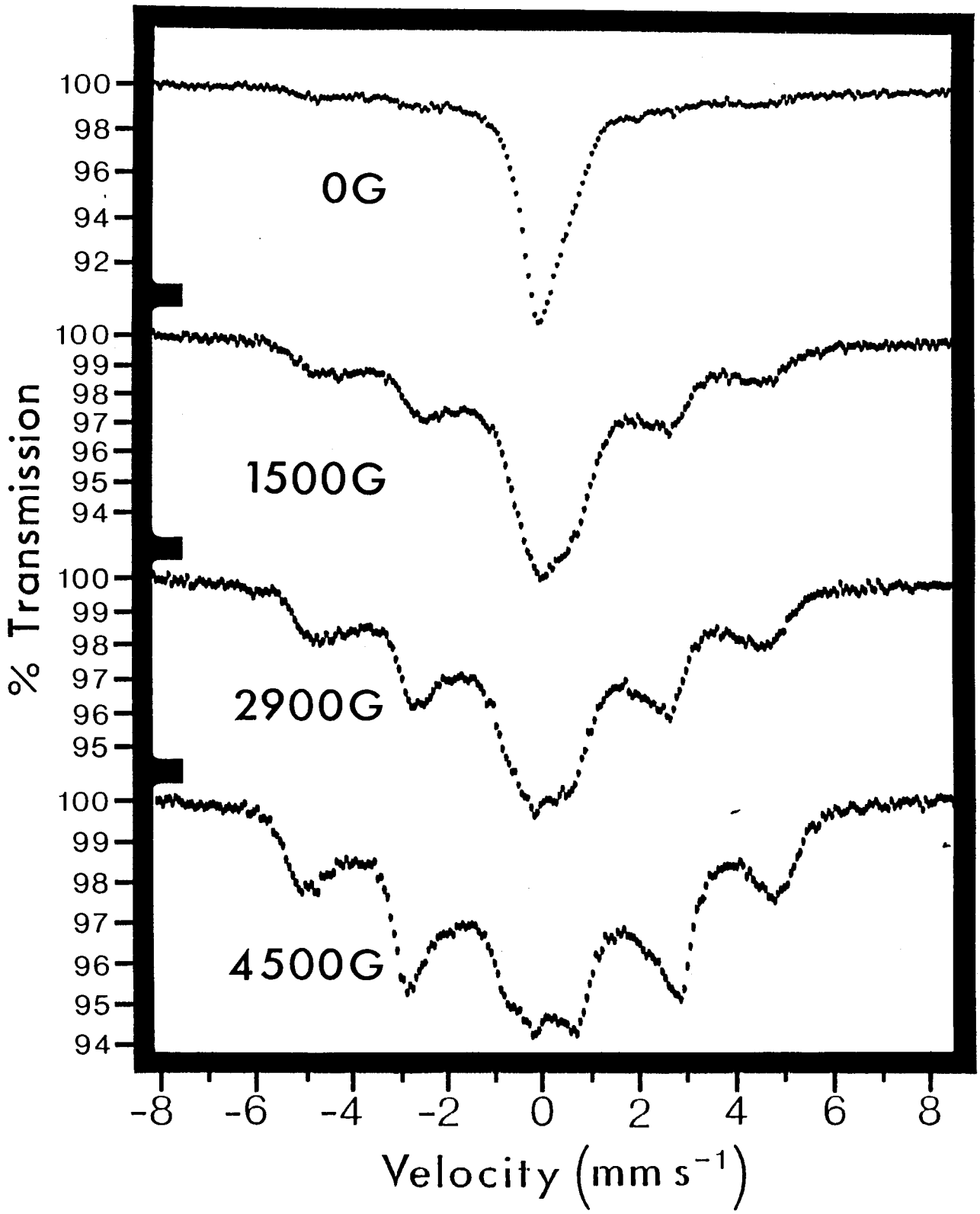

Fig. 6.37: RT ^{57}Fe Mössbauer spectra of Li_4CuFeS_2 in the presence of various external magnetic fields.

VII. CONCLUSIONS

1. The RT Mössbauer experiments were not very informative (cf. Clark's attempts). The *in situ* measurements in particular, were not as practical or as useful as we thought they might be. Nevertheless Mössbauer spectroscopy has proved to be a useful technique for studying the mechanism of discharge in these battery systems.

2. Thus low temperature Mössbauer and external magnetic field measurements provided very detailed information about the physical form of the iron particles formed in fully reduced FeS_2 cathodes. This is the first time that such measurements have been carried out on reduced cathodes. The average particle diameter of the iron in one of the cathodes was estimated to be 27 ± 1Å. It is of some interest that these experiments have provided examples of:

   i) superparamagnetism,
   ii) superferromagnetism,
   iii) surface effects,
   and iv) collective magnetic excitations

   all in the same system.

3. The formation of intermediates during discharge was found to be dependent on the rate of discharge and electrolyte. While no evidence for Li_2FeS_2 was found in FeS_2 cathodes discharged

at RT or at 55°C there was possible evidence for $Li_3Fe_2S_4$, (and other Li_xFeS_2 phases). Elemental iron was formed early in the discharge cycle as proposed by Clark *et al* [84]. The formation of iron particles:

$$FeS_2 \longrightarrow (Li_xFeS_2) \longrightarrow Fe^\circ$$

proceeds rapidly without attaining thermodynamic equilibrium and as a result only small quantities of intermediate are observed during discharge.

4. The mechanism for the discharge of an Li/FeS cell is apparently a one step process. No evidence for any intermediate(s) was obtained although low temperature spectra on partially discharged cathodes were not carried out. The iron particles present in fully reduced cathodes are larger than that found in analogous FeS_2 cathodes with comparable electrolyte and rate of discharge. This may in part be due to the difference in crystal structure of FeS compared with FeS_2 or different particle sizes in these two materials.

5. The Fe° particles produced upon chemical lithiation of $LiCuFeS_2$ are considerably smaller than the Fe° particles formed from FeS_2 chemically lithiated to the same extent.

6. This work has provided new information about Li_2FeS_2 and the first Mössbauer measurements on $Li_3Fe_2S_4$.

VII.2 Suggested Further Studies

The complexity of the Mössbauer spectrum of Li_2FeS_2 at 4.2°K suggests that further measurements between 77.4 and 4.2°K will be required to allow an interpretation of the spectra in terms of the various magnetic hfs components. It appears that some of the iron sites in Li_2FeS_2 at 4.2°K also experience electric quadrupole perturbations, and further experiments will be required to determine the magnetic properties.

The compound $Li_3Fe_2S_4$ is interesting as it possesses an internal magnetic field and a signicant electric quadrupole interaction. It is not possible to determine the hyperfine parameters such as H_{int}, the asymmetry parameter η, and the quadrupole coupling constant $\frac{1}{4}e^2qQ$ from the spectrum without first knowing the angle between the electric field gradient (EFG) tensor and the direction of the internal magnetic field. An x-ray crystal structure of $Li_3Fe_2S_4$ will be required to allow such an analysis.

While the *in situ* RT Mössbauer experiments did not prove to be very informative, future experiments in the presence of an applied external magnetic field could provide a method for *in situ* iron particle-size determination. The average Fe° particle size could be determined for different discharge rates and/or electrolytes. Similarily a study on the iron particle size at different stages of recharge should provide further insight into the poor reversibility of the Li/FeS_2 cell. These

experiments should be carefully designed and carried out in a short period of time in order to minimize the effects of diffusion of the particles to form larger particles. The external magnetic fields should also be large enough (~1T) in order to use the high field approximation for particle-size determination, and measurements must be carried out above the blocking temperature of the particles.

The work on the Li/FeS system is incomplete and will require low temperature Mössbauer experiments on partially discharged cathodes to determine whether intermediates are indeed formed. The *in situ* experiments discussed previously can also be extended for the Li/FeS system.

VIII. REFERENCES

[1] J.R.Gosselin, M.G.Townsend, and R.J.Tremblay, *Solid State Commun.*, **19**, 799, (1976).

[2] R.C.Cannon, C.C.Stone, and R.A.Wiesboeck, *Power Sources for Biomedical Implantable Applications and Ambient Temperature Lithium Batteries*, B.B.Owens and N.Margalit, Eds., 321, The Electrochemical Society, Inc., (1980).

[3] A.N.Dey, and B.P.Sullivan, *J. Electrochem. Soc.*, **117**, 222, (1970).

[4] G.Eichinger, *J. Electroanal. Chem.*, **74**, 183, (1976).

[5] S.B.Brummer, V.R.Koch, and R.D.Rauh, *Materials for Advanced Batteries*, D.W.Murphy, J.Broadhead and B.C.H.Steele, Eds., 123, Plenum Press, (1980).

[6] Y.Geronov, F.Schwager, and R.H.Muller, *J. Electrochem. Soc.*, **129**, 1422, (1982).

[7] G.Nazri, and R.H.Muller, *J. Electrochem. Soc.*, **132**, 1385, (1985).

[8] D.R.Vissers, Z.Tomczuk, and R.K.Steunenberg, *J. Electrochem. Soc.*, **121**, 665, (1974).

[9] R.A.Sharma, *J. Electrochem. Soc.*, **123**, 448, (1976).

[10] A.E.Martin, and Z.Tomczuk, *High Performance Batteries for Stationary Energy Storage and Electric Vehicle Propulsion: Progress Report for the Period October-December 1976*, Eds., P.A.Nelson *et al.*, **ANL-17-17**, 45-46, (April 1977).

[11] A.E.Martin, Z.Tomczuk, and M.F.Roche, *Argonne National Laboratory Report ANL-78-94*, 167, (1978).

[12] Z.Tomczuk, M.F.Roche and A.E.Martin, *Argonne National Laboratory Report ANL-79-39*, 66, (1979).

[13] Z.Tomczuk, S.K.Preto, and M.F.Roche, *J. Electrochem. Soc.*, **128**, 760, (1981).

[14] Z.Tomczuk, B.Tani, N.C.Otto, M.F.Roche, and D.R.Vissers, *J. Electrochem. Soc.*, **129**, 925, (1982).

[15] M.S.Whittingham, *Prog. Solid. St. Chem.*, **12**, 41-49, (1978).

[16] R.Brec, A.Dugast, and A.LeMehaute, *Mater. Res. Bull.*, **15**, 619, (1980).

[17] A.Dugast, R.Brec, G.Ouvard, and J.Rouxel, *Solid State Ionics*, **5**, 375, (1981).

[18] M.B.Clark, *Lithium Batteries*, J.P.Gabano, Ed., 115-136, (1984).

[19] C.Iwakura, N.Isobe and, H.Tamura, *Electrochimica Acta*, **28**, 277, (1983).

[20] H.Ikeda, S.Narukawa, and S.Nakaido, *21st Battery Symposium in Japan, Okayama*, Extended Abstract, 47, (November 1980).

[21] W.E.Aker, N.Margalit, D.P.Johnson, R.J.Ekern, N.A.Fleischer, and R.J.Brodd, *J. Electrochem. Soc.*, **131**, 1839, (1984).

[22] L.Néel, *Ann. Geophys.*, **5**, 99, (1949).

[23] W.F.Brown Jr., *J. Appl. Phys.*, **30**, suppl., 130S, (1959).

[24] W.F.Brown Jr., *J. Appl. Phys.*, **34**, 1319, (1963).

[25] W.F.Brown Jr., *Phys. Rev.*, **130**, 1677, (1963).

[26] H.H.Wickman, *Mössbauer Effect Methodology*, I.J.Gruverman, Ed., **2**, 39, Plenum Press, New York, (1966).

[27] S.Mørup, and H.Topsøe, *Appl. Phys.*, **11**, 63, (1976).

[28] S. Mørup, *Proc. Internat. Conf. Mössbauer Spectroscopy, Jaipur, India*, 178, (1981).

[29] J.E.Knudsen, and S.Mørup, *J. Phys.*, **41**, C1-155, (1980).

[30] G.von Eynatten, and H.E.Bömmel, *Appl. Phys.*, **14**, 415, (1977).

[31] C.S.Wang, and A.J.Freeman, *Phys. Rev.*, **B24**, 4364, (1981).

[32] S.Ohnishi, A.J.Freeman, and M.Weinert, *Phys. Rev.*, **B28**, 6741, (1983).

[33] S.Ohnishi, W.Weinert, and A.J.Freeman, *Phys. Rev.*, **B30**, 36, (1984).

[34] T.Shinjo, *J. Phys. (Paris) Colloq.*, **40**, (C-2), 63, (1979).

[35] H.Topsøe, J.A.Dumesic, and S.Mørup, *Applications of Mössbauer Spectroscopy*, R.L.Cohen, Ed., **Vol. II**, Academic Press, New York, 55, (1980).

[36] J.C.Walker, *International Conference on the Applications of the Mössbauer Effect, Jaipur, India*, Indian National Science Academy, New Delhi, 21, (1982).

[37] J.Korecki, *Hyperfine Interactions*, **40**, 89, (1988).

[38] W.Keune, J.Lauer, U.Gonser, and D.L.Williamson, *J. Phys. (Paris) Colloq.*, **40**, (C-2), 69, (1979).

[39] J.Lauer, W.Keune, and T.Shinjo, *Physica B+C*, **86 Part 3**, 1409, (1973).

[40] A.H.Owens, C.L.Chien, and J.C.Walker, *J. Phys. (Paris) Colloq.*, **40**, (C-2), 74, (1979).

[41] J.Korecki, and U.Gradmann, *Hyperfine Interactions*, **28**, 931, (1986).

[42] S.Hine, T.Shigematsu, T.Shinjo, and T.Takeda, *J. Phys. (Paris) Colloq.*, **40**, (C-2), 84, (1979).

[43] G.P.Stern, Z.O.Qiu, H.Tang, and J.C.Walker, *Hyperfine Interactions*, **41**, 709, (1988).

[44] R.Droste, G.Stern, and J.C.Walker, *J. Mag. Magn. Mat.*, **54-57**, 763, (1986).

[45] T.Shinjo, S.Hine, and T.Takeda, *J. Phys. (Paris) Colloq.*, **40**, (C-2), 86, (1979).

[46] J.L.Dormann, P.Renaudin, P.Gibart, and C.Sella, *J. Phys. (Paris) Colloq.*, **40**, (C-2), 96, (1979).

[47] J.L.Dormann, P.Gibart, and P.Renaudin, *J. Phys. (Paris) Colloq.*, **37**, (C-6), 281, (1976).

[48] T.Furubayashi, I.Nakatani, and N.Saegusa, *J. Phys. Soc. Jpn.*, **56**, 1855, (1987).

[49] H.M.Ziethen, G.Doppler, and A.X.Trautwein, *Hyperfine Interactions*, **42**, 1109, (1988).

[50] T.Nakamura, T.Shinjo, Y.Endoh, N.Yamamoto, M.Shiga, and Y.Nakamura, *Phys. Lett.*, **12**, 178, (1964).

[51] W.T.Oosterhuis, and K.Spartalian, *Applications of Mössbauer Spectroscopy*, R.L.Cohen, Ed., **Vol. I**, 141, Academic Press, New York, (1976).

[52] G.W.Simmons, and H.Leidheiser, *Applications of Mössbauer Spectroscopy*, R.L.Cohen, Ed., **Vol. I**, 85, Academic Press, New York, (1976).

[53] C.E.Johnson, and G.P.Glasby, *Nature (London)*, **222**, 376, (1969).

[54] R.M.Housley, R.W.Grant, A.H.Muir, M.Blander, and Abdel-Gawad, *Proc. Lunar Sci. Conf. Geochim. Cosmochim. Acta, 2nd, Suppl. 2*, **3**, 2125, (1971).

[55] D.W.Collins, J.T.Dehn, ad L.N.Mulay, *Mössbauer Effect Methodology*, I.J.Gruverman, Ed., **3**, 103, Plenum Press, New York, (1967).

[56] S.Mørup, J.A.Dumesic, and H.Topsøe, *Applications of Mössbauer Spectroscopy*, R.L.Cohen, Ed., **Vol. II**, Academic Press, New York, (1980).

[57] J.L.Dormann, *Rev. Phys. Appl.*, **16**, 275, (1981).

[58] S.Mørup, *Mössbauer Spectroscopy Applied to Inorganic Chemistry*, G.J.Long, Ed., **Vol. II**, 89, Plenum Press, New York, (1987).

[59] M.B.Madsen, S.Mørup, C.J.W.Koch, and O.K.Borggaard, *Surface Science*, **156**, 328, (1985).

[60] S.Mørup, and H.Topsøe, *Proc. Int. Conf. Mössbauer Spectrosc., Bucharest, Romania*, D.Barb, and D.Tarina, Eds., 229, (1977).

[61] S.Mørup, B.S.Clausen, and H.Topsøe, *J. Phys.*, **40**, C2-78, (1979).

[62] S.Mørup, B.R.Christensen, J.van Wonterghem, M.B.Madsen, S.W.Charles, and S.Wells, *J. Magn. Magn. Mat.*, **67**, 249, (1987).

[63] P.H.Christensen, S.Mørup, and J.W.Niemantsverdriet, *J. Phys. Chem.*, **89**, 4898, (1985).

[64] B.Rodmacq, *J. Phys. Chem. Solids*, **45**, 1119, (1984).

[65] S.Mørup, and H.Topsøe, *Appl. Phys.*, **11**, 63, (1976).

[66] S.Mørup, H.Topsøe, and J.Lipka, *J. Phys. (Paris) Colloq.*, **37** (C-6), 287, (1976).

[67] G.B.Raupp, and W.N.Delgass, *J. Catal.*, **58**, 348, (1979).

[68] J.Phillips, B.Clausen, and J.A.Dumesic, *J. Phys. Chem.*, **84**, 1814, (1980).

[69] A.P.Dalton, C.L.Honeybourne, and P.L.Plummer, *J. Phys. Chem. Solids*, **47**, 553, (1986).

[70] H.L.Wehner, G.Ritter, and H.H.F.Wegner, *Phys. Lett.*, **46A**, 333, (1974).

[71] J.M.Williams, D.P.Danson, and Chr.Janot, *Phys. Med. Biol.*, **23**, 835, (1978).

[72] I.Tamura and M.Hayashi, *Surface Science*, **146**, 501, (1984).

[73] S.C.Lin and J.Phillips, *J. Appl. Phys.*, **58**, 1943, (1985).

[74] D.G.Rancourt, S.R.Julian, and J.M.Daniels, *J. Magn. Magn. Mat.*, **49**, 305, (1986).

[75] S.Mørup, *J. Magn. Magn. Mat.*, **37**, 39, (1983).

[76] S.Mørup, M.B.Madsen, J.Franck, J.Villadsen, and C.J.W.Koch, *J. Magn. Magn. Mat.*, **40**, 163, (1983).

[77] D.G.Rancourt and J.M.Daniels, *Phys. Rev. B*, **29**, 2410, (1984).

[78] S.Mørup, P.H.Christensen, and B.S.Clausen, *J. Magn. Magn. Mat.*, **68**, 160, (1987).

[79] J.H.Kennedy and A.F.Sammells, *J. Electrochem. Soc.*, **121**, 1, (1974).

[80] C.A.Melendres and B.Tani, *J. Phys. Chem.*, **82**, 2850, (1978).

[81] A.J.Jacobsen and L.E.McCandlish, *J. Solid State Chem.*, **29**, 355, (1979).

[82] M.Eibschutz, *Physica*, **99B**, 145, (1980).

[83] S.Morzilli and B.Scrosati, *Electrochimica Acta*, **30**, 1271, (1985).

[84] J.C.Nardi, M.B.Clark, and W.P.Evans, *Symposium on Electric Power Sources in Horological and Microtechnical Products, Mulhause, France.*, Extended Abstract, 48, April (1981).

[85] M.S.Whittingham and M.B.Dines, *J. Electrochem. Soc.*, **124**, 1387, (1977).

[86] H.Gilman and F.K.Cartledge, *J. Organometal. Chem.*, **2**, 447, (1964).

[87] M.F.Lipton, C.M.Sorensen, A.C.Sadler, and R.H.Shapiro, *J. Organometal. Chem.*, **186**, 155, (1980).

[88] S.P.S.Badwal and R.J.Thorn, *J. Solid State Chem.*, **43**, 163, (1982).

[89] K.Ruebenbauer and T.Birchall, *Hyperfine Interactions*, **7**, 125, (1979).

[90] S.L.Ruby, *Mössbauer Effect Methodology*, I.S.Gruverman, Ed., **8**, 263, Plenum Press, New York, (1973).

[91] C.Wivel and S.Mørup, *J. Phys. E: Sci. Instrum.*, **14**, 605, (1981).

[92] R.S.Preston, S.S.Hanna, and J.Heberle, *Phys. Rev.*, **128**, 2207, (1962).

[93] B.H.Armstrong, *J. Quant. Spectrosc. Radiat. Transfer.*, **7**, 61, (1967).

[94] G.Xiao and C.L.Chien, *Phys. Rev. B*, **35**, 8763, (1987).

[95] R.J.Pollard, *Hyperfine Interactions*, **40**, 417, (1988).

[96] F.Schmidt, A.Quazi, A.X.Trautwein, G.Doppler, and H.M.Ziethen, *Z. Phys. D: Atoms, Molecules and Clusters*, **3**, 303, (1986).

[97] S.Bjärmann and R.Wappling, *J. Mag. Magn. Mat.*, **40**, 219, (1983).

[98] R.J.Batchelor, F.W.B.Einstein, C.H.W.Jones, R.Fong, and J.R.Dahn, *Phys. Rev. B*, **37**, 3699, (1988).

[99] R.Fong, M.Sc. thesis, (1987).

[100] H.M.Gager and M.C.Hobson Jr., *Catal. Rev.*, **11**, 117, (1975).

[101] J.A.Morice, L.V.C.Rees, and D.T.Rickard, *J. Inorg. Nucl. Chem.*, **31**, 3797, (1969).

[102] A.J.Stone, *Chem. Phys. Lett.*, **6**, 331, (1970).

[103] J.W.Niemantsverdriet, A.M.van der Kraan, W.N.Delgass, and M.A.Vannice, *J. Phys. Chem.*, **89**, 67, (1985).

[104] U.Herr, J.Jing, R.Birringer, U.Gonser, and H.Gleiter, *Appl. Phys. Lett.*, **50**, 472, (1987).